UNIVERSITY OF ICELAND

GRÓ · GTP Geothermal Training Programme

unesco Centre Under the auspices of UNESCO

M.S. Thesis

in Earth Sciences

Major and Trace Elements Geochemistry of Natural Waters in Meru, Tanzania

Sadock Josephat Zakaria

June 2023

FACULTY OF EARTH SCIENCES

Major and Trace Elements Geochemistry of Natural Waters in Meru, Tanzania

Sadock Josephat

Dissertation submitted in partial fulfilment of a
Magister Scientiarum degree in Earth Sciences

M.S. Committee
Andri Stefánsson
Finnbogi Óskarsson

Examiner
Daði Þorbjörnsson

Faculty of Earth Sciences
School of Engineering and Natural Sciences
University of Iceland
Reykjavik, June 2023

Major and Trace Elements Geochemistry of Natural Waters in Meru, Tanzania

Water Geochemistry in Meru, Tanzania
Dissertation submitted in partial fulfilment of an *M.S.* degree in Earth Sciences

Faculty of Earth Sciences
School of Engineering and Natural Sciences
University of Iceland
Sturlugata 7
101, Reykjavik
Iceland

Telephone: 525 4000

Bibliographic information:
Sadock Josephat, 2023, *Major and Trace Elements Geochemistry of Natural Waters in Meru, Tanzania,* MS dissertation, Faculty of Earth Sciences, University of Iceland, 74 pp.

Abstract

The geochemistry of major and trace elements and stable isotopes of surface and groundwaters in the upper flanks of Mt. Meru volcano was assessed. The study area is in the volcanic province of northern Tanzania, in the Gregory Rift of the East Africa Rift System. This study involved spring-, stream-, river-, lake-, and groundwaters. PHREEQC was used for the calculation of aqueous speciation and mineral saturation indices.

The studied waters are of meteoric origin as indicated by $\delta^{2}H\text{-}H_2O$ and $\delta^{18}O\text{-}H_2O$, with Na-HCO_3 composition. The chemistry of the studied waters is mainly controlled by progressive dissolution of rocks at low temperatures as indicated by the correlation between major constituents (Na, K, Mg, SO_4, and Cl). Two possible end-member water compositions, non-reacted rainwater and reacted water have been identified, and other spring-, river- and groundwaters fall between these two end members. The saline lakes are formed by evaporation of waters sourced at higher altitudes. Dissolution of carbonates, mixing with biogenic and atmospheric CO_2, and input of deep volatiles are suggested based on $\delta^{13}C\text{-}CO_2$.

The element mobility relative to Na is generally low in the studied waters, suggesting that many elements are incorporated into weathering minerals. Multiple mineral equilibria geothermometry suggests a possible low-temperature (<100 °C) geothermal system on the Eastern flank of Mt. Meru. The concentrations of As, Fe, Hg, Mn, Mo, U, Na, Cl, SO_4, and NO_3 in some samples and F in nearly all samples are higher than the permissible limits defined by local and international health guidelines.

Útdráttur

Efnafræði yfirborðsvatns og grunnvatns í hlíðum Meru-fjalls í Tansaníu var rannsökuð. Rannsóknarsvæðið er innan eldvirka beltisins í Norður-Tansaníu, sem aftur tilheyrir Gregory-rekbeltinu í eystri grein Sigdalsins mikla í Austur-Afríku. Sýnum var safnað af grunnvatni, vatni úr lindum, lækjum, ám og stöðuvötnum og þau greind með tilliti til aðalefna, snefilefna og stöðugra samsætna. Forritið PHREEQC var notað til að reikna jafnvægissamsetningu vatnsins og mettunarstig steinda.

Samsætur vetnis og súrefnis (δ^2H-H_2O og δ^{18}O-H_2O) gefa til kynna að uppruna vatnsins megi rekja til úrkomu og ráðandi jónir í því eru Na^+ og HCO_3^-. Fylgni milli styrks aðalefna vatnsins (Na, K, Mg, SO_4 og Cl) gefur til kynna að efnasamsetningin stjórnist fyrst og fremst af upplausn bergs við fremur lágt hitastig. Greina má tvær vatnsgerðir, mikið og lítið hvarfað vatn, sem gætu verið endaþættir í blandlíkani þar sem efnasamsetningu annars linda-, straum- og grunnvatns mætti skýra með blöndun endaþáttanna tveggja. Söltu vötnin á svæðinu hafa orðið til við uppgufun aðrunnins vatns. Kolefnissamsætur (δ^{13}C-CO_2) sýna að uppruna CO_2 má rekja til upplausnar karbónatsteinda, blöndunar við CO_2 af lífrænum uppruna, úr lofti, og af djúpstæðari uppruna.

Flest frumefni í vatninu sem hér var til skoðunar eru minna hreyfanleg en Na, sem bendir til þess að mörg þeirra sitji eftir í veðrunarsteindum. Efnahitamælir sem byggir á mörgum steindajafnvægjum samtímis gefur til kynna að hugsanlega megi finna lághitakerfi (<100 °C) í austurhlíðum Meru-fjalls. Styrkur As, Hg, Fe, Mn, Mo, U, Na, Cl, SO_4, og NO_3 er yfir heilsuverndarmörkum í nokkrum sýnum og styrkur F yfir heilsuverndarmörkum í öllum sýnum.

Dedication

This dissertation is dedicated to my lovely wife Olivia Josephat who has been taking care of our son Joseph and daughter Sabina alone during my time in Iceland.

Table of Contents

List of Figures

List of Tables

Acknowledgements

The completion of this thesis is a remarkable achievement to finishing my journey towards the award of *Magister Scientiarum* degree in Earth Sciences. I thank Almighty God for such a Blessing.

I am thankful to GRÓ.GTP under the auspices of UNESCO for financially supporting my MSc studies at the University of Iceland. In conjunction, I thank the GRÓ.GTP staff Dr. Guðni Axelsson (Director), Ingimar G. Haraldsson (Deputy Director), Málfríður Ómarsdóttir (Project Manager), and Dr. Vigdís Harðardóttir (Operations Manager) for their support throughout my studies.

I am indebted to my supervisors Andri Stefánsson (Professor of Geochemistry at University of Iceland) and Finnbogi Óskarsson (Chemist at Iceland GeoSurvey). Thank you for your time, dedication, patience, and guidance throughout the preparation of this thesis and my MSc studies in general at the University of Iceland. The knowledge gained from you will constitute an important part in my further carrier and I am looking forward to working with you in the future. I also thank the examiner of this thesis Daði Þorbjörnsson (Geologist at Iceland GeoSurvey) for reviewing this work.

I am gratitude to my current employer Tanzania Geothermal Development Company Ltd (TGDC) for granting me the study leave and allowing me to use the water chemistry data of the Mt. Meru area for my thesis. I also thank the Government of Tanzania for granting me the permit required for a civil servant to be abroad.

I also thank the colleagues GRÓ.GTP fellows whom we shared moments and made the stay in Iceland contended. I would like to mention a few, Makoye Didas thank you for the assistance with Inkscape, Daniel Gustavo and Tingting Zheng thank you for the assistance with Grapher. Araksan Ahmed and Zelalem Abebe, those weekends and late-night discussions in Gamli Garður were awesome. TGDC colleague Philibert Philmon (Geophysicist) is also acknowledged for a discussion on the geology of the study area.

Finally, I am thankful to my family for their support during my MSc studies. My father and late mom have always been a source of inspiration in life. Thank you for the advice and prayers. My wife and our kids Joseph and Sabina have been a big motivation in my undertakings, thank you so much.

1 Introduction

Geochemical and hydrological factors and processes among others control water composition. For instance water-rock interaction, mixing of waters of variable sources, evaporation and input of deep gases may all contribute to the chemical composition of natural waters (White 2020). Moreover, the chemical and isotope composition of natural waters can provide insight into some of the key hydrogeological features of groundwater systems, both thermal and non-thermal systems. For instance the stable isotopes of water (δ^2H and $\delta^{18}O$) can be used to trace the water sources, progressive water-rock interaction and evaporation processes (Allegre, 2008; Sharp, 2017). In addition, non-reactive elements, for example B and Cl, have been used to evaluate the progress of water-rock interaction and mixing of waters of variable origin (e.g., Arnórsson and Andrésdóttir, 1995) whereas the reactive elements, for example Si, Na, K, Ca, Mg, Al and Fe, are incorporated into secondary and weathering minerals (Kaasalainen and Stefánsson, 2012).

Trace element composition of natural waters has received less attention than major element chemistry. Most previous studies on trace element chemistry in groundwater systems have focused on their concentrations rather than quantifying the processes controlling their composition. However, such studies (e.g., Kaasalainen and Stefánsson, 2012) have demonstrated that trace elements geochemistry can be quantified in a similar manner as many major elements, i.e., by studying water mixing and water-rock interaction.

Previous hydrogeological and geochemical studies at Mt. Meru volcano (Tanzania) and the surrounding areas have postulated groundwater composition at Mt. Meru to be controlled by the aquifer lithology and climate factors including high precipitation and temperature (Bennett et al., 2022; Makoba and Muzuka, 2019; Tomašek et al., 2022). High precipitation and warm temperature are associated with enhanced dissolution of rocks (e.g., Gislason, 2008). Water hosted in the fractured volcanic rocks, breccia, and tuff formations has lower concentrations of dissolved elements compared to the water hosted in lahars, which are more susceptible to weathering. Moreover, the deep circulating groundwater evinces lower concentrations of dissolved elements than shallow circulating water, attributed to slower weathering and dissolution rate of aluminosilicate minerals composing the deep aquifer than the pyroclastic deposits that form the shallower aquifers (Bennett et al., 2021).

Water quality at Mt. Meru volcano and surroundings is poor and often unacceptable due to elevated concentrations of dissolved elements, for example F, Na, K, SO_4, Cl, and NO_3 (Bennett et al., 2022; Makoba and Muzuka, 2019; Malago et al., 2020). Uranium (U) and Mo above health limits have been identified in some water sources (Tomašek et al., 2022).The composition of such water has been linked to the interaction with the alkaline rocks and influence of hydrothermal fluids (e.g., Bennett et al., 2021; Ghiglieri et al., 2012). In contrast the geochemistry of trace elements is not well understood as well as the mobility of various elements, both in thermal and non-thermal waters.

The purpose of this study is to investigate the geochemistry of major and trace elements in the ground-, surface- and lake waters at Mt. Meru volcano and the areas around. It focuses on the origin of the waters and processes affecting water composition, mobility of major and trace elements, characterization of end-member water sources as well as assessing the overall water quality with respect to major and trace elements.

2 Study Area

2.1 Location and Climate

The study area of the present study is on the eastern side of Mt. Meru volcano and surroundings and lies at an elevation of 1230 to 4565 meters above sea level (m AMSL). Mount Meru is in the Arusha National Park, Tanzania. The climate is semi-arid with cold and dry season from June to September while the warm and wet season is between October and May. However, at the summit of the Mt. Meru volcano, the temperature drops to below freezing point.

2.2 Geological Background

Mt. Meru is a stratovolcano in the eastern branch (Gregorian rift) of the East Africa Rift System (EARS). This rift is a 6,000 km long intra-continental structure generally trending north-south (Chorowicz, 2005; Roberts, 2002). It extends from northeast of Africa in the Gulf of Aden to eastern Africa in Mozambique (Figure 2- 1). The EARS is observed as a succession of basins bordered by the uplifted blocks while the central part is subsiding, and it has two main branches which are the eastern and the western branches.

The Gregory rift extends from the Gulf of Aden to Ethiopia and Kenya and ends in the rift basins of the northern Tanzania volcanic zone (Chorowicz, 2005; Mahecha, 2019). High relief areas in the EARS corresponds to the Ethiopian dome, Kenyan dome and Tanzanian dome (Chorowicz, 2005) and are attributed to volcanism, tectonic belts, and graben shoulders. The eastern branch has more volcanic activity than the western branch and is believed to have more geothermal potential.

The EARS is comprised of elongated zones of thinned continental crust because of intrusions in the upper mantle, which results to thermal uplift (Chorowicz, 2005; Mahecha, 2019). This agrees with the thermal flux anomaly identified at the collision boundaries (Didas et al., 2022). The rift generally trends north-south, however, the trend varies locally from one area to another reflecting the pre-existing geologic conditions. For example, the eastern and western branches run around the stable Tanzanian craton indicating that rifting could not penetrate this formation (Figure 2- 1).

The evolution and propagation of the EARS is attributed to the rising mantle plume (Delcamp et al., 2013). This plume has been detected by gravity and seismic imaging and also indicated by the noble gases provenance (Halldórsson et al., 2014). The formation of domes, upper mantle thinning, intrusion and thermal uplift is analogue to early stage of passive continental margin preceding opening of the ocean (Chorowicz, 2005).

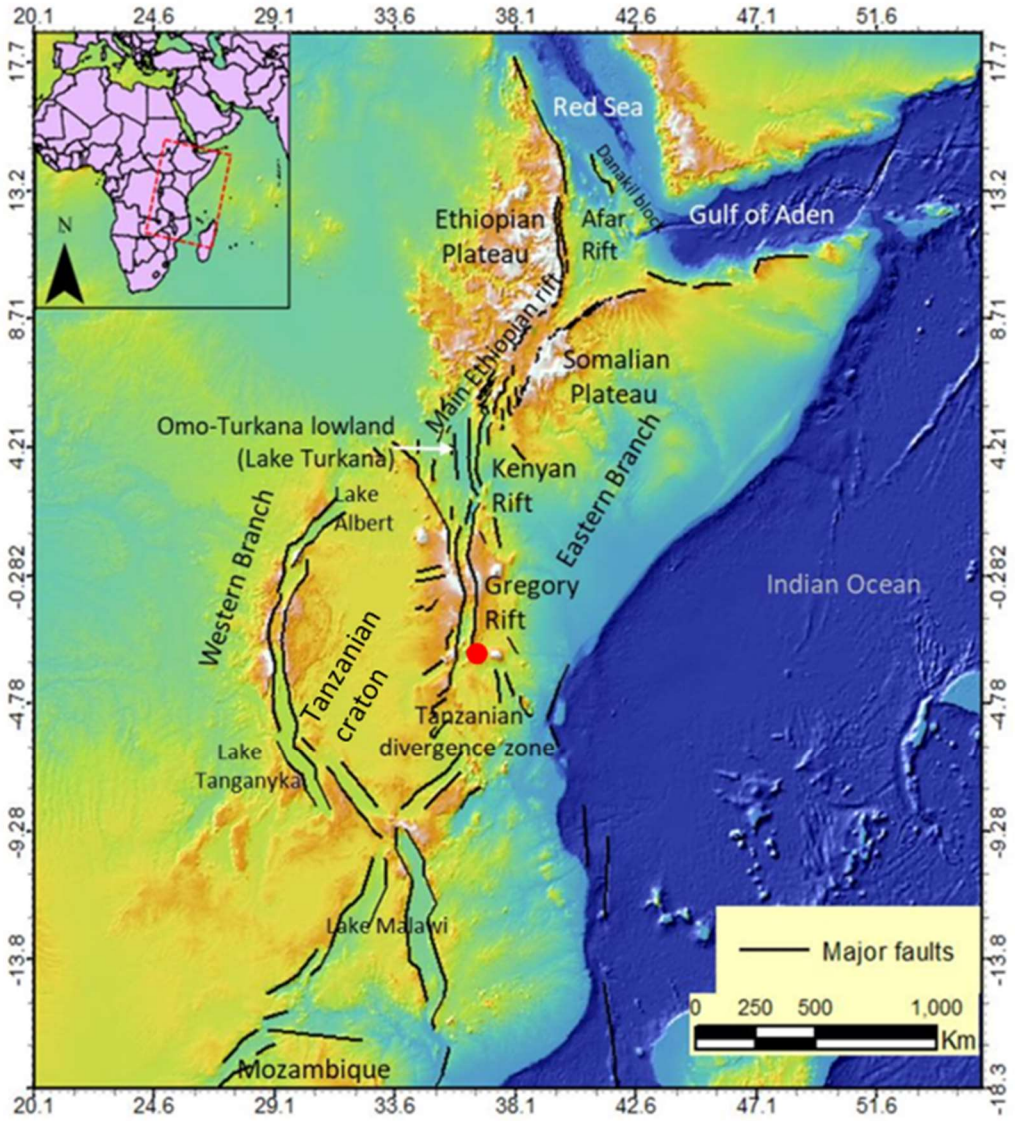

Figure 2- 1: Digital elevation map of the Eastern Africa showing the East African Rift System (EARS) (Kebede, 2021). The location of the study area is indicated by the red dot.

The northern Tanzania divergence is characterized by a 50-80 km wide depression (Le Gall et al. 2008). The depressions trend N-S in Magadi (south of Kenya) to the Natron-Manyara basin, NE-SW in the Ngorongoro-Eyasi depression and NW-SE in the Pangani rift basin in Tanzania (Dawson 1992). The Eyasi, Manyara and Pangani fault system form the main diverging rift structure of the northern Tanzania divergence zone (NTDZ), bordered by the Tanzanian craton on the west and the Precambrian Mozambique belt rocks on the east (Le Gall et al., 2008; Roberts, 2002).

Volcanoes in the NTDZ occur in alignments forming linear trends which can be correlated to the rift structures. The alignments recognized in the area are the N-S trend from Natron to Oldonyo Lengai, Kerimasi and Manyara, the NE-SW trend encompassing the Eyasi structure, Balangida fault and the volcanoes of Ngorongoro, Tarosero, Essimingor and Burko. Other trends are the ENE-WSW Meru trend evidenced by the alignment of Ngorongoro-Monduli-Meru-Kilimanjaro volcanoes (Figure 2- 2) and the NW-SE trend indicated by the Engaruka basin and fissure eruption southeast of Kilimanjaro and Pangani

basin (Delcamp et al., 2013; Le Gall et al., 2008). This suggest that magmatism in the NTDZ is structural controlled.

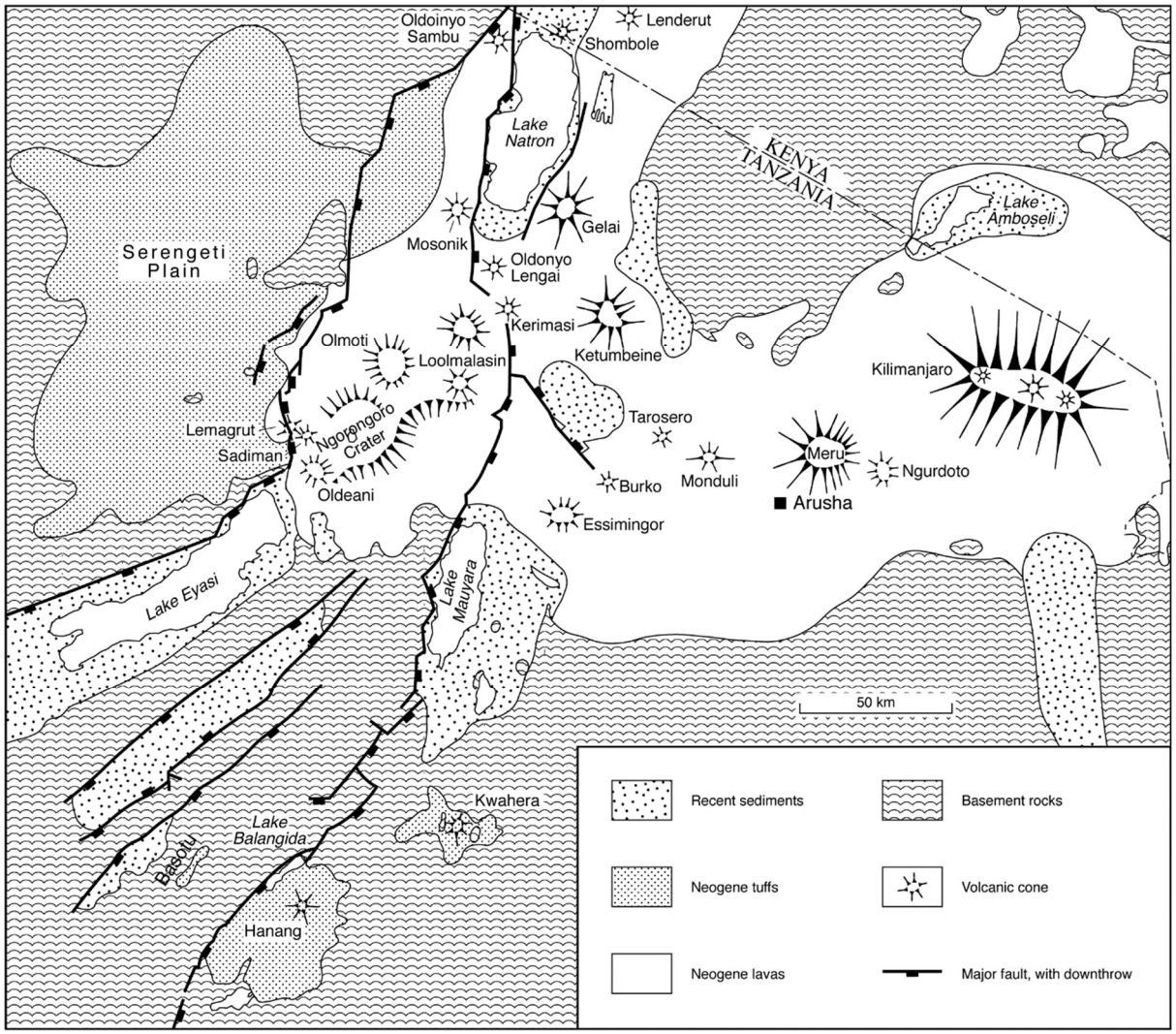

Figure 2- 2: Map showing volcanoes and tectonic lineament in the Northern Tanzania Divergence Zone (Foster et al., 1997).

The Northern Tanzania Volcanic Province (NTVP) recorded a complex history of faulting, volcanism, and sedimentation. The early deformation is indicated by the mid-Tertiary faulting which caused uplifting of the Lake Victoria and the Masai blocks (Dawson, 1992). This occurred concurrently with sedimentation due to erosion of the uplifted blocks. Volcanism in the area produced several shield volcanoes which ejected alkali basalts, trachytes and phonolites. These volcanoes include Ngorongoro, Gelai, Shira and Mawenzi of Kilimanjaro, Oldoinyo Sambu, Elanairobi, Olmoti, Loolmalasin, Lemagrut, Oldeini, Ketumbeine and Tarosero. This was followed by a phase of volcanic activity with different explosivity and volcanic products. Volcanoes erupted in this phase included Meru, Monduli, Oldoinyo Lengai, Burko, Kerimas, Kwaraha and Hanang. The chronology and stratigraphy in the NTDZ have been detailed described by Roberts (2002) and Wilkinson et al. (1986).

Volcanic activity in the northern Tanzania is younger than its northern counterparts in Kenya and Ethiopia where magmatism started 30 Ma in Lake Tana, Ethiopia (Chorowicz, 2005; Dawson, 1992). This suggest southern migration of the mantle plume (Dawson, 2008; Roberts, 2002). Alkaline volcanism in Meru occurred in hiatus and the early events were 2.0–1.5 Ma followed by other events 0.35-0.16 Ma (Roberts, 2002; Wilkinson et al., 1986). The main Meru cone building eruption occurred 0.16-0.06 Ma followed by small events which were observed until the 20th century (Wilkinson et al., 1986). The last documented eruption in Meru occurred at ash cone in 1910 and produced black ash at the top of ash cone (Delcamp et al., 2013; Ghiglieri et al., 2010; Wilkinson et al., 1986) which is a resurgent volcano erupted after the collapse of the main Meru volcano on its eastern flank. An ash cone is emplaced in the Meru crater and believed to be still growing (Delcamp et al., 2013).

The surface geology is dominated by volcanics (Figure 2- 3). Volcanic tuffs are distributed throughout the northern volcanic province of Tanzania (Dawson, 1992). Other rock units include basaltic lava flows, nephelinite, pyroclastic deposits, tuffs and volcanic breccia which contain phonolite clasts associated with Meru and Ngurdoto crater eruptions (Roberts 2002). Debris avalanche characterized by presence of large boulders within fine matrix which is a result of collapse of the Mt. Meru volcano, cover a large area on the eastern flank of Mt. Meru volcano. The main cone of Meru is peralkaline trachyte, phonolites and nephelinites while carbonatite lava and pyroclactics occur with nepheline at Oldoinyo Lengai, Hanang, Kwaraha and Kerimasi (Dawson, 1992).

Mt. Meru volcano collapsed on its eastern flank ~7800 years ago resulting in a lahar covering an area of ~1500 km^2 to the northeast, east and southeast of the volcano up to the foot of Mt. Kilimanjaro volcano (Wilkinson et al., 1986). This wide spread of lahar was aided by the presence of large quantity of water that acted as lubricant (Delcamp et al., 2016) and was followed by construction of lava dome and ash cone in the 3.5 km diameter Meru crater on the eastern flank of the volcano (Roberts, 2002; Wilkinson et al., 1986).

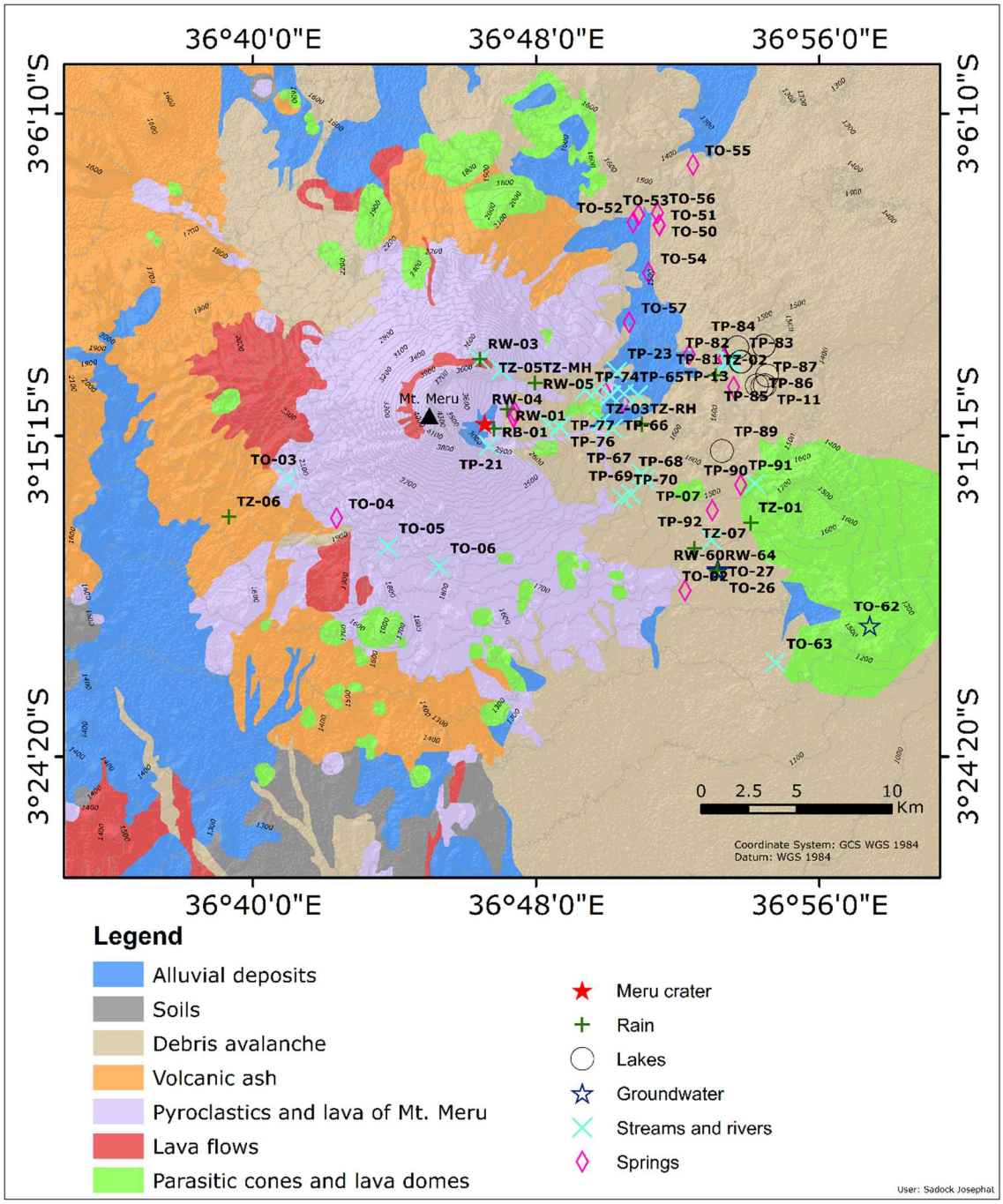

Figure 2- 3: Geological map of Mt. Meru volcano area modified from Tomašek et al. (2022). The locations of sampling sites in the present study are also indicated.

2.3 Hydrogeology

Hydrology in the area is influenced by Mt. Meru volcano. The drainage system is radial from higher to lower elevation with streams and rivers, while lakes occur only to the eastern side of the volcano (Figures 2-3 and 5-7). Water flow is complicated by tectonic structures such as grabens, faults, eruptive activity, lava domes, vegetation cover, thermal regime, and tholoids (Delcamp et al., 2016; Ghiglieri et al., 2010).

The hydrological model of Mt. Meru volcano can be explained as the typical mature volcano where aquifers developed at temperate conditions when recharge was higher than discharge (Delcamp et al., 2016). The episodes of Meru volcano collapse, which cut one third of the volcano, disrupted the aquifer leading to loss of large quantity of stored water and this water acted as a lubricant for lahar flow (Delcamp et al., 2013). However, the aquifer may have redeveloped following the post collapse eruption leading to emplacement of ash cone in the collapse scur.

Water flow in the area has been categorized into local, intermediate, and regional flow systems by Bennett et al. (2021). The regional flow system has been regarded as deeper with longer residence time while the local and intermediate flow are shallow with short residence time (Figure 2- 4). However, controls of the water composition and mixing trends between different endmembers were not well established and are described in this study.

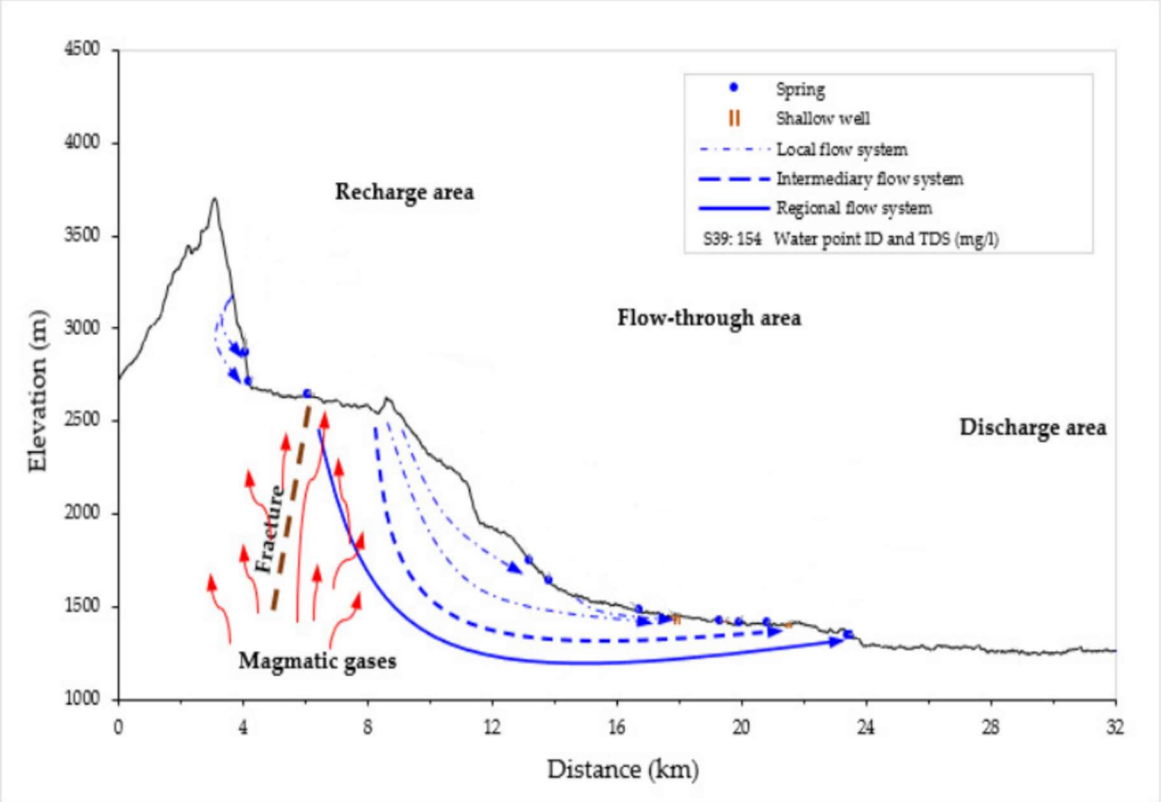

Figure 2- 4: Hydrological model of the Mt. Meru proposed by Bennett et al. (2021).

2.4 Geothermal Activity

The northern volcanic province of Tanzania is characterized by various geothermal activity like thermal springs, deposits, and mineral alteration. Thermal springs in this zone indicate great variability in discharge temperatures and chemical composition between specific prospect areas. The known discharge temperatures range from 20 °C to 71 °C, pH from 7.4 to 10, and composition ranging from Na-Cl to Na-HCO_3 waters.

At Mt. Meru fumarolic activity was observed after the 1910 ash cone eruption but vanished after 1954 (Ghiglieri et al., 2010; Wilkinson et al., 1986). At present, the evidence of this fumarolic activity is presented by fossil argillic alteration observed at the ash cone. High heat flux in the order of 90-104 mW/m^2 has been identified in the Northern Tanzania Divergence Zone by Didas et al. (2022).

The Njekukumia springs are located at high elevation and in thick vegetation cover and display high dissolved solute content compared to other springs in the area. A few other springs at lower elevation on the eastern and north-eastern flanks of Mt. Meru volcano display similar composition as the Njekukumia springs including springs in the Lendoiya and Ngarenayuki villages. Such high content of dissolved elements may be signs of thermal water. However, the geothermal activity at Mt. Meru is poorly characterized and in fact mostly unknown. Reservoir temperatures in the range of 50 - 90 °C have been estimated based on geothermometry with water circulation depth down to ~1.5 km assuming a geothermal gradient of 45 °C/km (Bennett, 2022).

Alteration minerals in the area were mapped by remote sensing and laboratory analysis of rock samples. Minerals identified include ferric oxide, alunite, calcite, and kaolinite. Analysis of rock and soil samples confirmed the occurrence of alunite together with levynite, K-feldspars, hematite and halloysite (Mahecha, 2019). Native sulfur, which is commonly observed in association with steam-heated acid-sulfate waters was observed at the ash cone. Most of these alteration minerals were observed in the Meru crater and the peak of ash cone and are typical mineralogy associated with argillic alteration (Mahecha, 2019; Mahecha et al., 2021).

3 Methods

3.1 Sampling and Analysis

Water samples were collected on the upper flanks of Mt. Meru volcano in 2017, in total 64 samples of springs, streams, rivers, lakes, and groundwater. In addition to the surface and groundwater samples, rainwater was collected from different locations in the Arusha National Park and outside the park (Figure 2- 3). On-site measurements of water temperature, pH, EC, and redox potential (ORP) were conducted using a WTW Multimeter. The pH was measured by a combination pH electrode inbuilt in a multimeter and was calibrated using 4.0, 7.0 and 10.0 buffer solutions whereas the EC electrode was calibrated using KCl solution.

Water samples were collected for the analysis of anions (F, Cl, Br, ΣCO_2, SO_4, NO_3 and PO_4), major and trace cations (Na, K, Ca, Mg, Si, Al, Fe, B, Sr, As, Ba, Be, Bi, Cd, Ce, Co, Cr, Cs, Cu, Dy, Er, Eu, Ga, Gd, Ge, Hf, Hg, Ho, In, La, Li, Lu, Mn, Mo, Nb, Nd, Ni, Pb, Pr, Rb, Sb, Sc, Se, Sm, Sn, Sr, Ta, Tb, Te, Th, Ti, Tl, Tm, U, V, W, Y, Yb, Zn, and Zr), and selected stable isotope ratios (δ^2H-H_2O, $\delta^{18}O$-H_2O, and $\delta^{13}C$-CO_2).

Samples for analysis of anions were collected into polyethylene (PE) bottles with no further sample treatment. Samples for analysis of cations (major and trace) were filtered using PE syringes fitted with disposable 0.45 µm cellulose acetate filters, collected in PE bottles and acidified with 1 mL ultrapure 65% HNO_3 in 100 mL sample. Samples for analysis of stable water isotopes (δ^2H-H_2O and $\delta^{18}O$-H_2O) were collected in brown glass bottles with double stoppers. Samples for analysis of $\delta^{13}C$-CO_2 were filtered using PE syringes fitted with disposable 0.45 µm cellulose acetate filters and collected into glass bottles with no further treatment.

The water samples were analyzed at the Groundwater Resources, Soil as a Resource and Resource Geochemistry laboratories of Federal Institute for Geosciences and Natural Resources (BGR) in Hanover, Germany. The concentrations of anions (F, Cl, Br, SO_4, ΣCO_2, PO_4, and NO_3) were determined by ion chromatography (Dionex-2000). Major cations (Na, K, Mg, Ca, Si, Fe, Al) were analyzed using Spectro Arcos Inductively Coupled Plasma Optical Emission Spectroscopy (ICP-OES) while trace elements (B, Sr, As, Ba, Be, Bi, Cd, Ce, Co, Cr, Cs, Cu, Dy, Er, Eu, Ga, Gd, Ge, Hf, Hg, Ho, In, La, Li, Lu, Mn, Mo, Nb, Nd, Ni, Pb, Pr, Rb, Sb, Sc, Se, Sm, Sn, Sr, Ta, Tb, Te, Th, Ti, Tl, Tm, U, V, W, Y, Yb, Zn, and Zr) were determined using Agilent 7800 Inductively Coupled Plasma Mass Spectrometry (ICP-MS). Determination of δ^2H-H_2O and $\delta^{18}O$-H_2O was done using Picarro L2130-i Cavity ring-down laser spectrometer, and $\delta^{13}C$-CO_2 was analysed using thermo scientific MAT 253 isotope ratio mass spectrometer.

The average charge balance error for the analytical results is -0.1%. Data with charge balance error within the range of ±10% were used in further assessment while data out of this range were considered of low quality and not further considered. Therefore, data for 55 samples were used while data from nine samples were discarded.

3.2 Calculations of Aqueous Speciation and Mineral Saturation Indices

The PHREEQC (version 3.7.3) computer program and the llnl.dat database (Parkhurst and Appelo, 1999) were used to calculate the aqueous speciation, charge balance, activities, and activity coefficients of different aqueous species from component concentrations. PHREEQC calculates the concentration and activities of the species from a component concentration by simultaneously solving the mass balance, mass action and activity coefficient equations at the specified Eh, pH and temperature.

PHREEQC was also used to calculate the saturation indices of different minerals. The saturation index (SI), which is used to assess the mineral-fluid equilibria, is calculated by subtracting the logarithm of equilibrium constant (K) from the logarithm of reaction quotient (Q) for a particular reaction.

$$SI = \log Q - \log K \quad (1)$$

If SI<0 the water is undersaturated with respect to the mineral, which could thus be dissolving, if SI=0 the water and mineral are at equilibrium, and if SI>0 the water is supersaturated and the mineral under consideration could be forming (precipitating). The saturation states of studied waters were assessed with respect to albite, K-feldspar, K-mica, chalcedony, calcite, chlorite, alunite, kaolinite, gibbsite, hematite, goethite, quartz, talc, analcime, fluorite, and illite, chrysotile. These minerals have been identified in the area, while others are minerals commonly observed in low temperature environments.

To estimate the subsurface temperature, such a mineral-fluid saturation was assumed using a multi-mineral equilibria geothermometry approach (Reed and Spycher, 1984). This technique involves calculation of the saturation index of relevant secondary minerals and solving the temperature where the mineral saturation indices are at equilibrium.

3.3 Water Quality

To assess the quality of surface and groundwater, concentration of potential toxic elements including As, B, Ba, Cd, Cr, Cu, F, Fe, Hg, Mn, Mo, Ni, Pb, Sb, Se, U, and Zn and major constituents (Na, Cl, SO_4, NO_3) were compared with the Tanzanian guidelines (TBS, 2008) and international guidelines (WHO, 2022). Constituents whose concentrations were above the health limits including As, Fe, Mo, U, Hg, Mn, F, Na, Cl, SO_4, and NO_3 were inferred to be of concern while elements whose concentrations were below the limits defined by the guidelines including Ba, B, Cd, Cr, Cu, Mn, NH_4, Ni, Pb, Sb, Se, and Zn were assumed to be of less concern to human health. The elements with high relative mobility in water were considered hydrophilic thus preferentially partition into water and could have a concerning impact when the concentration is above the limits.

3.4 Relative Mobility of Elements

The relative mobility (RM) of elements in the surface waters and groundwater in the upper flanks of Mt. Meru volcano was calculated from the relationship,

$$RM = \left(\frac{Ci}{Na}\right)w \Big/ \left(\frac{Ci}{Na}\right)r \qquad (2)$$

where Ci is the concentration of element *i* in water ′w′ and in rocks ′r′ in mmol/kg normalized to the concentration of sodium ′Na′. Sodium was selected as the reference element because it is abundant both in water and in the reference rock and it is the highly mobile cation (Gislason et al., 1996).

The chemical composition of nephelinites, which were used as reference rocks due to their abundance in the area (BGR, 2018; Dawson, 2008; Roberts, 2002) is reported in Table 1. These are whole rock geochemistry data. Elements with RM above the reference suggest they are controlled by dissolution of primary rocks while elements with low RM indicate they are retained in the host rocks or uptake by the secondary minerals.

Table 1: Chemical composition of the nephelinites in the study area used for calculation of elemental relative mobility based on whole rock geochemistry. Data from (Roberts, 2002).

Major elements (wt-%)	
SiO_2	48.43
Al_2O_3	17.70
Fe_2O_3	8.76
FeO	6.30
MgO	2.32
CaO	6.46
Na_2O	8.30
K_2O	4.25
TiO_2	2.23
MnO	0.20
P_2O_5	0.55
Total	100.78
LOI	0.46
Trace elements (ppm)	
Ba	1630.29
Co	15.11
Cr	11.13
Cu	24.84
Ga	25.50
Hf	10.52
Nb	196.67
Ni	9.40
Pb	16.08
Rb	108.89
Sc	23.53
Sr	1669.76
Ta	10.19
Th	13.66
U	4.87
V	134.29
Y	39.16
Zn	118.07
Zr	476.90
REE (ppm)	
La	135.00
Ce	235.67
Pr	25.40
Nd	86.37
Sm	14.12
Eu	4.33
Gd	14.44
Tb	1.64
Dy	7.66
Ho	1.38
Er	3.87
Tm	0.51
Yb	3.09
Lu	0.44

4 Results

4.1 Major Element Composition

The major element composition of springs, streams, rivers, lakes, and cold groundwaters used in this study are given in Table 2.

Spring waters are characterized by discharge temperatures of 14.0-24.1 °C, pH of 6.3-8.9, EC of 242-9320 µS/cm, redox potential of -70 to 308 mV, and SiO_2 (4.4-72.1 ppm). Sodium (Na) dominates the cations (38.5-2294 ppm), followed by K (13.7-327 ppm), Ca (1.01-20.8 ppm), and Mg (0.351-6.78 ppm). Anions are dominated by, ΣCO_2 (98.1-3062 ppm), followed by SO_4 (2.07-1437 ppm), Cl (2.86-203 ppm), and F (1.43-77.9 ppm). The isotopic composition of water is δ^2H-H_2O of -35.6 to -10.5 ‰ and $\delta^{18}O$-H_2O of -6.83 to -2.49 ‰ and for dissolved inorganic carbon is $\delta^{13}C$-CO_2 of -16.6 to -0.29 ‰. Among the springs, Njekukumia springs indicate the highest concentration of major elements (except for NO_3) compared to other springs and they occur as outliers in the box and whisker plots (Figure 4-1).

Rivers and streams water have temperatures of 12.3-33.8 °C, pH of 6.3-9.6, EC of 109-5360 µS/cm, redox potential of 15-317 mV, and SiO_2 (6.1-51 ppm). The concentration of major metals is Na (14.4-1211 ppm), K (7.5-207 ppm), Ca (1.42-18.7 ppm), and Mg (0.245-5.2 ppm). The concentration of major anions was dominated by ΣCO_2 (41.1-1801 ppm), SO_4 (0.124-564 ppm), Cl (1.45-167 ppm), and F (0.248-71.9 ppm). The isotope composition for these waters are δ^2H-H_2O of -35.3 to -8.1 ‰, $\delta^{18}O$-H_2O of -6.81 to -2.25 ‰, and $\delta^{13}C$-CO_2 of -17.1 to 1.21 ‰.

The lake waters are the most saline in the study area with temperatures of 18.4-28.2 °C, pH of 7.1-9.9, EC of 1004-43600 µS/cm, and redox potential of -270 to 116 mV. The composition of major cations is dominated by Na (163-14350 ppm), K (89.4-1830 ppm), Ca (1.09-19 ppm), and Mg (2.18-9.31 ppm). Major anions are ΣCO_2 (556-13125 ppm), SO_4 (22.5-3186 ppm), Cl (29-1611 ppm), and F (2.77-1180 ppm). SiO_2 content for the lake waters is 2-52.2 ppm and isotopic composition of δ^2H-H_2O is -8.8 to 37 ‰, and $\delta^{18}O$-H_2O is -2.6 to 6.73 ‰. The saline-alkaline lakes indicate the highest concentration of Na, K, Mg, Al, Cl, F, SO_4, and ΣCO_2 among the studied waters (Figure 4-1).

Groundwater had measured temperatures of 22-25 °C, pH of 6.5-8.6, EC of 257-786 µS/cm, redox potential of 59-238 mV, and SiO_2 (33.3-57.6 ppm). The determined concentration of major cations is dominated by Na (52.6-154 ppm), followed by K (13-33.9 ppm), Ca (2.86-5.49 ppm), and Mg (0.431-5.41 ppm). Major anion composition is dominated by ΣCO_2 (142-494 ppm), SO_4 (0.372-13.4 ppm), Cl (4.38-16.2 ppm), and F (4.24-15.7 ppm). The isotope composition was δ^2H-H_2O of -27.3 to -18.3 ‰, $\delta^{18}O$-H_2O of -5.67 to -3.97 ‰, and $\delta^{13}C$-CO_2 of -15.7 to -5.9 ‰.

The studied waters were classified using the Piper plot (Figure 4-2). This diagram indicates that both the springs-, lakes-, ground- streams and rivers water are dominated by $NaHCO_3$ composition.

Table 2: Major element and stable isotopes composition of waters in the upper flanks of Mt. Meru volcano[a].

Sample	Coordinates		Altitude	Type	Name	Temp.	EC	ORP	pH	SiO_2	Na	K	Ca	Mg	Al	Fe	F	Cl	ΣCO_2	SO_4
	Easting (m)	Northing (m)	m			˚C	µS/cm	mV		ppm	ppm	ppm	ppm	ppm	ppm	ppm	ppm	ppm	ppm	ppm
TP-18	254346	9641038	2580	S	Njekukumia	23	4465	280	7.9	32.2	1075	220	5.53	2.95	0.020	0.036	64.9	176	1592	375
TP-58	254362	9641031	2615	S	Njekukumia	23	4760	215	7.8	32.5	1064	218	5.67	2.92	0.028	0.069	50.0	181	1651	379
TO-55	263717	9654153	1350	S		24	3400	205	8.2	26.2	767	101	9.59	3.03	0.024	0.039	26.4	103	1001	448
TP-79	265345	9644054	1462	S	Lendoiya	23	3800	-70	8.3	4.40	816	134	2.12	1.94	0.136	0.070	46.9	104	1223	336
TP-80	265366	9644115	1458	S	Lendoiya	22	9320	92	8.3	19.9	2294	327	16.5	4.97	0.565	2.584	77.9	203	3062	1437
TP-88	265866	9642597	1443	S	Ngongongare	20	3650	na	8.9	7.00	876	97.2	4.95	1.55	0.378	0.233	58.5	71.7	1232	288
TO-02	263341	9632016	1312	S	SE TFS	22	787	270	6.7	60.2	141	27.5	20.8	6.78	0.027	0.048	3.03	6.48	279	11.9
TO-04	245095	9635740	1900	S		15	242	245	7.9	57.2	38.5	13.7	5.61	1.88	0.055	0.053	1.55	2.86	98	2.07
TP-07	264759	9636186	1431	S	Makroso	20	951	249	8.6	24.7	215	27.4	4.62	0.675	0.039	0.045	22.7	26.1	317	36.3
TO-50	261959	9651001	1434	S	N of ANP	22	1078	244	7.5	51	204	43.8	15.2	4.15	0.007	0.040	7.81	19.4	392	46.2
TO-52	260591	9651154	1449	S	N of ANP	24	824	228	7.7	55.1	162	28	12.9	2.21	0.247	0.108	6.64	15.3	332	16.9
TO-53	260864	9651555	1426	S	N of ANP	24	966	207	8.7	24.3	213	21.1	3.38	0.462	0.096	0.077	10.7	31.8	352	29.4
TO-54	261401	9648522	1453	S	Olkungw'ado	19	797	308	7.6	53.1	155	30.0	9.04	2.56	0.006	0.038	6.54	17.1	301	26.7
TO-56	261860	9651645	1418	S	N of ANP	21	1035	215	7.8	52.5	206	35.9	16.7	3.16	0.043	0.058	7.92	17.6	418	28.8
TO-57	260393	9645956	1493	S	N of ANP	17	463	251	7.2	49.5	88.3	22.5	3.26	0.606	0.022	0.048	4.54	8.4	177	8.52
TP-59	254386	9641304	2543	S	N of Njeku	14	1368	204	8.6	42.2	268	70.4	1.01	0.351	0.047	0.058	28.5	31.8	438	74.7
TP-90	266246	9637514	1557	S		21	329	106	6.8	33.1	43.4	31.3	8.12	3.72	0.296	2.031	1.43	6.64	124	8.81
TO-78	263539	9644291	1513	S	Momella	22	1883	na	8.4	8.40	402	68.5	2.05	1.42	0.084	0.085	22.5	58.5	631	106
TP-08	266047	9644674	1475	L	Lekandiro	25	10260	78	9.3	bdl	2790	260	2.08	7.12	bdl	bdl	223	403	3124	745
TP-09	267428	9644748	1445	L	Tulusia	25	36500	58	9.7	bdl	11710	1430	9.32	8.13	bdl	bdl	1070	1570	11732	1442
TP-10	267614	9643205	1441	L	Big Momella	28	43600	35	9.8	52.2	14350	1830	9.60	9.31	0.023	0.202	1180	1611	13125	3186
TP-11	267497	9642695	1436	L	Rishateni	28	31100	32	9.8	bdl	9770	1360	7.70	3.58	bdl	bdl	900	1039	10250	505
TP-13	266218	9643915	1448	L	Small Momella	27	10010	116	9.5	16.5	2610	360	1.09	3.95	0.331	0.082	245	262	3008	678
TP-82	266260	9643924	1439	L	Small Momella	24	9460	110	9.3	2.40	2247	322	1.61	4.79	0.337	0.139	154	242	2851	624
TP-83	266053	9644671	1466	L	Lekandiro	23	8830	101	9.0	2.00	2165	198	3.26	5.62	1.240	0.125	129	317	2664	623
TP-84	267438	9644746	1441	L	Tulusia	24	24700	84	9.7	10.4	6805	857	7.66	4.6	0.014	0.150	436	924	6825	935

TP-86	267079	9642689	1443	L	Big Momella	20	6340	0	8.8	11.2	1569	163	10.9	2.91	0.573	0.708	103	184	2145	530
TP-87	267365	9642642	1438	L	Rishateni	22	23200	55	9.9	19.4	6097	863	5.12	2.18	0.095	0.130	391	685	6432	424
TP-17	258971	9640797	1890	SR	Miriakamba	20	1640	172	8.7	25.3	339	80.6	5.85	1.76	0.037	0.060	24.4	47.3	530	106
TP-12	265743	9643867	1454	SR	Lendoiya	34	4540	15	8.5		1090	190	3.32	2.1	bdl	bdl	71.9	126	1671	296
TO-03	242533	9637822	1971	SR	TFS area	16	447	250	7.5	44.6	87.6	22.3	5.25	0.898	0.017	0.048	7.90	4.77	173	8.73
TO-05	247796	9634262	1939	SR	TFS area	17	180	279	8.0	45.3	30.4	11	3.47	0.986	0.018	0.045	2.48	2.28	68.8	1.96
TP-19	253689	9643454	3168	SR	Jiwe la lami	12	151	245	6.3	36.0	18.9	10.8	6.32	1.32	0.030	0.046	0.248	2.63	54.4	3.48
TP-21	253064	9639554	2648	SR	Meru crater	12	277	266	8.0	33.5	55.5	7.50	3.25	0.997	0.040	0.057	12.1	1.45	92.3	8.14
TP-67	261075	9638095	1601	SR		20	240	148	7.7	51.0	38.0	14.0	5.69	1.08	0.088	0.242	1.01	5.82	93.8	1.7
TP-72	258108	9642451	1959	SR	Jiwe la lami	15	138	177	7.6	41.8	22.7	8.39	1.94	0.584	0.085	0.120	0.66	5.02	51.1	0.124
TP-81	265734	9643856	1444	SR	Lendoiya	25	5360	103	8.4	6.10	1211	191	6.41	2.33	0.362	0.919	57.9	132	1801	564
TP-14	260860	9642171	1601	SR	Ngarenayuki	18	2340	132	8.8	30.3	495	120	6.76	2.16	0.033	0.045	35.3	84.3	703	179
TP-15	260110	9642238	1639	SR	Tulusia	17	1427	137	8.6	23.8	281	75.7	3.71	0.896	0.027	0.042	39.4	31.0	431	80.8
TO-06	250479	9633228	1852	SR	Navaru	16	192	317	8.4	45.3	37.1	9.20	1.87	0.451	0.045	0.066	4.85	2.44	70	1.97
TP-23	259751	9643374	1670	SR	Nasula	18	390	278	8.0	38.4	77.3	20.5	1.53	0.245	0.038	0.070	11.7	5.91	136	7.90
TP-24	258679	9642399	1813	SR	Lenganassa	16	914	244	8.4	24.2	186	47.7	1.67	0.43	0.022	0.044	32.2	16.0	284	42.8
TP-25	259445	9642157	1762	SR	Tulusia	17	1423	223	8.2	23.1	291	74.3	3.59	0.882	0.023	0.047	39.2	31.1	443	81.0
TO-63	268094	9628261	1230	SR	Maji ya chai	22	295	222	7.0	26.3	44.8	16.9	12.8	2.99	0.358	1.142	1.75	6.37	115	1.30
TP-66	259561	9640440	1798	SR		16	1811	119	8.8	30.0	346	88.4	5.13	1.54	0.041	0.057	22.4	62.8	537	124
TP-68	261245	9637775	1602	SR		23	250	82	6.9	42.6	15.5	23.2	18.7	5.2	0.075	0.284	0.732	5.64	104	0.403
TP-92	264735	9634650	1403	SR	Maji ya Chai	19	727	35	8.2	33.8	145	29.0	5.82	1.17	0.209	0.799	11.06	16.3	263	17.8
TP-73	258680	9642408	1794	SR	Lenganassa	16	836	167	8.3	26.0	160	42.2	1.42	0.358	0.029	0.049	19.0	14.6	250	36.9
TP-74	259387	9642169	1755	SR	Tulusia	16	1365	118	8.7	24.7	261	70.7	3.39	0.795	0.032	0.049	28.2	29.3	430	76.4
TP-22	256174	9640662	2270	SR	Njeku	16	4500	209	9.6	32.1	1030	207	5.46	2.8	0.025	0.040	65.2	167	1430	358
TP-76	256769	9640523	2163	SR	Njeku-Maio	15	1675	136	8.9	31.6	404	103	5.64	1.69	0.035	0.048	26.8	72.7	625	155
TP-77	256759	9640579	2130	SR	Maio	16	4570	129	9.1	32.4	979	204	5.38	2.6	0.030	0.056	52.6	167	1414	356
TP-65	260860	9642171	1601	SR	Ngarenanyuki	16	1707	215	8.9	30.9	332	83.7	5.21	1.54	0.065	0.068	21.2	58.3	505	122
TO-26	265061	9633129	1390	G	Mbega lodge	25	275	238	7.6	45.9	52.6	13.0	2.86	0.675	0.032	0.059	4.39	5.56	102	5.22
TO-27	265025	9633064	1415	G	Mbega lodge	23	571	207	8.6	33.3	111	32.2	3.02	0.431	0.024	0.050	15.7	16.2	183	13.4

Continued

Table 2: Major element and stable isotopes composition of waters in the upper flanks of Mt. Meru volcano (Continued).

Sample	Type	NO_3	PO_4	δ^2H-H_2O	$\delta^{18}O$-H_2O	$\delta^{13}C$-CO_2
		ppm	ppm	‰	‰	‰
TP-18	S	0.23	0.88	-35.5	-6.73	-3.1
TP-58	S	0.02	0.96	-35.6	-6.83	-0.8
TO-55	S	16	0.54	-26.1	-5.20	-7.2
TP-79	S	0.04	0.29	-23.1	-4.62	-5.7
TP-80	S	0.444	0.88	-13.1	-3.17	-0.3
TP-88	S	1.48	0.92	-15.7	-3.48	na
TO-02	S	85.2	0.06	-21.9	-4.41	-16.1
TO-04	S	1.96	0.07	-23.8	-5.09	-16.6
TP-07	S	0.628	0.64	-22.5	-4.86	-12.3
TO-50	S	24.6	1.17	-27.8	-5.60	-7.9
TO-52	S	2.87	0.49	-28.3	-5.74	-5.0
TO-53	S	0.89	0.35	-28.2	-5.75	-7.6
TO-54	S	3.15	1.34	-28.5	-5.10	-7.0
TO-56	S	2.28	1.25	-28.6	-5.79	-3.0
TO-57	S	3.76	0.37	-26.3	-5.53	-8.7
TP-59	S	0.23	1.09	-27.4	-5.66	-4.5
TP-90	S	0.379	3.29	-10.5	-2.49	-3.0
TO-78	S	0.681	0.56	-26.3	-5.33	na
TP-08	L	0.19	bdl	28.0	5.23	na
TP-09	L	0.24	bdl	32.1	5.97	na
TP-10	L	0.31	15.3	37.0	6.39	na
TP-11	L	0.18	bdl	35.6	6.73	na
TP-13	L	0.06	1.23	29.6	5.20	na
TP-82	L	0.208	1.48	22.7	3.86	na
TP-83	L	2.6	2.62	15.9	2.85	na
TP-84	L	0.176	5.12	9.7	1.80	na

TP-86	L	3.32	10.2	2.2	0.13	na
TP-87	L	0.562	7.29	14.9	2.87	na
TP-17	SR	0.94	0.55	-25.3	-5.38	-4.2
TP-12	SR	0.21	bdl	-11.1	-2.25	-1.7
TO-03	SR	4.24	0.38	-35.3	-6.50	-15.0
TO-05	SR	1.03	0.14	-23.0	-5.03	-15.3
TP-19	SR	5.52	bdl	-15.1	-3.68	-17.1
TP-21	SR	0.025	0.7	-14.6	-3.62	-8.3
TP-67	SR	0.22	0.16	-16.4	-4.22	-15.1
TP-72	SR	bdl	0.04	-14.4	-3.79	-8.7
TP-81	SR	0.069	0.4	-17.7	-3.85	na
TP-14	SR	0.43	0.59	-30.0	-6.00	na
TP-15	SR	1.03	0.71	-26.1	-5.38	na
TO-06	SR	0.713	0.41	-30.1	-5.97	-9.7
TP-23	SR	0.625	0.86	-34.7	-6.81	-10.4
TP-24	SR	0.533	1.14	-24.7	-5.35	-6.2
TP-25	SR	0.932	0.73	-27.3	-5.70	-3.8
TO-63	SR	0.38	1.15	-15.3	-3.77	-8.3
TP-66	SR	0.81	0.57	-27.6	-5.71	-2.9
TP-68	SR	0.02	0.68	-8.4	-2.45	-0.1
TP-92	SR	0.467	0.58	-18.1	-4.28	-9.5
TP-73	SR	0.34	1.15	-25.6	-5.42	-4.5
TP-74	SR	1.36	0.78	-26.2	-5.52	-3.3
TP-22	SR	0.04	0.87	-35.1	-6.63	-1.7
TP-76	SR	0.186	0.58	-30.2	-6.01	-2.6
TP-77	SR	0.212	0.94	-33.8	-6.56	-1.5
TP-65	SR	0.85	0.55	-26.7	-5.57	-3.2
TO-26	G	2.19	0.2	-27.3	-5.67	-5.9
TO-27	G	0.931	0.62	-20.8	-4.83	-15.7

[a] S = springs, L = lakes, SR = streams and rivers, G = groundwater, na = not analyzed, bdl = below detection limit

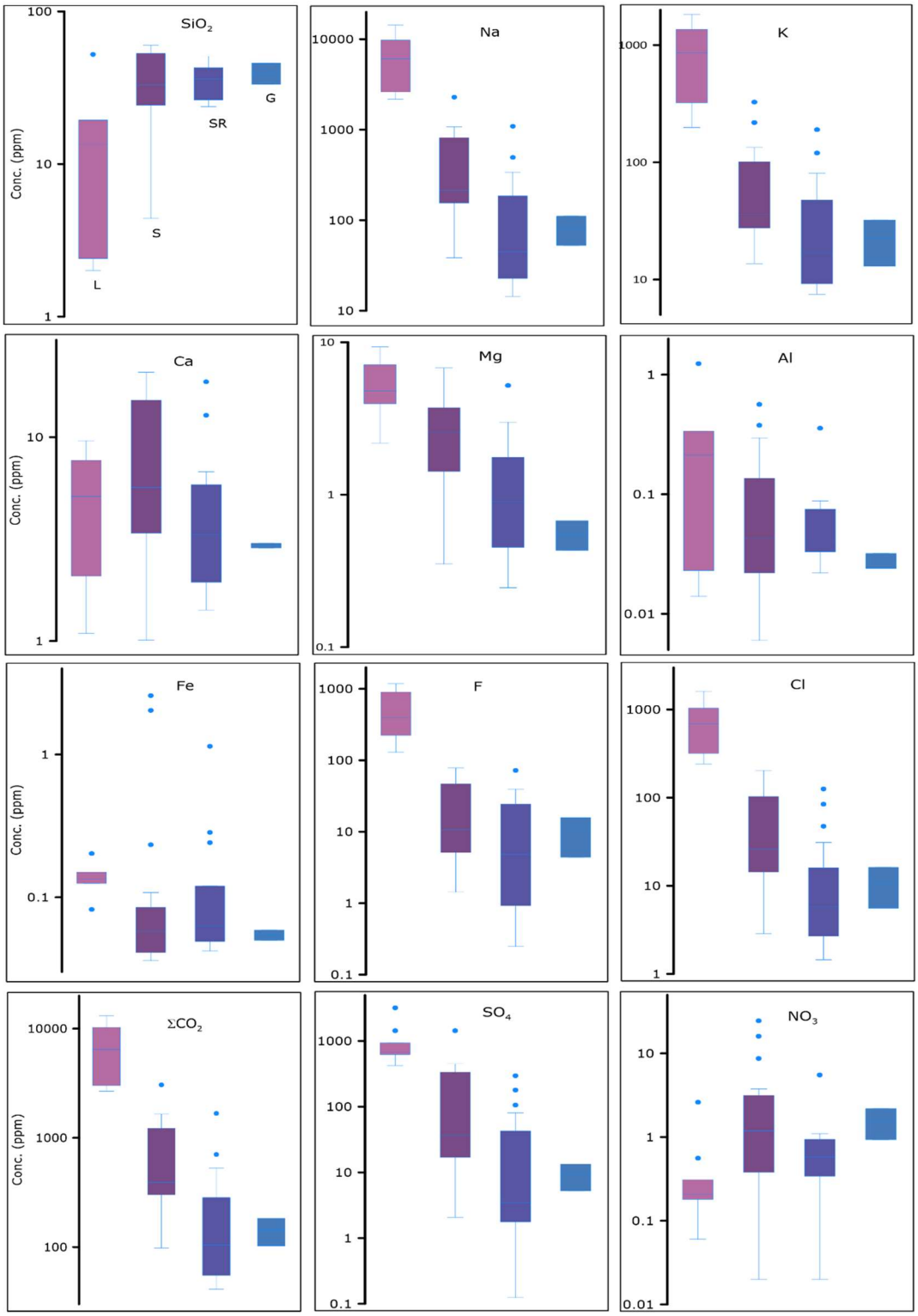

Figure 4-1: Box and whisker plot showing concentration ranges for the major constituents in different waters of the upper flanks of Mt. Meru volcano. The letter L represents lakes, S represents springs, SR represents streams and rivers, G represents groundwater. The Njekukumia springs have the highest concentrations among the springs and plot as outliers (except for NO_3).

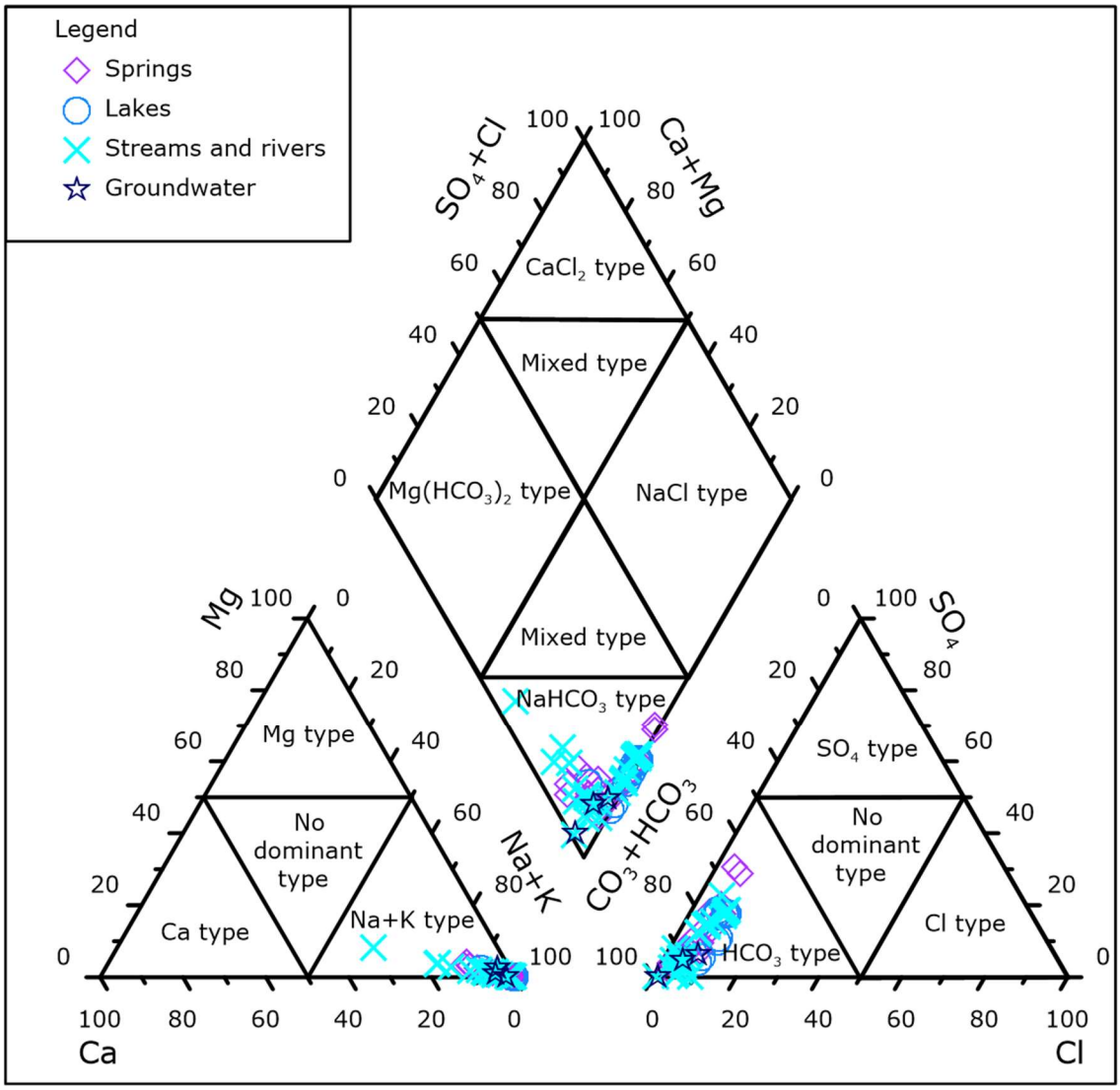

Figure 4-2: Piper plot showing the classification of springs-, lake-, ground-, stream- and river waters in the upper flanks of Mt. Meru volcano. The dominant anion in the area is ΣCO_2 while the dominant cation is Na. The composition of surface and groundwaters is therefore predominantly $NaHCO_3$.

4.2 Trace Element Composition

The concentration of trace metals in the studied waters is presented in Table 3.

The concentrations of trace alkali metals (Li, Rb, Cs) range between 0.005 ppb and 1179 ppb. Lithium concentrations are 0.4-105 ppb, Rb concentrations are 2-1179 ppb, and Cs concentrations are 0.005-0.725 ppb. The highest concentration of Li up to 94 ppb was detected in the springs. In the high pH saline-alkaline lakes, an elevated concentration of Li is observed reaching 64 ppb. The highest concentrations of Cs and Rb are 0.723 ppb and 1179 ppb, respectively, observed in the saline-alkaline lakes which have the highest pH

among other waters. Significantly high concentrations of Rb reaching 291 ppb are observed in spring waters as well.

The concentrations of trace alkaline earth metals (Be, Sr, Ba) are 0.008 ppb to 947 ppb. The concentrations of Be are 0.008-1.43 ppb, Sr concentrations are 25-947 ppb and Ba concentrations are 0.427-175 ppb. The highest concentration of Be, Sr and Ba (up to 1.43 ppb, 947 ppb and 175 ppb, respectively) are detected in springs while significantly high concentrations of Sr reaching up to 720 ppb are detected in the saline-alkaline lakes.

The concentration of As, Cr, Ni, Pb, Se, Sn, Tl, V, and Zn range between 0.002 ppb and 3506 ppb. The concentrations of As are 0.046-32.8 ppb, of Cr are 0.4-16.2 ppb, Ni concentrations are 3.35-32.6 ppb, Pb concentrations are 0.146-1.31 ppb, concentrations of Se are 0.15-2.95 ppb, Sn concentration of 0.014-0.4 ppb, Tl concentrations of 0.002-0.07 ppb, V concentrations are 0.678-562 ppb, and concentrations of Zn are 0.479-3506 ppb. The highest values of concentrations of As, Cr, Ni, Pb, Se, Sn, Tl, V, and Zn were measured in the spring waters. Among the springs, Njekukumia springs are characterized by the highest concentrations of trace elements which occur as outliers compared to other springs.

The concentrations of B, Cd, Ga, Ge, Hf, Hg, Ho, In, Mo, Nb, Sb, Sc, Ta, Tb, Te, Th, Ti, U, W, Y, Zr range between 0.001 ppb and 2044 ppb. The concentrations of B are 3.73-2044 ppb, Cd are 0.003-1.1 ppb, Ga are 0.008-19 ppb, Ge are 0.001-0.385 ppb, Hf are 0.001-2.23 ppb, Hg are 0.003-3.95 ppb, Ho are 0.001-0.1 ppb, In are 0.001-0.008 ppb, Mo are 0.21-1558 ppb, Nb are 0.019-3.54 ppb. The concentrations of Sb are 0.017-0.8 ppb, Sc are 0.096-5.3 ppb, Ta are 0.001-0.652 ppb, Tb are 0.001-0.1 ppb, Te are 0.034-5 ppb, Th are 0.001-1 ppb, Ti are 0.6-240 ppb, U are 0.011-598 ppb, W concentrations are 0.093-971 ppb, Y are 0.021-3.01 ppb, Zr are 0.06-802 ppb. These elements indicated highest concentrations in the saline-alkaline lakes.

The concentrations of Mn, Co, and Cu ranges between 0.04 ppb and 165 ppb. The concentration of Mn is 0.8-165 ppb, Co is 0.04-0.604 ppb, and Cu is 0.4-5.74 ppb. The elevated concentration of these metals was indicated in the rivers.

The rare earth elements (REEs) including La, Ce, Pr, Nd, Sm, Eu, Gd, Tb, Dy, Ho, Er, Tm, Yb, and Lu indicated concentrations between 0.001 and 6.5 ppb. The concentrations of these elements are mostly below 1 ppb and values reaching 1 ppb were detected in a few samples. High concentration of La reaching 3.48 ppb is detected in the rivers, while in the saline-alkaline lakes concentration reaching 2 ppb was detected. Cerium is the most abundant REE with concentration reaching 6.5 ppb in river waters and 4.7 ppb in saline-alkaline lakes. The highest concentration of Nd (2.4 ppb) is detected in the alkaline lake waters while highest concentration of 2.27 ppb is observed in river waters. The Maji ya Chai River (TO-63) which has been identified to have the highest concentration of La, Ce, and Nd also exhibits high concentration of Cu and the highest concentration of Fe among the studied waters. Other REEs exhibit concentration magnitudes below 1 ppb.

Table 3: Trace elements composition in the studied waters of the upper flanks of Mt. Meru volcano.

Sample	Type	As	B	Ba	Be	Bi	Cd	Ce	Co	Cr	Cs	Cu	Dy	Er	Eu	Fe	Ga	Gd	Ge	Hf	Hg	Ho
		ppb	ppb	ppb	ppb	ppb	ppm	ppb	ppb	ppb	ppb	ppb	ppb	ppb	ppb	ppb	ppb	ppb	ppb	ppb	ppb	ppb
TP-18	S	32.8	629	6.49	1.43	bdl	0.227	0.037	0.086	11.1	0.077	0.881	0.002	0.004	0.002	36	0.117	0.002	0.131	0.079	0.526	0.001
TP-58	S	23.9	376	6.3	0.71	bdl	0.24	0.03	0.09	8.6	0.05	1	bdl	bdl	bdl	69	0.11	bdl	bdl	0.06	bdl	bdl
TO-55	S	3.34	60	175	bdl	bdl	0.07	0.09	0.4	9.7	0.1	3.9	bdl	0.01	0.04	39	0.13	0.03	bdl	bdl	bdl	bdl
TP-79	S	0.17	117	0.9	bdl	bdl	0.07	0.08	0.04	0.4	bdl	0.6	bdl	bdl	bdl	70	0.84	bdl	bdl	0.06	bdl	bdl
TP-80	S	na	na	na	na	na	na	na	na	na	na	na	na	na	na	2584	na	na	na	na	na	na
TP-88	S	3.56	151	1.8	bdl	bdl	0.05	0.61	0.29	9.4	0.04	1.8	0.05	0.02	0.01	233	5.36	0.06	bdl	0.08	bdl	bdl
TO-02	S	0.24	9.6	5.1	0.102	bdl	0.003	0.046	0.07	7.4	0.139	0.944	0.006	0.003	0.002	48	0.021	0.007	0.011	bdl	0.012	0.001
TO-04	S	0.28	3.73	1.75	0.029	0.004	0.007	0.189	0.044	7.5	0.026	0.554	0.005	0.006	0.003	53	0.021	0.008	0.004	0.007	bdl	0.001
TP-07	S	3.48	29.9	0.498	0.038	bdl	0.013	0.087	0.052	7.6	0.265	0.448	0.004	0.007	bdl	45	1.9	bdl	0.008	0.004	0.092	0.001
TO-50	S	2.02	46	2.84	0.058	bdl	0.012	0.004	0.074	8.73	0.017	2.03	0.003	0.003	0.001	40	0.023	bdl	bdl	0.003	bdl	bdl
TO-52	S	1.83	13	6.01	0.022	bdl	0.015	0.301	0.081	8.44	0.044	0.76	0.013	0.007	0.006	108	0.135	0.018	bdl	0.014	bdl	0.001
TO-53	S	3.64	28	4.19	0.008	bdl	0.014	0.176	0.096	8.58	0.009	0.68	0.008	0.004	0.004	77	0.577	0.008	bdl	0.011	bdl	0.002
TO-54	S	1.9	25	3.68	0.035	bdl	0.013	0.007	0.073	8.05	0.119	0.83	0.001	0.002	0.001	38	0.008	bdl	bdl	bdl	bdl	bdl
TO-56	S	1.37	32	10.7	0.015	bdl	0.012	0.163	0.115	9.08	0.021	1.62	0.007	0.01	0.007	58	0.049	0.014	bdl	0.003	bdl	0.003
TO-57	S	1.56	16	1.79	0.157	bdl	0.009	0.088	0.069	7.97	0.031	1.71	0.006	0.006	0.003	48	0.032	0.005	bdl	bdl	bdl	0.002
TP-59	S	7	98	0.56	0.085	bdl	0.018	0.128	0.08	8.39	0.01	0.71	0.004	0.004	0.003	58	0.029	0.007	bdl	0.012	bdl	0.001
TP-90	S	bdl	bdl	bdl	bdl	bdl	bdl	bdl	bdl	bdl	bdl	bdl	bdl	bdl	bdl	2031	bdl	bdl	bdl	bdl	bdl	bdl
TO-78	S	0.401	111	0.9	bdl	bdl	0.1	0.11	0.16	16.2	0.05	3.2	0.03	0.01	bdl	85	1.37	bdl	bdl	bdl	bdl	bdl
TP-08	L	bdl	bdl	bdl	bdl	bdl	bdl	bdl	bdl	bdl	bdl	bdl	bdl	bdl	bdl	bdl	bdl	bdl	bdl	bdl	bdl	bdl
TP-09	L	bdl	bdl	bdl	bdl	bdl	bdl	bdl	bdl	bdl	bdl	bdl	bdl	bdl	bdl	bdl	bdl	bdl	bdl	bdl	bdl	bdl
TP-10	L	25.9	2044	22	0.101	0.004	1.1	3.45	0.31	8.7	0.725	0.525	0.073	0.149	0.01	202	10	0.08	0.385	2.23	3.95	0.031
TP-11	L	bdl	bdl	bdl	bdl	bdl	bdl	bdl	bdl	bdl	bdl	bdl	bdl	bdl	bdl	bdl	bdl	bdl	bdl	bdl	bdl	bdl
TP-13	L	3.9	480	5.53	0.038	bdl	0.161	0.314	0.196	9.6	0.152	0.759	0.049	0.063	0.013	82	5.95	0.042	0.029	0.352	0.822	0.013
TP-82	L	3.32	409	6.1	bdl	bdl	0.14	0.34	0.18	9.7	0.04	1	0.06	0.07	0.01	139	5.54	bdl	bdl	0.28	bdl	bdl
TP-83	L	5.69	440	6.4	0.07	bdl	0.12	0.94	0.39	9.8	0.19	2.6	0.15	0.11	0.04	125	5.87	0.1	bdl	0.68	bdl	0.02
TP-84	L	19.4	1657	27	bdl	bdl	0.8	4.7	0.5	12.3	bdl	5.3	0.9	0.5	0.2	150	19	0.6	bdl	0.8	bdl	0.1

TP-86	L	bdl	bdl	bdl	bdl	bdl	bdl	bdl	bdl	bdl	bdl	bdl	bdl	bdl	bdl	708	bdl	bdl	bdl	bdl	bdl	bdl
TP-87	L	10.5	1271	bdl	bdl	bdl	1	1	bdl	12.2	bdl	3.9	0.3	0.2	bdl	130	4.52	bdl	bdl	1.1	bdl	bdl
TP-17	SR	3.17	109	1.86	0.017	bdl	0.018	0.089	0.062	10.1	0.027	1.05	0.004	0.008	0.002	60	0.124	0.002	0.012	0.005	0.119	0.002
TP-12	SR	bdl	bdl	bdl	bdl	bdl	bdl	bdl	bdl	bdl	bdl	bdl	bdl	bdl	bdl	bdl	bdl	bdl	bdl	bdl	bdl	bdl
TO-03	SR	1.83	9.93	0.977	0.09	bdl	0.006	0.027	0.058	8.2	0.017	0.576	0.001	0.002	0.002	48	0.028	0.004	0.001	0.001	bdl	bdl
TO-05	SR	0.51	4.04	0.387	0.01	bdl	0.007	0.029	0.055	7.8	0.01	0.872	0.007	0.002	0.002	45	0.03	0.008	0.01	bdl	bdl	0.001
TP-19	SR	0.08	28.6	5.66	0.009	bdl	0.014	0.085	0.239	14.4	0.04	1.84	0.005	0.004	0.003	46	0.115	0.01	0.17	0.001	0.008	0.001
TP-21	SR	0.1	10.5	13.1	0.12	0.002	0.02	4.215	0.543	13.1	0.021	3.64	0.095	0.064	0.061	57	0.573	0.206	0.288	0.02	0.003	0.021
TP-67	SR	0.18	15	1.44	0.029	bdl	0.011	0.685	0.281	8.23	0.031	1.58	0.028	0.024	0.011	242	0.065	0.045	bdl	0.016	bdl	0.005
TP-72	SR	0.103	7	0.45	0.019	bdl	0.05	0.463	0.174	8.51	0.017	1.15	0.032	0.016	0.011	120	0.046	0.031	bdl	0.01	bdl	0.005
TP-81	SR	na	na	na	na	na	na	na	na	na	na	na	na	na	na	919	na	na	na	na	na	na
TP-14	SR	9.48	264	4.73	0.183	bdl	0.052	0.125	0.08	10.1	0.092	1.88	0.009	0.011	0.004	45	0.165	0.009	0.022	0.012	0.236	0.004
TP-15	SR	4.7	93.2	1.05	0.032	bdl	0.018	0.049	0.054	7.4	0.025	1.09	0.003	0.003	0.001	42	0.124	0.004	0.001	0.003	0.123	bdl
TO-06	SR	1.79	4.05	0.91	0.01	bdl	0.009	0.152	0.059	7.4	0.06	0.76	0.005	0.006	0.002	66	0.056	0.005	0.009	0.004	bdl	0.001
TP-23	SR	31.7	667	5.07	0.78	bdl	0.212	0.077	0.087	11.5	0.047	0.943	0.008	0.004	0.004	70	0.098	0.004	0.059	0.046	0.55	0.002
TP-24	SR	5.92	51.2	0.427	0.054	bdl	0.013	0.183	0.149	14.6	0.021	1.66	0.004	0.004	0.002	44	0.117	0.009	0.119	0.002	0.037	0.002
TP-25	SR	9.28	137	1.41	0.085	bdl	0.017	0.057	0.114	13.9	0.032	1.87	0.002	0.001	bdl	47	0.45	0.006	0.075	0.002	0.171	bdl
TO-63	SR	0.316	17	5.9	0.192	0.007	0.027	6.5	0.474	9.49	0.01	5.74	0.226	0.113	0.103	1142	0.487	0.382	bdl	0.067	bdl	0.04
TP-66	SR	5.52	138	4.5	0.09	bdl	0.04	0.16	0.09	9.4	0.07	1.5	0.03	0.01	bdl	57	0.08	bdl	bdl	bdl	bdl	bdl
TP-68	SR	0.161	28	10.3	0.025	bdl	0.033	0.565	0.604	9.67	0.017	4.6	0.022	0.017	0.014	284	0.039	0.04	bdl	0.011	bdl	0.005
TP-92	SR	2.28	26	1.06	0.065	bdl	0.014	1.17	0.318	9.05	0.11	3.7	0.034	0.027	0.016	799	1.1	0.055	bdl	0.03	bdl	0.007
TP-73	SR	5.79	60	0.65	0.04	bdl	0.006	0.114	0.078	8.32	0.016	1.74	0.007	0.004	0.003	49	0.256	0.004	bdl	0.005	bdl	0.002
TP-74	SR	4.93	98	1.27	0.037	bdl	0.016	0.122	0.073	8.36	0.019	1.39	0.009	0.007	0.003	49	0.19	0.005	bdl	0.008	bdl	0.002
TP-22	SR	3.18	18.9	0.299	0.048	0.002	0.01	0.087	0.168	15.5	0.011	1.25	0.006	0.002	0.001	40	0.075	0.009	0.179	0.007	0.009	0.001
TP-76	SR	8.34	177	4	0.19	bdl	0.07	0.11	0.1	8.4	0.04	1.3	bdl	0.03	bdl	48	0.09	bdl	bdl	bdl	bdl	bdl
TP-77	SR	23.5	374	4.9	0.41	bdl	0.27	0.08	0.07	8.2	0.05	1	0.01	bdl	bdl	56	0.12	bdl	bdl	0.07	bdl	bdl
TP-65	SR	5.64	128	3.8	0.12	bdl	0.04	0.27	0.1	8.7	0.04	1.9	0.02	bdl	bdl	68	0.18	0.02	bdl	0.03	bdl	bdl
TO-26	G	7.29	212	1.54	0.075	bdl	0.021	0.068	0.118	14.4	0.025	1.9	0.001	0.005	0.001	59	0.275	0.005	0.032	0.004	0.211	bdl
TO-27	G	2.84	84.1	1.31	0.018	0.002	0.02	0.1	0.124	13.5	0.036	4.44	0.002	0.005	0.001	50	1.16	0.008	0.141	0.006	0.129	bdl

Continued

Table 3: Trace elements composition in the studied waters of the upper flanks of Mt. Meru volcano (Continued).

Sample	Type	In	La	Li	Lu	Mn	Mo	Nb	Nd	Ni	Pb	Pr	Rb	Sb	Sc	Se	Sm	Sn	Sr	Ta	Tb
		ppb	ppb	ppb	ppb	ppb	ppb	ppb	ppb	ppb	ppb	ppb	ppb	ppb	ppb	ppb	ppb	ppb	ppb	ppb	ppb
TP-18	S	0.004	0.012	94	0.001	3.69	68	2.019	0.005	18.1	0.203	0.003	291	0.33	1.64	2.95	0.003	0.062	695	0.023	0.001
TP-58	S	bdl	0.01	54.1	bdl	1.3	288	1.5	bdl	4.4	0.3	bdl	220	0.24	1.6	bdl	bdl	0.2	775	0.04	bdl
TO-55	S	bdl	0.074	4.5	bdl	6	369	0.53	0.07	4.6	0.9	0.01	105	0.12	0.2	bdl	bdl	0.4	907	0.02	bdl
TP-79	S	bdl	0.054	5.1	bdl	0.8	195	0.21	0.03	bdl	bdl	bdl	90	bdl	0.2	bdl	bdl	bdl	240	0.02	bdl
TP-80	S	bdl	bdl	bdl	bdl	bdl	bdl	bdl	bdl	bdl	bdl	bdl	bdl	bdl	bdl	bdl	bdl	bdl	1100	bdl	na
TP-88	S	bdl	0.428	3.9	bdl	19.5	209	0.78	0.16	4.7	0.4	0.08	73	0.09	0.49	bdl	0.03	bdl	295	0.04	bdl
TO-02	S	bdl	0.039	0.99	0.001	9.41	1.21	0.074	0.027	3.9	0.194	0.006	48.4	0.062	0.377	0.98	0.007	0.024	253	0.001	0.001
TO-04	S	bdl	0.084	1.34	bdl	1.27	0.52	0.142	0.035	3.82	0.186	0.013	18.2	0.036	0.214	0.16	0.004	0.024	83	0.002	0.001
TP-07	S	bdl	0.019	0.41	0.001	1.03	7.92	0.094	0.014	3.52	0.165	0.002	36.4	0.158	0.153	0.3	0.004	0.014	91	0.08	bdl
TO-50	S	bdl	0.01	1.9	0.001	1.2	36.3	0.077	0.005	4.1	0.21	0.001	69.8	0.107	0.57	bdl	bdl	0.07	520	0.008	bdl
TO-52	S	bdl	0.211	0.4	bdl	2.07	13.3	0.242	0.092	3.9	0.23	0.035	42	0.095	0.53	bdl	0.038	0.07	308	0.01	0.003
TO-53	S	bdl	0.121	2.8	0.001	1.97	37.4	0.079	0.08	4.1	0.22	0.018	28	0.213	0.3	bdl	0.013	0.06	167	0.014	bdl
TO-54	S	bdl	0.005	2.7	bdl	10.1	26.1	0.068	0.004	3.9	0.2	bdl	49	0.081	0.42	bdl	bdl	0.07	269	0.003	bdl
TO-56	S	bdl	0.174	0.4	0.002	13.4	20	0.124	0.093	4.5	0.23	0.027	46.5	0.056	0.6	bdl	0.017	0.11	470	0.005	0.002
TO-57	S	bdl	0.07	12.8	bdl	1.35	11	0.107	0.037	3.7	0.19	0.014	22.3	0.149	0.4	bdl	0.004	0.06	106	0.002	0.001
TP-59	S	bdl	0.063	21.4	bdl	1.5	85	0.142	0.036	4.1	0.21	0.015	57.6	0.1	0.37	bdl	0.007	0.06	90	0.023	bdl
TP-90	S	bdl	bdl	bdl	bdl	bdl	bdl	bdl	bdl	bdl	bdl	bdl	bdl	bdl	bdl	bdl	bdl	bdl	207	bdl	bdl
TO-78	S	bdl	0.067	5.5	bdl	4.3	102	0.21	0.06	8.1	0.5	bdl	53	0.06	bdl	bdl	bdl	0.2	101	bdl	bdl
TP-08	L	bdl	bdl	bdl	bdl	bdl	bdl	bdl	bdl	bdl	bdl	bdl	bdl	bdl	bdl	bdl	bdl	bdl		bdl	bdl
TP-09	L	bdl	bdl	bdl	bdl	bdl	bdl	bdl	bdl	bdl	bdl	bdl	bdl	bdl	bdl	bdl	bdl	bdl		bdl	bdl
TP-10	L	0.008	0.083	26.9	0.052	58.4	410	3.54	0.081	3.35	0.208	0.011	1179	0.548	5.3	1.9	0.025	0.14	637	0.652	0.007
TP-11	L	bdl	bdl	bdl	bdl	bdl	bdl	bdl	bdl	bdl	bdl	bdl	bdl	bdl	bdl	bdl	bdl	bdl		bdl	bdl
TP-13	L	bdl	0.114	18	0.011	8.97	81	0.305	0.142	4.21	0.206	0.029	269	0.124	0.642	0.15	0.028	0.036	87	0.197	0.006
TP-82	L	bdl	0.143	10	0.03	9.8	378	0.29	0.12	4.4	0.4	0.03	236	0.08	1.2	bdl	bdl	0.3	108	0.09	bdl
TP-83	L	bdl	0.724	5	0.01	21.7	362	1.27	0.78	4.3	0.3	0.19	169	0.2	0.6	bdl	0.1	0.2	156	0.06	0.02
TP-84	L	bdl	2	15	bdl	76	1558	2.1	2.4	bdl	bdl	0.7	603	bdl	4.5	bdl	0.9	bdl	796	0.2	0.1

TP-86	L	bdl	bdl	bdl	bdl	bdl	bdl	bdl	bdl	bdl	bdl	bdl	bdl	bdl	bdl	bdl	bdl	bdl	523	bdl	bdl
TP-87	L	bdl	0.3	64	bdl	bdl	1028	1.5	bdl	bdl	bdl	bdl	674	0.8	2.7	bdl	bdl	bdl	586	0.1	bdl
TP-17	SR	bdl	0.049	14.8	0.001	2.1	22	0.161	0.028	4.61	0.216	0.009	49.3	0.09	0.21	0.43	0.003	0.031	206	0.016	0.001
TP-12	SR	bdl	bdl	bdl	bdl	bdl	bdl	bdl	bdl	bdl	bdl	bdl	bdl	bdl	bdl	bdl	bdl	bdl	0	bdl	bdl
TO-03	SR	bdl	0.023	5.13	bdl	1.35	3.03	0.076	0.005	4.04	0.184	0.004	17.3	0.149	0.194	0.35	0.002	0.038	151	0.013	bdl
TO-05	SR	bdl	0.07	1.07	0.001	1.28	0.54	0.032	0.034	3.96	0.167	0.009	9.8	0.037	0.082	0.11	bdl	0.062	112	0.001	0.001
TP-19	SR	bdl	0.086	5.76	bdl	9.01	0.75	0.065	0.066	32.6	0.265	0.011	17.3	0.022	0.271	0.17	0.01	0.037	313	0.001	0.001
TP-21	SR	bdl	2.26	3	0.007	36.1	0.21	1.467	1.49	8.71	1.31	0.383	2	0.068	0.096	0.16	0.205	0.083	31	0.003	0.024
TP-67	SR	bdl	0.29	0.8	0.002	42.1	1.91	0.271	0.187	4.1	0.27	0.051	16.6	0.03	0.48	bdl	0.036	0.06	150	0.008	0.004
TP-72	SR	bdl	0.352	0.6	0.001	9.66	1.12	0.094	0.199	4.3	0.21	0.066	8.83	0.023	0.36	bdl	0.038	0.05	55	0.003	0.005
TP-81	SR	na	na	na	na	na	na	na	na	na	na	na	na	na	na	na	na	na	420	na	na
TP-14	SR	bdl	0.072	59.1	0.002	2.4	40.9	0.412	0.072	5.01	0.195	0.02	117	0.191	0.449	1.14	0.002	0.033	420	0.034	0.001
TP-15	SR	bdl	0.039	18.3	bdl	1.29	16.6	0.101	0.022	3.57	0.146	0.007	51.1	0.124	0.184	0.46	0.009	0.037	180	0.022	0.001
TO-06	SR	bdl	0.148	1.34	bdl	1.57	0.64	0.106	0.07	3.68	0.202	0.027	12.2	0.154	0.275	0.06	0.007	0.007	29	0.008	0.003
TP-23	SR	0.002	0.037	105	0.001	2.69	68.8	1.595	0.028	5.42	0.224	0.007	286	0.362	1.49	2.94	bdl	0.033	51	0.027	bdl
TP-24	SR	bdl	0.105	16.2	bdl	4.18	4.23	0.128	0.072	10.2	0.298	0.014	25.5	0.26	0.437	0.37	0.015	0.058	83	0.008	0.001
TP-25	SR	0.001	0.041	37.8	bdl	2.98	15.8	0.13	0.014	7.11	0.263	0.005	52.6	0.204	0.254	0.63	0.007	0.039	185	0.011	0.001
TO-63	SR	bdl	3.48	0.6	0.013	19.7	3.92	1.21	2.27	5	0.38	0.59	13.7	0.05	0.29	bdl	0.339	0.06	259	0.024	0.043
TP-66	SR	bdl	0.086	22.6	bdl	2.2	119	0.29	0.05	4.2	0.2	0.02	67	0.2	0.3	bdl	0.03	0.2	351	0.01	bdl
TP-68	SR	bdl	0.251	0.5	0.002	165	2.01	0.133	0.192	4.9	0.26	0.051	30.8	0.037	0.4	bdl	0.033	0.06	472	0.003	0.005
TP-92	SR	bdl	0.527	1.9	0.004	23	23.3	0.586	0.326	4.7	0.26	0.094	31.8	0.1	0.21	bdl	0.05	0.06	149	0.017	0.008
TP-73	SR	bdl	0.076	14.3	bdl	1.48	50	0.112	0.043	4	0.2	0.015	32.4	0.246	0.33	bdl	0.011	0.06	73	0.016	0.001
TP-74	SR	bdl	0.072	19.6	0.001	1.89	87.2	0.144	0.055	4.1	0.2	0.012	53.7	0.134	0.23	bdl	0.008	0.07	178	0.014	0.001
TP-22	SR	0.001	0.054	13	0.001	5.99	3.73	0.059	0.021	9.12	0.326	0.007	6.3	0.13	0.359	0.27	0.006	0.074	686	0.008	bdl
TP-76	SR	bdl	0.091	27	bdl	1.6	141	0.47	0.09	4.4	0.3	0.02	85	0.13	0.6	bdl	bdl	bdl	432	0.01	bdl
TP-77	SR	bdl	0.018	53	bdl	1.7	280	1.15	0.07	4.5	0.3	bdl	212	0.28	1.3	bdl	bdl	bdl	746	0.01	bdl
TP-65	SR	bdl	0.139	21.6	bdl	2.3	113	0.34	0.07	4.3	0.3	0.03	64	0.07	0.4	bdl	0.03	bdl	332	0.01	bdl
TO-26	G	0.002	0.048	49.7	0.001	2.94	24.6	0.132	0.026	6.94	0.281	0.008	78.3	0.17	0.192	0.62	0.006	0.047	22	0.015	bdl
TO-27	G	0.001	0.064	15.5	0.001	2.36	8.11	0.112	0.045	6.98	0.888	0.01	35.8	0.073	0.236	0.24	0.001	0.066	88	0.006	0.001

Continued

Table 3: Trace elements composition in the studied waters of the upper flanks of Mt. Meru volcano (Continued).

Sample	Type	Te	Th	Ti	Tl	Tm	U	V	W	Y	Yb	Zn	Zr
		ppb	ppm	ppb	ppb	ppb	ppb	ppb	ppb	ppb	ppb	ppb	ppb
TP-18	S	0.034	0.003	7.18	bdl	0.001	31.7	562	126	0.042	0.006	0.891	180
TP-58	S	bdl	bdl	7.1	bdl	bdl	29.2	401	112	0.03	0.01	bdl	142
TO-55	S	0.3	bdl	5.1	0.07	d	57	37.4	12.6	0.18	bdl	3506	3.23
TP-79	S	bdl	bdl	2.9	bdl	d	8.71	0.99	28.9	0.07	bdl	bdl	17.9
TP-80	S	na	na	na	na	na	na	na	na	na	na	na	na
TP-88	S	bdl	0.06	23	bdl	bdl	26.7	4.07	71.6	0.27	0.03	bdl	12.8
TO-02	S	bdl	0.003	0.8	bdl	0.001	3.85	6.08	0.153	0.05	0.006	1.15	0.078
TO-04	S	bdl	0.031	2.43	bdl	bdl	1.09	3.21	0.308	0.04	0.006	0.55	0.355
TP-07	S	0.017	0.011	1.51	bdl	0.001	9.6	17.2	24.6	0.062	0.008	0.479	0.309
TO-50	S	0.02	bdl	0.6	0.008	bdl	15.9	25.2	4.33	0.037	0.005	1.5	0.06
TO-52	S	0.03	0.046	7.41	0.015	0.002	6.36	30.9	2.73	0.062	0.003	1.4	1
TO-53	S	bdl	0.021	4.63	0.006	bdl	12.1	41.1	11.8	0.061	0.006	1.2	0.445
TO-54	S	0.03	bdl	0.69	0.006	bdl	6.51	19.7	4.36	0.021	bdl	1.2	0.116
TO-56	S	bdl	0.018	1.86	0.017	bdl	7.55	24.9	1.85	0.105	0.007	1.5	0.349
TO-57	S	bdl	0.011	1.87	0.004	bdl	3.34	11.7	3.06	0.07	0.004	1.3	0.131
TP-59	S	bdl	0.012	2.89	bdl	bdl	1.65	35	38.7	0.05	0.004	1	1.41
TP-90	S	bdl	bdl	bdl	bdl	bdl	na	bdl	bdl	bdl	bdl	bdl	bdl
TO-78	S	0.3	bdl	3.8	0.04	bdl	3.23	3.68	24.7	0.06	bdl	bdl	3.12
TP-08	L	bdl	bdl	bdl	bdl	bdl	bdl	bdl	bdl	bdl	bdl	bdl	bdl
TP-09	L	bdl	bdl	bdl	bdl	bdl	bdl	bdl	bdl	bdl	bdl	bdl	bdl
TP-10	L	0.208	0.399	240	bdl	0.037	363	24.9	971	0.44	0.269	0.98	802
TP-11	L	bdl	bdl	bdl	bdl	bdl	bdl	bdl	bdl	bdl	bdl	bdl	bdl
TP-13	L	0.035	0.046	11.8	bdl	0.011	47	3.8	210	0.555	0.053	0.839	81.6
TP-82	L	bdl	0.06	15	bdl	0.01	47.3	2.67	202	0.56	0.06	bdl	77.6
TP-83	L	0.2	0.2	23	bdl	0.02	67.8	5.09	233	1.14	0.09	bdl	72.1
TP-84	L	5	0.6	127	bdl	bdl	598	26.9	956	3.01	0.6	bdl	285

TP-86	L	bdl	bdl	bdl	bdl	bdl	bdl	bdl	bdl	bdl	bdl	bdl	bdl
TP-87	L	bdl	1	130	bdl	bdl	228	15.5	770	2.61	0.3	bdl	575
TP-17	SR	bdl	0.009	1.9	bdl	0.001	6.39	23.9	25.8	0.051	0.006	1.01	1.26
TP-12	SR	bdl	bdl	bdl	bdl	bdl	bdl	bdl	bdl	bdl	bdl	bdl	bdl
TO-03	SR	bdl	0.005	0.86	bdl	bdl	2.08	12	3.05	0.033	0.003	0.535	0.087
TO-05	SR	bdl	0.006	1.02	bdl	0.001	0.188	3.96	0.778	0.032	0.003	0.438	0.062
TP-19	SR	bdl	0.001	1.28	bdl	0.001	0.019	0.977	0.334	0.044	0.005	1.91	0.148
TP-21	SR	bdl	0.036	62.2	0.002	0.007	0.058	1.59	0.222	0.577	0.051	153	1.15
TP-67	SR	bdl	0.043	7.25	0.006	0.002	0.071	2.39	0.44	0.172	0.017	1.8	0.871
TP-72	SR	0.02	0.026	3.75	0.006	0.002	0.044	2.1	0.093	0.155	0.014	1.4	0.633
TP-81	SR	na	na	na	na	na	na	na	na	na	na	na	na
TP-14	SR	bdl	0.009	2.9	bdl	0.002	10.2	178	57.6	0.138	0.007	0.764	30.9
TP-15	SR	bdl	0.005	1.03	bdl	bdl	5.46	34.4	36.4	0.043	0.007	0.839	0.581
TO-06	SR	bdl	0.029	2.96	bdl	0.001	0.282	7.51	2.11	0.038	0.006	0.742	0.376
TP-23	SR	0.034	0.011	8.67	bdl	0.001	30.8	537	125	0.071	0.009	1.4	160
TP-24	SR	bdl	0.015	2.17	bdl	0.001	1.37	32.5	9.58	0.053	0.007	1.48	0.356
TP-25	SR	bdl	0.013	1.3	bdl	bdl	4.22	51.1	40.4	0.028	0.004	1.33	0.444
TO-63	SR	0.03	0.127	32	0.014	0.02	0.923	8.57	0.917	1.35	0.114	3.5	4.68
TP-66	SR	0.2	bdl	3.1	bdl	bdl	6.64	104	35.8	0.14	0.02	bdl	18.8
TP-68	SR	0.02	0.038	4.57	0.003	0.002	0.051	1.37	0.113	0.163	0.012	4.3	0.99
TP-92	SR	bdl	0.074	18.8	0.005	0.004	4.43	12.3	14.3	0.276	0.023	2	2.23
TP-73	SR	0.02	0.025	1.76	bdl	bdl	2.73	32.1	27.6	0.059	0.002	1.3	0.443
TP-74	SR	0.03	0.015	1.98	0.003	0.001	5.54	35.3	39.1	0.071	0.005	1.4	0.725
TP-22	SR	bdl	0.029	3.13	bdl	bdl	0.247	10.5	2.2	0.029	0.004	1.86	0.351
TP-76	SR	bdl	bdl	1.9	bdl	bdl	8.17	155	49.2	0.09	0.01	bdl	29.8
TP-77	SR	0.3	bdl	6.4	bdl	bdl	26.2	366	106	0.05	bdl	bdl	123
TP-65	SR	0.4	bdl	3.9	0.04	bdl	6.16	93.6	33.5	0.17	0.03	bdl	15.4
TO-26	G	bdl	0.006	2.2	bdl	0.001	7.32	56.5	51.3	0.052	0.004	1.34	0.857
TO-27	G	bdl	0.017	3.23	bdl	bdl	1.67	12.1	30.8	0.04	0.005	18.9	0.234

5 Discussion

5.1 Water Sources

The majority of waters at Mt. Meru follow closely the water isotope ratio (δ^2H and $\delta^{18}O$) of the global meteoric water line (GMWL) and display similar values as the local precipitation, indicating a local meteoric water source of the surface and groundwaters (Figure 5- 1).

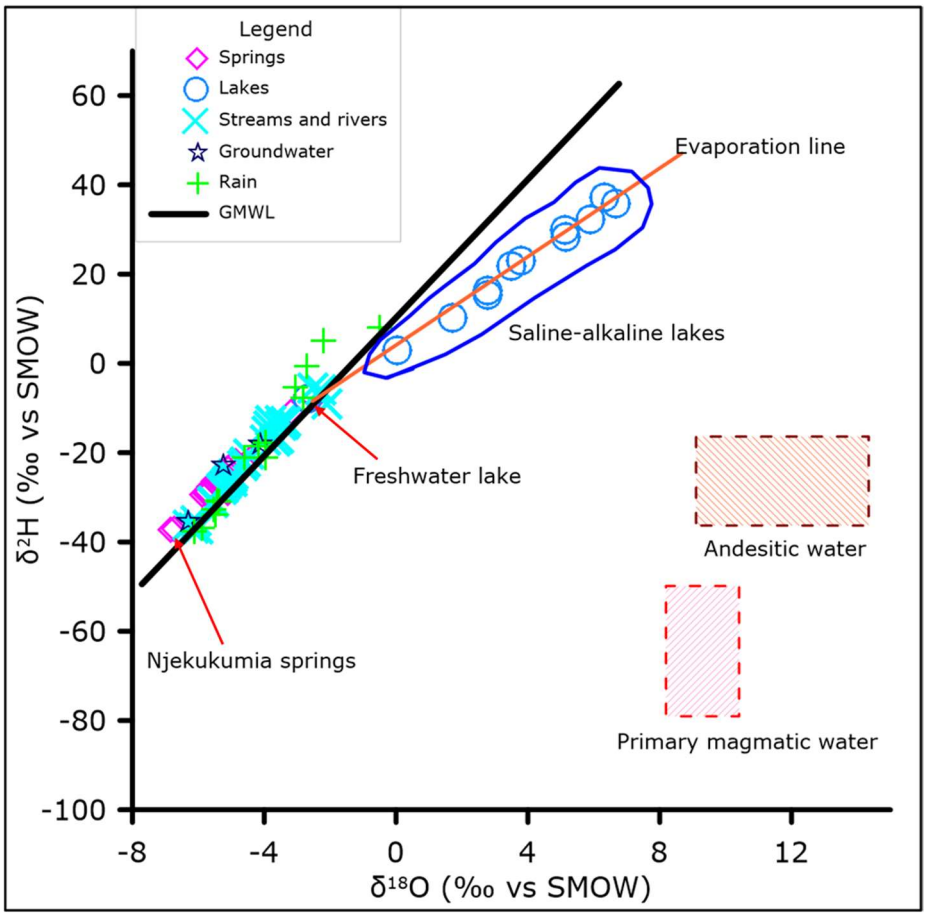

Figure 5- 1: Correlation plot of $\delta^{18}O$-H_2O vs δ^2H-H_2O in per mil against standard mean ocean water (SMOW) for the rain-, spring-, stream-, river-, lake-, and groundwaters in Meru. The GMWL is defined by the modern day global meteoric water line equation $\delta^2H = 8\delta^{18}O + 10$ (Craig, 1961). This plot suggests that the surface and groundwaters in Meru are of meteoric water origin. End-member composition for andesitic and primary magmatic water are taken from Benavente et al. (2016) and Giggenbach (1992).

The streams, rivers, and freshwater lake plot along the GMWL trend whereas groundwaters are slightly shifted to lower $\delta^{18}O$ values similar to the local precipitation. The saline-alkaline

lakes waters display higher δ^2H and $\delta^{18}O$ ratios compared to other water samples in the area. The lake samples follow a line with a slope of 4.91 corresponding to an enrichment resulting from free evaporation in the closed basin (Craig, 1961; Sharp, 2017).

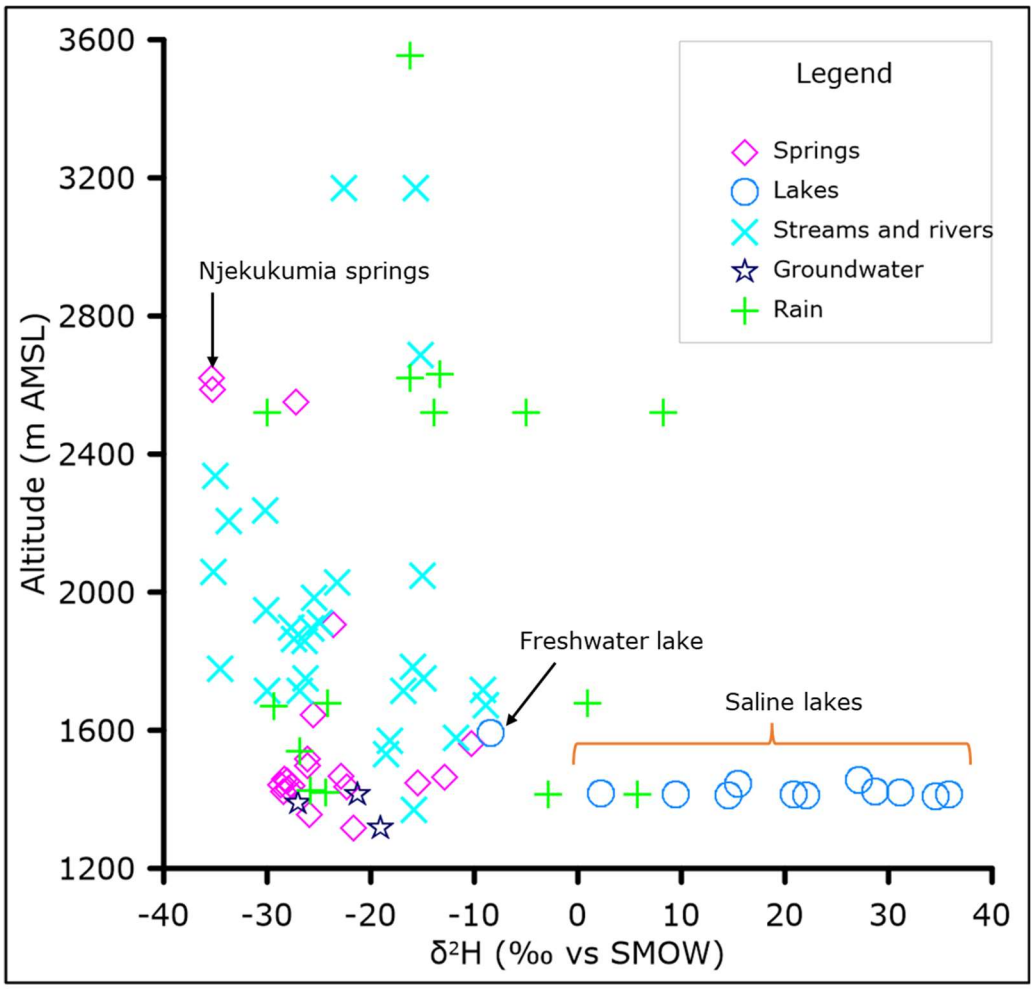

Figure 5- 2: Correlation plot of altitude and δ^2H-H_2O for different waters in the upper flank of Mt. Meru volcano. This plot suggests that variability of δ^2H-H_2O at Mt. Meru is due to altitude effect and evaporation.

Moreover, the water samples show distinguished decrease in δ^2H with increasing altitude consistent with fractionation processes as a function of pressure and temperature (Sharp, 2017; White, 2020). Some rainwater samples indicate enrichment in δ^2H compared to springs, streams and rivers in the similar altitude suggesting they were evaporated prior to analysis (Figure 5- 2).

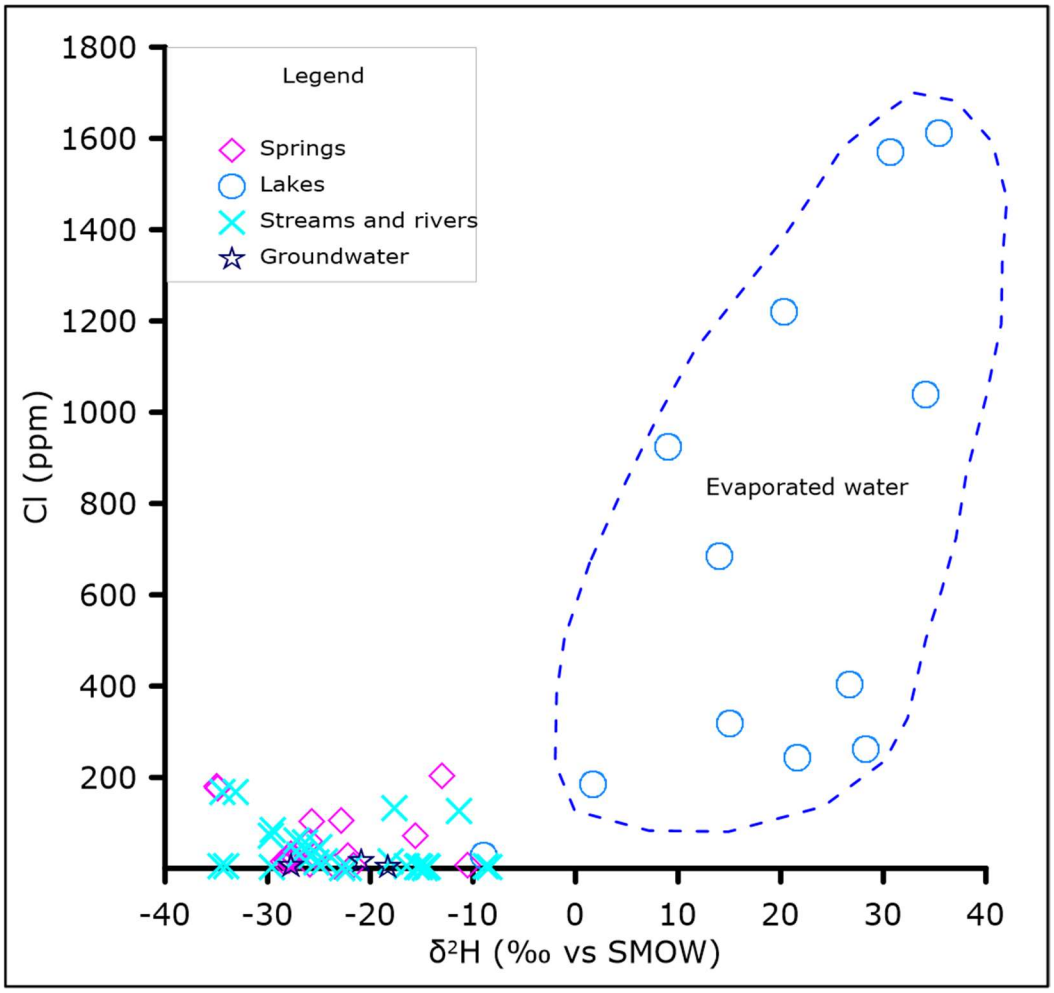

Figure 5- 3: Correlation plot of chloride and δ^2H-H_2O for the surface and groundwaters in the upper flanks of Mt. Meru volcano.

The shift in water isotopes in the saline-alkaline lakes of Mt. Meru is consistent with high concentration of dissolved constituents in these lakes. Similar enrichment has been observed in the Olkaria Domes and Olkaria East high temperature geothermal reservoir fluid and in the Nakuru and Elementaita rift lakes in Kenya (Mutonga, 2015). The chloride vs δ^2H-H_2O plot suggest that most waters at Mt. Meru show low Cl concentrations and the δ^2H isotope ratios are controlled by precipitation altitude. The saline-alkaline lake waters are enriched in all major elements with somewhat irregular δ^2H isotope ratios presumably caused by open system evaporation and condensation processes (Figure 5- 3). No obvious signs of thermal water inputs are observed, for example decreasing Mg content and increasing SiO_2 concentration with δ^2H water ratios of the saline-alkaline lake waters.

5.2 Relative Mobility of Elements

The relative mobility (RM) of a particular element can be used to gain insight into its behavior upon water-rock interaction. Assuming Na (i.e., the reference element) to be mobile, lower RM suggests uptake of the element into secondary minerals. Almost all elements show lower mobility compared to Na (Figure 5-4).

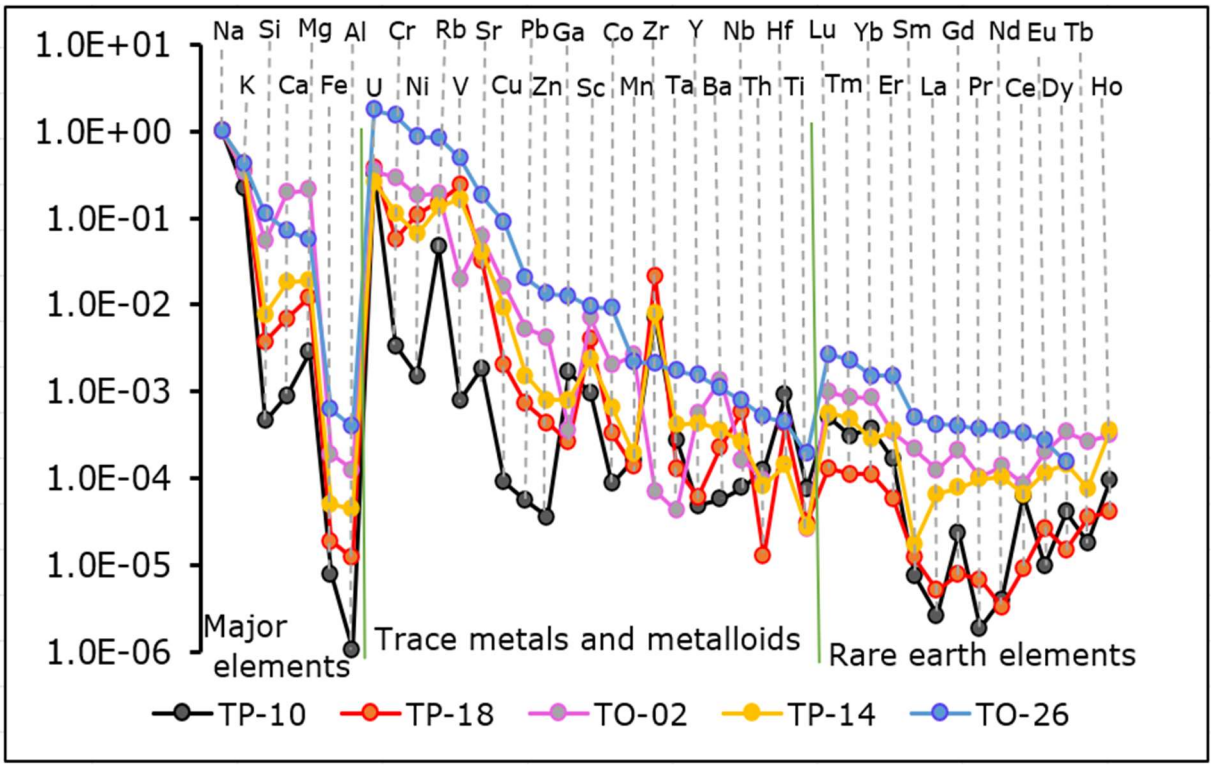

Figure 5- 4: Relative mobility of major-, trace-, and rare earth elements in different water types in the Mt. Meru volcano area. TP-18 is the Njekukumia spring, TP-02 is a dilute cold spring. TP-14 is Ngarenayuki river, TP-10 is the saline-alkaline Big Momella lake, and TO-26 is groundwater.

Among major elements, Na and K are the most mobile whereas Al and Fe are the least mobile. Other major elements (Si, Ca, and Mg) also show reduced mobility relative to Na suggesting that majority of these elements are retained within alteration minerals upon water-rock interaction. The low mobility of Al and Fe suggest they are completely retained into alteration and weathering minerals like aluminium silicates and/or oxides and hydroxides.

Trace elements show similar span in RM values as major elements. In all waters, U, Cr, Ni, Rb, V, Sr and Cu show the highest mobility while Th and Ti are the least mobile among trace elements. The elements with high mobility are probably controlled by dissolution of primary rocks while elements with low mobility are likely incorporated in the secondary minerals. The relatively high aqueous mobility of some trace elements is consistent with the aqueous speciation distribution predominated by simple ions (Rb^{+}, Sr^{+2}, and Ni^{+2}) or formation of highly soluble oxyanion complexes in water (U). In other cases, the RM of some elements is unknown due to lack of data on trace element composition of rocks in the study area.

The Rare Earth Elements (REE) have similar chemical properties and generally display low solubilities, however they can be mobilized and fractionated during surface alteration of rocks (Wayne Nesbitt, 1979). The REE generally show low relative mobility in the surface and groundwaters (Figure 5- 4) suggesting they are mostly retained in the host rocks and

incorporated into alteration and weathering minerals. This behaviour was also observed in the weathering profile by Middelburg et al. (1988). The aqueous mobility of the REE gradually increases with increasing atomic number thus the heavy rare earth elements (HREE) are slightly mobile compared to the light rare earth elements (LREE) suggesting increasing solubility. The increase in solubility with increasing atomic number is consistent with preferential leaching of HREE from host rocks compared to LREE (Wayne Nesbitt 1979) while LREE are preferentially enriched in the rock residue (Braun et al., 1993).

The variability in the magnitude and pattern of RM in different waters can be attributed to different and complex processes such as incongruent dissolution of these elements from the host rocks, redox processes, uptake by secondary minerals, ion exchange between minerals, and transport reactions (Aiuppa et al., 2005, 2006; Middelburg et al., 1988). It may also indicate that these waters interact with different rocks, not only nephelinites as assumed in this study but also other rock types for example phonolites, tephriphonolite, phonotephrite which were also identified at Mt. Meru (Roberts, 2002).

5.3 Aqueous Speciation and Mineral Saturation Indices

The geochemical behavior of elements including reactivity and precipitation into alteration and weathering minerals largely depends on their aqueous speciation. The speciation calculation indicates ligands in the studied waters are Cl as Cl^-, CO_2 as HCO_3^- and CO_3^{2-}, F as F^-, Br as Br^-, N as NO_3^-, and S as SO_4^{2-}. Following the results of aqueous speciation in the studied waters, elements were categorized as follows.

Category 1 for elements occurring as simple ions only. This includes Cs^+, Ga^{3+}, Hg^{2+}, In^{3+}, K^+, Li^+, Na^+, Ni^{2+}, Rb^+, Sc^{3+}, Sr^{2+}, and Tl^+ which occur in unpaired elemental states. This behavior can be related to low polarizability of these elements in the solution hence they are more attracted to water than other ligands (Aiuppa et al., 2000).

Category 2 for elements occurring as simple ions and forming complexes. The speciation of these elements is dominated by unpaired ions but also form several complexes. These include Ba, Be, Ca, Cd, Co, Fe, Mg, Mn, and Zn. Speciation of Sr is dominated by Sr^{2+} (90.5 %) and complexing with carbonate forming $SrCO_3$ in the saline-alkaline lakes (9.5 %). Ba is dominated by Ba^{2+} (95 %) while complexing with carbonate forming $BaCO_3$ in the saline alkaline lakes account for 5 %. Be is dominated by Be^{2+} (72 %) while oxy- compound BeO_2^{2-} accounts for 18 %. Ca and Mg are dominated by Ca^{2+} and Mg^{2+} ions with abundance of 69 %, while $CaCO_3$ & $MgCO_3$, and $CaHCO_3^+$ & $MgHCO_3^+$ account for 18 % and 13 %, respectively. Co is dominated by hydroxy(oxo)cobalt ($HCoO_2^-$) (68 %) and Co^{2+} is 32 %. Speciation of Fe is dominated by $FeHCO_3^+$ (50 %), $FeCO_3$ (27 %) and Fe^{2+} (23 %). Cd is dominated by Cd^{2+} (55 %), $CdCl^+$ (31 %), and $Cd(CO_3)_2^{2-}$ (14 %) which occur in the saline lakes. Speciation of Mn is dominated by Mn^{2+} (56 %) and $MnCO_3$ (44 %) and speciation of Zn is dominated by Zn^{2+} (78 %), $ZnHCO_3^+$ (16 %), and $Zn(OH)_2$ (6 %). Formation of carbonate complexes with these metals in the saline-alkaline lakes can be linked to the plenty availability of this ligand because of evaporative concentration while formation of hydroxy-compound with Co can be linked with the oxidizing conditions of up to +116 mV in these lakes.

Category 3 for elements mainly forming complex with dissolved inorganic carbon. This group include Ce, Cu, Dy, Er, Eu, Gd, Ho, La, Lu, Nd, Pb, Pr, Sm, Tb, Tm, U, Y, and Yb. Among theseCu, Pb, and U complex 100 % with CO_2 forming $CuCO_3$ or $Cu(CO_3)_2^{2-}$, $PbCO_3$ or $Pb(CO_3)_2^{2-}$, and $UO_2(CO_3)_3^{4-}$, respectively. Other elements in this group form complexes mainly with dissolved CO_2 and to a small proportion complex with fluoride.

Category 4 for elements forming oxy- and hydroxy- complexes. These are Al, As, B, Cr, Hf, Mo, Sb, Se, Si, Sn, Th, Ti, V, W, and Zr. Among these, B, Cr, Hf, Sb, Sn, Ti, and Zr completely form hydroxy- complexes. Mo, Se, V, and W completely form oxy- complexes. Th is dominated by hydroxy- compounds and a small proportion of fluoride complexes. SiO_2 dissolves forming SiO_2 in springs, streams, rivers, and groundwater, and $NaHSiO_3$ in the saline-alkaline lakes. Arsenic completely forms the oxyfluoride complex (AsO_3F^{2-}) and Al is dominated by oxy- and fluoride compounds. Formation of $NaHSiO_3$ in saline-alkaline lakes can be linked to the high concentration of Na in these lakes caused by evaporative concentration.

Speciation results indicate that the most important ligands in the waters of the upper flanks of Mt. Meru volcano are dissolved carbon (HCO_3^- and CO_3^{2-}), fluoride (F^-), and water (OH^-). The abundance of complexes formed between the metals and chloride (Cl^-) and sulfate (SO_4^{2-}) is low compared to other ligands. The number of complexes formed between these ligands and different metals can be associated with the reactivity/affinity of these metals with such ligands.

Knowing the aqueous species concentrations, the relevant mineral saturation indices can be estimated (Figure 5-5). Various secondary minerals including ferric oxide, alunite, gibbsite, kaolinite, levynite, K-feldspars, hematite, smectite, halloysite, carbonates, and native sulfur have been identified at Mt. Meru (Lyu et al., 2018; Mahecha, 2019). Among the identified minerals, some are typical argillic alteration minerals (acid sulfate alteration) like ferric oxide, alunite, gibbsite, kaolinite, hematite, and native sulfur whereas others, for example halloysite are low temperature weathering minerals while K-feldspar can be observed in both low and high temperature conditions as well as in igneous rocks.

Alunite ($KAl_3(SO_4)_2(OH)_6$) is undersaturated in the studied waters suggesting that it is unstable. In fact, its occurrence can be related to argillic alteration rather than weathering and low temperature alteration. The minerals analcime, hematite, K-feldspar, and goethite are, in contrast, supersaturated and may form.

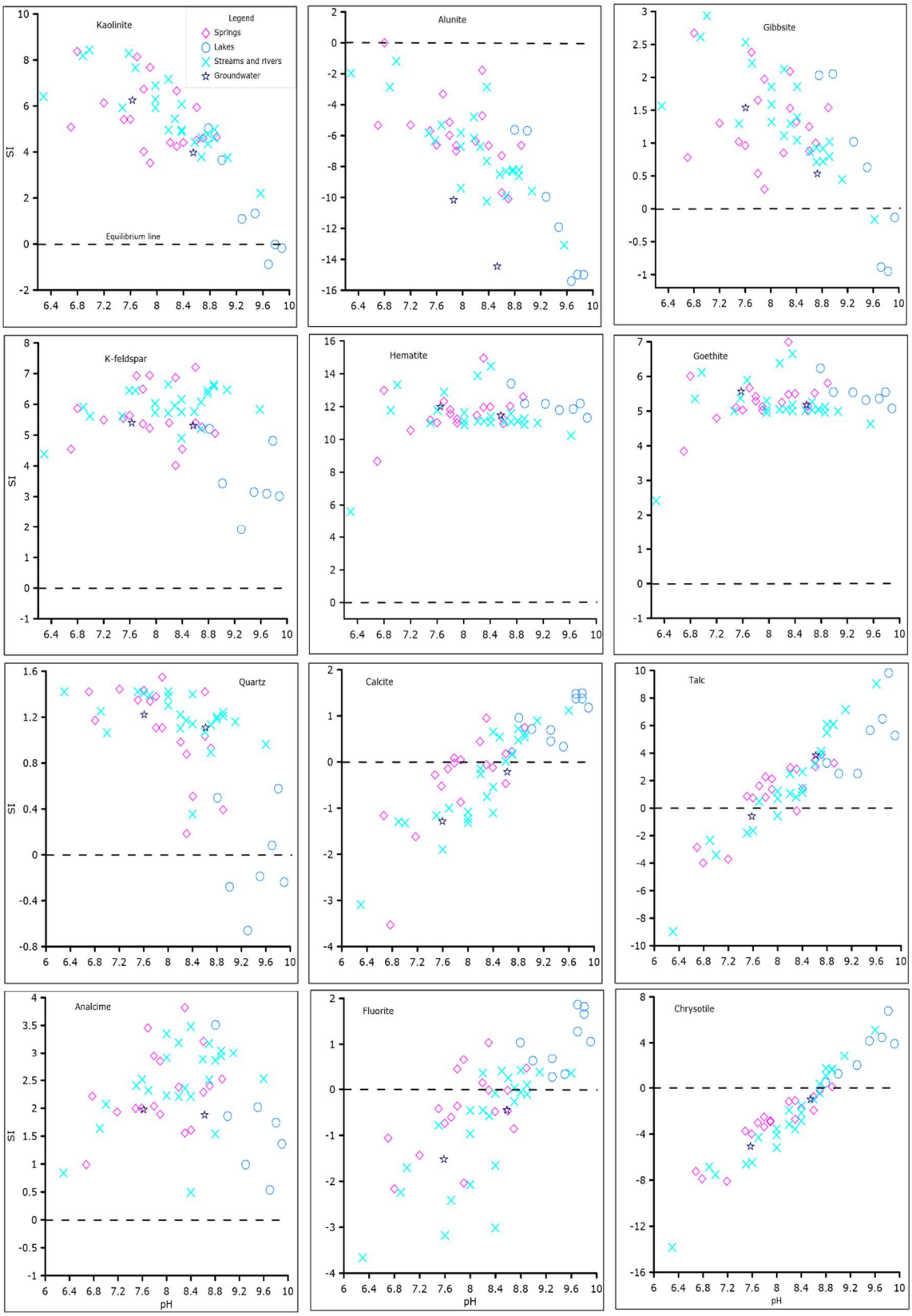

Figure 5- 5: Correlation plots for saturation index (SI) and pH showing the saturation states of water with respect to secondary minerals in the study area.

The saturation index of kaolinite, alunite, gibbsite, analcime, and K-feldspar, and quartz decreases with increasing pH with significant decreases at pH above 8. This is because of the dissociation of aqueous silicic acid to form $H_3SiO_4^-$ at pH > 8 therefore the activity of H_4SiO_4 decreases hence log Q value for species that include the H_4SiO_4 (Brady and Walther, 1989; White, 2020). The saturation indices of other minerals, calcite, fluorite, and Mg-silicates (chrysotile and talc) increase with increasing pH while hematite and goethite seem to be pH independent in the range of the studied waters.

Most of the elements, both major and trace elements, show low RM and are presumably taken up by secondary minerals either as major elements or substitute elements. The supersaturation of water with Al and Fe secondary minerals is consistent with the low RM indicated by Al and Fe (Figure 5- 4). Trace elements indicated to have low RM could be substituting for major elements in the forming secondary minerals (Figure 5- 5). For example, Mn, Ni and Co could be substituting for Fe while the trivalent metals like Sc could be substituting for Al. The elements Ba and Sr are known to be incorporated in the Al-silicates (Kaasalainen and Stefánsson, 2012) and references therein. Formation of low temperature weathering minerals at Mt. Meru could be enhanced by humid and temperate climate (Lyu et al., 2018).

5.4 Water–Rock Interaction and Mixing

In general, the process of water-rock interaction influencing water composition at Mt. Meru may be described by an incongruent weathering of nephelinites. Such would imply primary minerals and glasses to be dissolved to variable degree and other weathering minerals formed that have different relative elemental composition to the primary minerals.

The wide variability in the composition of the studied waters may be due to difference in the specific lithology interacting with water, varying degree of dissolution, difference in residence time, and admixture of volatiles of deep provenance in some of these waters. The waters at high altitude (except the Njekukumia springs) are dilute indicating they are less reacted. Enrichment of dissolved constituents increases with decreasing altitude indicating water-rock reaction time is an important factor controlling water composition thus waters at low altitude are more reacted.

The composition of the studied waters suggest that it is controlled by chemical weathering (dissolution of rocks at low temperature) without significant input of geothermal water. The positive correlation between major constituents like Na, K, Mg, SO_4 and the conservative Cl (Figure 5- 6) and trace elements vs Cl (Figure 5- 8) suggest progressive water rock interaction at low temperature and mixing of variable reacted non-thermal waters as the dominant processes controlling water composition.

The increase of Mg concentration with increasing Cl is indicative of low temperature water-rock interactions (weathering) and that with more rocks being dissolved the more Mg gets into the water. The concentration of SiO_2 in the studied waters is low indicative of typical continental rock weathering. The lack of linear trend on the SiO_2 vs Cl plot suggests insignificant input of geothermal fluid. Furthermore, the positive correlation of ΣCO_2 and Cl suggest the CO_2 to originate mainly from dissolution carbonates, possibly trona identified in the area.

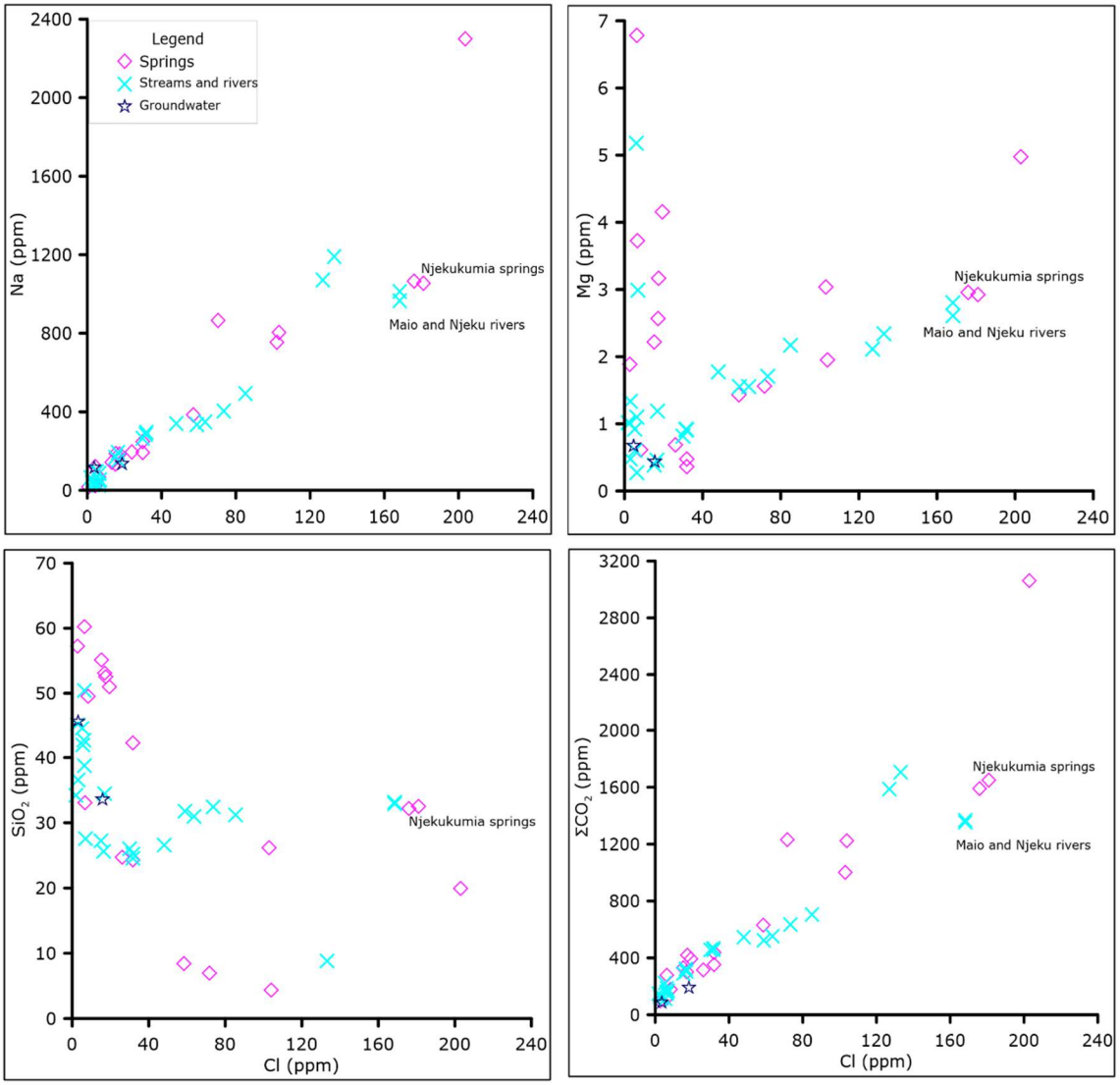

Figure 5- 6: Correlation plot of Cl and Na, Mg, SiO_2 and ΣCO_2 in the surface and groundwater on the upper flanks of Mt. Meru volcano. These plots suggest that the composition of the spring-, stream-, river-, and groundwater is mainly controlled by weathering of rocks at low temperature.

The dissolution of rocks may be enhanced by admixture of volcanic gases in some springs indicated by relatively high concentration of rock forming elements than in other springs. During chemical weathering CO_2 is converted to HCO_3 leading to increased concentration of HCO_3 with increasing concentration of dissolved rock forming elements which is considered as the index of water-rock-gas interaction (Aiuppa et al., 2000, 2005). Equation (3) indicates an example of CO_2 consuming reaction during chemical weathering of rocks.

$$CaAl_2Si_2O_8 + 2CO_2 + 3H_2O = Al_2Si_2O_5(OH)_4 + 2HCO_3^- + Ca^{2+} \quad (3)$$

Anorthite kaolinite

In addition to the interaction of water with alkali volcanic rocks, composition may also be influenced by the dissolution of evaporites that form on the surface during the dry season due to enhanced evaporation and get flushed at the onset of rainy season (Malago et al., 2020; Nanyaro et al., 1984).

The composition of the waters at Mt. Meru is also affected by the mixing of waters from different sources. There are possible two end-member water compositions in the study area, which are dilute waters (non-reacted or waters with low residence time) and more reacted waters. The non-reacted water has low concentration of dissolved constituents, while the reacted is somewhat mineralized. The reacted waters are indicated by for example the Njekukumia springs and few other springs (Figure 5- 8) whereas other springs, rivers, streams, and groundwater indicate varying degrees of mixing with non-reacted water. The reacted water end-member may be enhanced by dissolution of rocks by action of CO_2 charged water as a result of input of CO_2 from deep sources (Ghiglieri et al., 2012; Grassa et al., 2006).

The hydrological flow map indicates how the springs, streams and rivers join and mix in the study area (Figure 5- 7). The Maio and Njeku rivers are the highest mineralized among streams and rivers (Table 2) suggesting they mix with reacted waters possibly from springs (Figure 5- 8 and Figure 5- 9). Upon mixing, the mobile elements like Cl, B, As, and Li (Aiuppa et al., 2005, 2006; Kaasalainen and Stefánsson, 2012), indicate linear trends (Aiuppa et al., 2006; Arnórsson, 1985; Kaasalainen and Stefánsson, 2012). The elements Na, K, F, and SO_4 are also mobile upon mixing (Figure 5- 8) while others including SiO_2, Fe, Al, Ca, W, Sb, Sr, V, U, W, Zr do not show linear trend with chloride suggesting they react upon mixing.

Along the river flow path, the increasing dilution/mixing is evident. Two samples were collected in the Ngarenanyuki river, TP-14 was collected upstream close to the mini-hydropower plant in the Arusha National Park (ANP) while TP-65 was collected downstream close to the ANP headquarters. Analysis of the two samples indicate a systematic decrease in the physicochemical parameters and major elements in a 2.5 km river flow path. EC, Na, K, Ca, Mg, Fe, F, Cl, ΣCO_2, and SO_4 decreased by different order of magnitudes between 20 % and 40 %.

However, there was no river identified to join Ngarenanyuki river between the two sampling points (Figure 5- 7), although there may be small streams or underground sources not detected by remote sensing (SRTM) which may be causing dilution. Considering the significant change in the chemical composition of Ngarenanyuki river in such a short flow path (2.5 km), it indicates that geochemical processes operate at relatively high rate in the surface conditions.

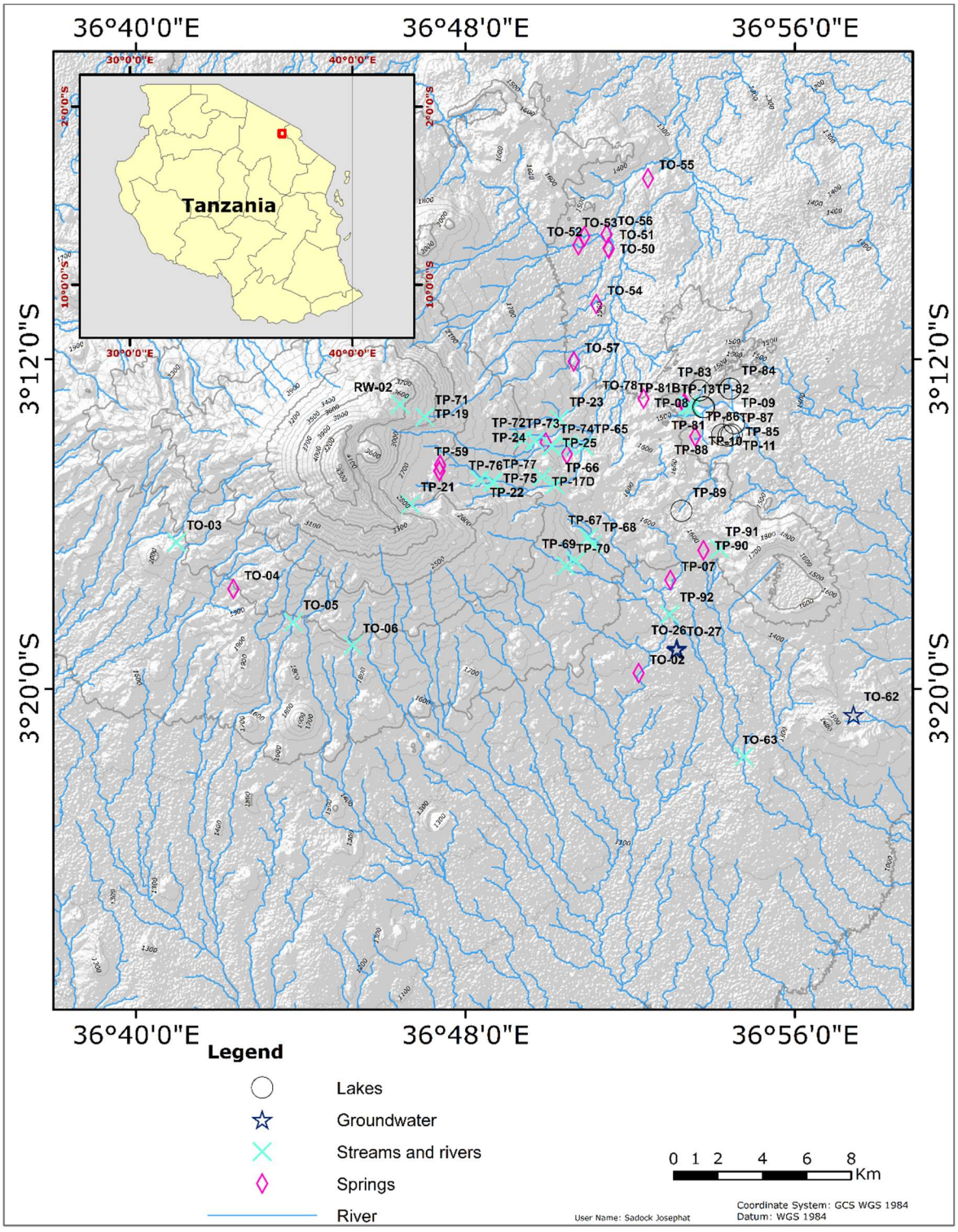

Figure 5- 7: Map showing hydrology in the Mt. Meru area. Sampling sites for this study and sample numbers are also indicated.

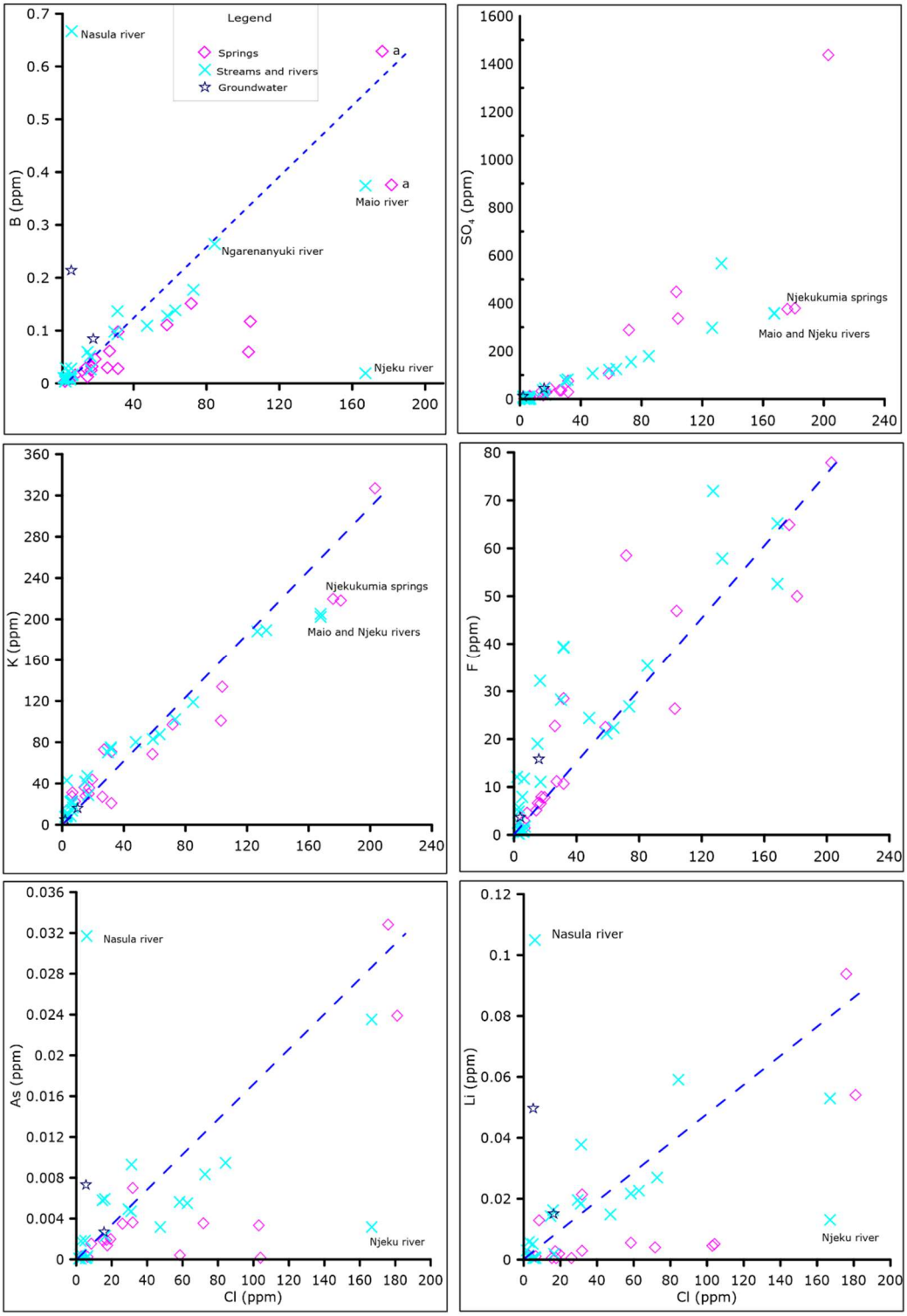

Figure 5- 8: Correlation plots for chloride and boron, sulfate, potassium, fluoride, arsenic, and lithium in the spring-, stream-, river- and groundwaters. The letter 'a' represents Njekukumia springs.

Nasula river is characterized by high concentration of some trace elements (Figure 5- 8 and Table 3). The highest concentration of B (667 ppb), Li (105 ppb), Sb (0.362 ppb), Sr (941 ppb), As (31.7 ppb), and W (125 ppb) were identified in this river compared to other studied

waters. However, this river evinces low concentration of major elements. This river is located on the lower altitude, 1670 m AMSL compared to the Njekukumia springs 2615 m AMSL on the eastern flank of Mt. Meru volcano. The low concentration of major elements and high concentration of trace elements may be associated with non-congruent dissolution of host rocks and a range in geochemical behaviors between the major and trace elements.

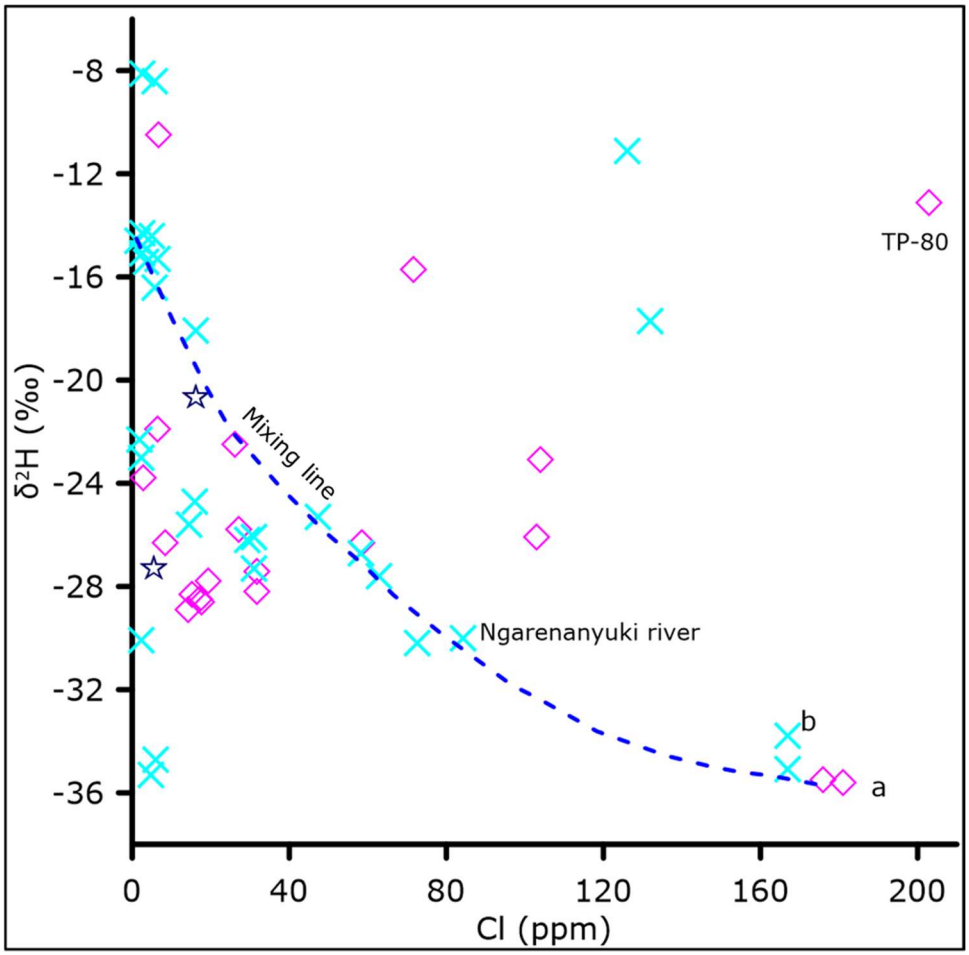

Figure 5- 9: Correlation plot of δ^2H-H_2O and chloride for the spring-, stream-, river-, and groundwaters in the upper flank of Mt. Meru volcano. The letters 'a' represent Njekukumia springs while 'b' represent the Maio and Njeku rivers.

Based on the composition of the studied waters, two end-member water compositions are inferred at Mt. Meru. These include the dilute (nearly fresh rainwater) and the reacted waters (possibly with some input of deep gases). Other waters are the results of mixing between the two endmembers.

5.5 Carbon Source in the Water at Meru

The studied waters are enriched in CO_2 similar to many other areas in the East African Rift System. Dissolved carbon concentrations show positive correlation with many other elements, for example Na, K, Mg, and Ca suggesting the source of CO_2 being progressive water-rock interaction with carbon rich rocks. Alternatively, magmatic degassing through Mt. Meru is another possibility for the sources of CO_2. The $\delta^{13}C$-CO_2 data support such a hypothesis, with mixing of CO_2 of deep origin characterized by CO_2 with $\delta^{13}C$ similar to mantle gas and surface CO_2 of atmospheric and biogenic origin (Figure 5- 10) (Chiodini et al., 2008; Delalande et al., 2011; Grassa et al., 2006).

Carbon dioxide is among the least soluble volatile in melts at high pressure resulting in degassing potentials from deep levels through the crust to surface without any magma transfer or deep geothermal activity (e.g., Ranta et al., 2023). Also, the input of deep provenance volatiles into the Njekukumia springs is supported by the presence of acid-sulfur alteration mineralogy in the vent of ash cone ~2 km west of these springs. Fumarolic activities were also observed at the ash cone vent until 1954 (Ghiglieri et al., 2010; Wilkinson et al., 1986). However, a recent attempt to map such activities in June 2017 using thermal imaging camera could not identify a thermal anomaly in the area. There have also been field observations in October 2016, June 2017, July 2018, and June 2021 but no fumarolic activities have been identified. The Lendoiya springs at low altitude also suggest input of deep CO_2.

It is likely that the flux of volatiles from deep provenance has been largely quenched by cold water flowing from the high altitudes of Mt. Meru volcano, regarded as the recharge zone. The volatiles from deep sources may be carried with groundwater water along the flow path. It is also possible that hydrothermal degassing may have decreased due to recession of the water table; however, no clear signs of thermal waters at Mt. Meru were observed in this study.

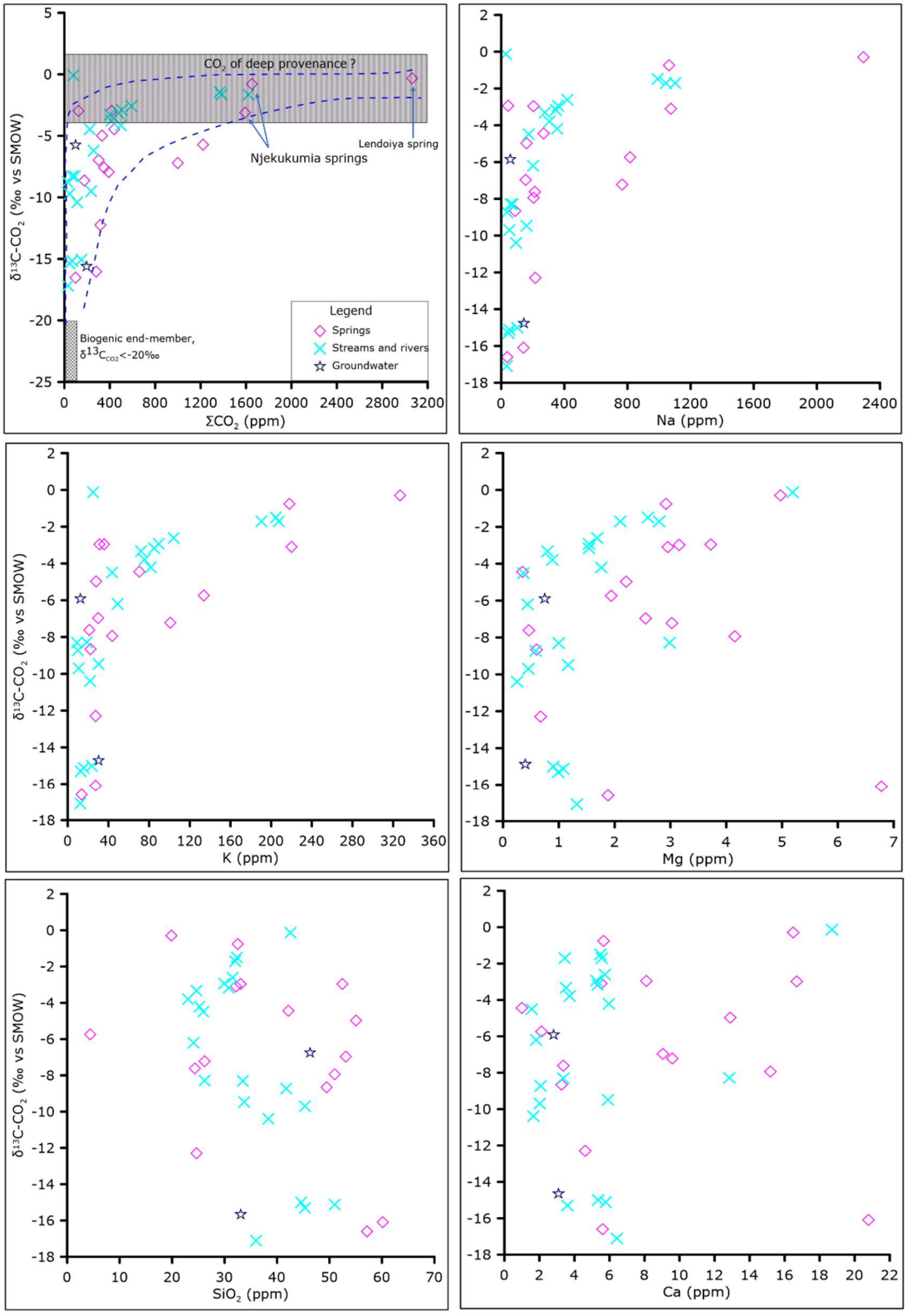

Figure 5- 10: Correlation plot of $\delta^{13}C$-CO_2 and ΣCO_2, Na, K, Mg, SiO_2 and Ca for the springs-, streams-, rivers-, and groundwater while $\delta^{13}C$-CO_2 was not analyzed in the lake samples. The end-member composition for $\delta^{13}C$-CO_2 is from Chiodini et al. (2008) and Grassa et al. (2006).

5.6 Geothermal Fluids at Mt. Meru

The reacted water at high altitude indicated by Njekukumia springs, discharge waters with a little elevated temperature (23 °C) compared to nearby springs and local ambient temperature (12 °C). Such is in line with previous studies at Mt. Meru (Bennett, 2022; Bennett et al., 2021; Ghiglieri et al., 2012) suggest the occurrence of thermal waters. The thermal water may be a result of shallow circulation of meteoric water and heat mining from the cooling rocks while input of deep gas to these springs is suggested based on $\delta^{13}C\text{-}CO_2$.

To characterize the potential temperatures of such thermal waters, the multi-mineral equilibria geothermometry approach (Reed and Spycher, 1984) was applied. Minerals which are commonly observed in low temperature systems including chalcedony, illite, K-feldspar, chlorite, fluorite, albite, and calcite were used. The results (Figure 5- 11) indicate potentially somewhat higher temperatures than observed at surface, i.e. between ~50 and 100 °C. Previous reservoir temperature estimation at Mt. Meru using quartz geothermometer suggested a temperature of 50 - 90 °C (Bennett, 2022), however, quartz is not an applicable geothermometer at <180-200 °C.

Moreover, the two springs (Figure 5- 11) indicate a similar range of reservoir temperature and identical chemical composition suggesting they originate from the same source. However, the temperature indicated by these springs may be non-relevant since water in these springs may represent a complex mixture of non-thermal waters of different origin (reacted and dilute cold waters) and potential thermal water as well. The results point towards a possible low-temperature thermal water (<100 °C) on the eastern flank of Mt. Meru whereas signs of intensive geothermal activity and a high-temperature geothermal system are lacking.

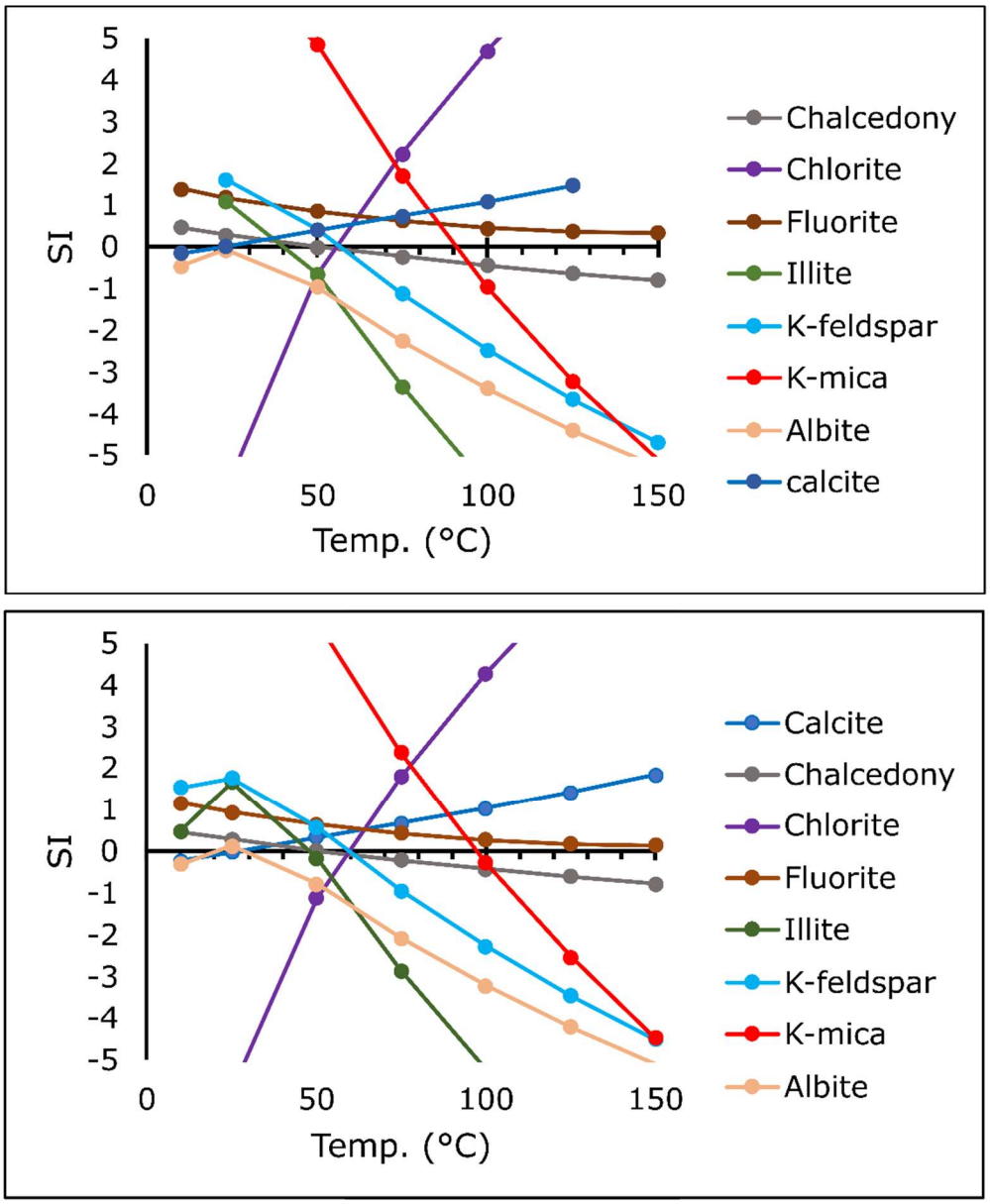

Figure 5- 11: Temperature versus saturation index plots for the Njekukumia springs, sample TP-18 (top) and TP-58 (bottom).

5.7 Water Quality

The constituents of water affect taste, color, appearance, smell, and general quality of water. It is therefore of paramount importance to ensure that water supplied to communities is of an acceptable quality following the established heath guidelines. In this study the Tanzania Bureau of Standards (local) health guidelines (TBS, 2008) and international health guidelines (WHO, 2022) were used to assess the quality of the studied waters. This study assessed the trace heavy elements and major elements, however assessment focusing on the major elements has been extensively done (e.g., Bennett et al., 2022; Chacha et al., 2018; Ghiglieri et al., 2010; Makoba and Muzuka, 2019; Malago et al., 2017).

These studies indicated that many water sources have unacceptable quality due to high concentration of F, Na, K, Cl, SO_4 and NO_3 above the health limits. The high concentration of fluoride in waters has been linked to the interaction with the alkaline rocks in the area while influence of deep provenance volatiles has also been suggested (Bennett et al., 2021; Ghiglieri et al., 2012, this study). Interaction of waters with alkaline rocks as source of high dissolved constituents including fluoride is supported by undersaturation of nephelinites (which are the most abundant rocks in the area) in the studied waters (Figure 5- 12). The studied waters evince low concentration of nitrate and phosphate suggesting water quality issue is associated with natural processes rather than anthropogenic activities.

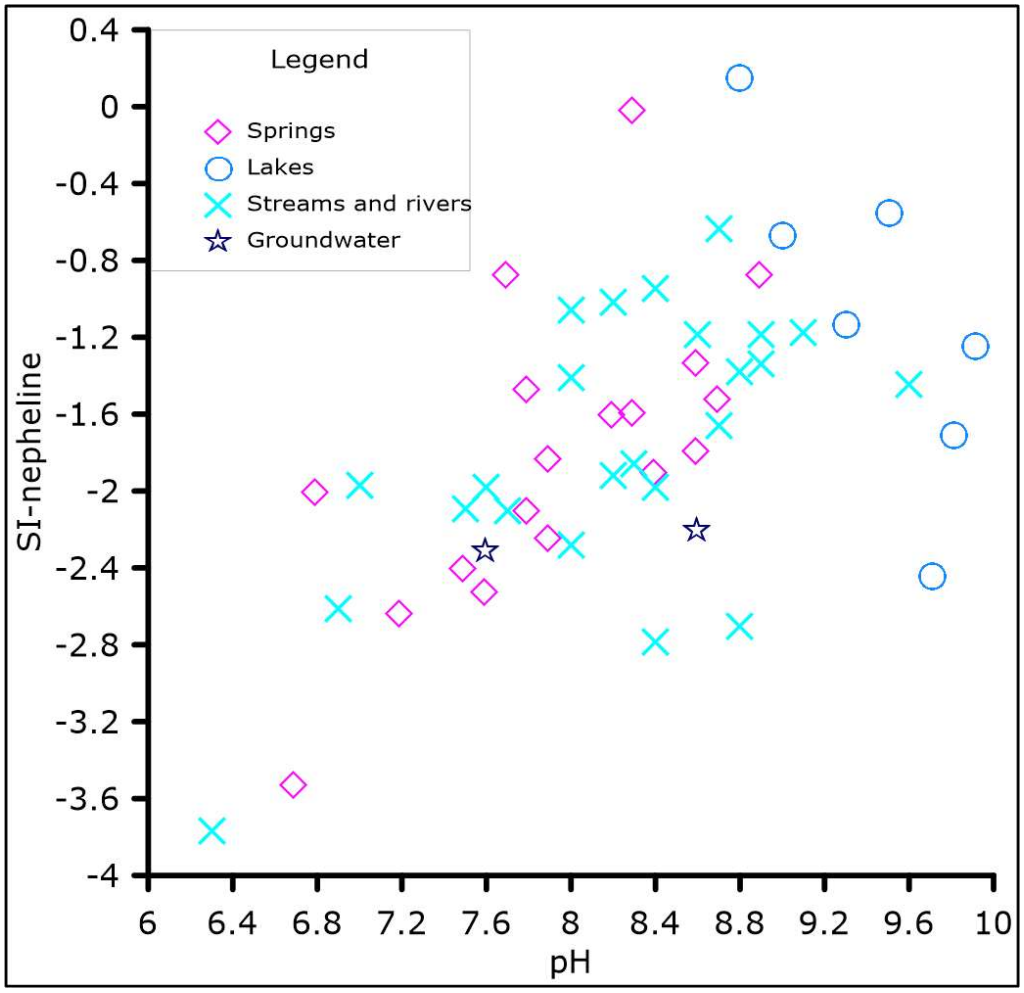

Figure 5- 12: Correlation plot for saturation index of nepheline and pH in the surface and groundwaters in the Mt. Meru area. Nepheline is supersaturated in only one lake sample and is undersaturated in other waters, hence it could be dissolving in the studied waters.

The water sources with concentration of dissolved constituents above the health guidelines can be linked with input of deep volatiles, evaporative concentration, mixing with reacted water end-member, dissolution of continental rocks, and high flow rate in the rivers contributing to high chemical denudation of Fe from the host rocks (Gislason, 2008). High concentration of As and Mo has also been identified in the rift lakes of Nakuru and Naivasha in Kenya and have been associated with volcanic activity (Jirsa et al., 2013).

Apart from Fe, elements with low to moderate relative mobility e.g., Al, Ti, Y, Pb, Ba, Cu, Se, and Zn seem to be of less concern since they are preferentially retained in the host rocks or incorporated in the secondary minerals. However, concentrations of Fe reaching 2.6 ppm and 1.142 ppm were identified in springs and rivers, respectively (Figure 5-13). Elements with high relative mobility e.g., U, Cr, Ni preferentially partition into the aqueous phase hence they may be of concern. Since U is the most mobile (Figure 5- 4), this can explain why its concentration is above the health limits in some springs and alkaline lakes.

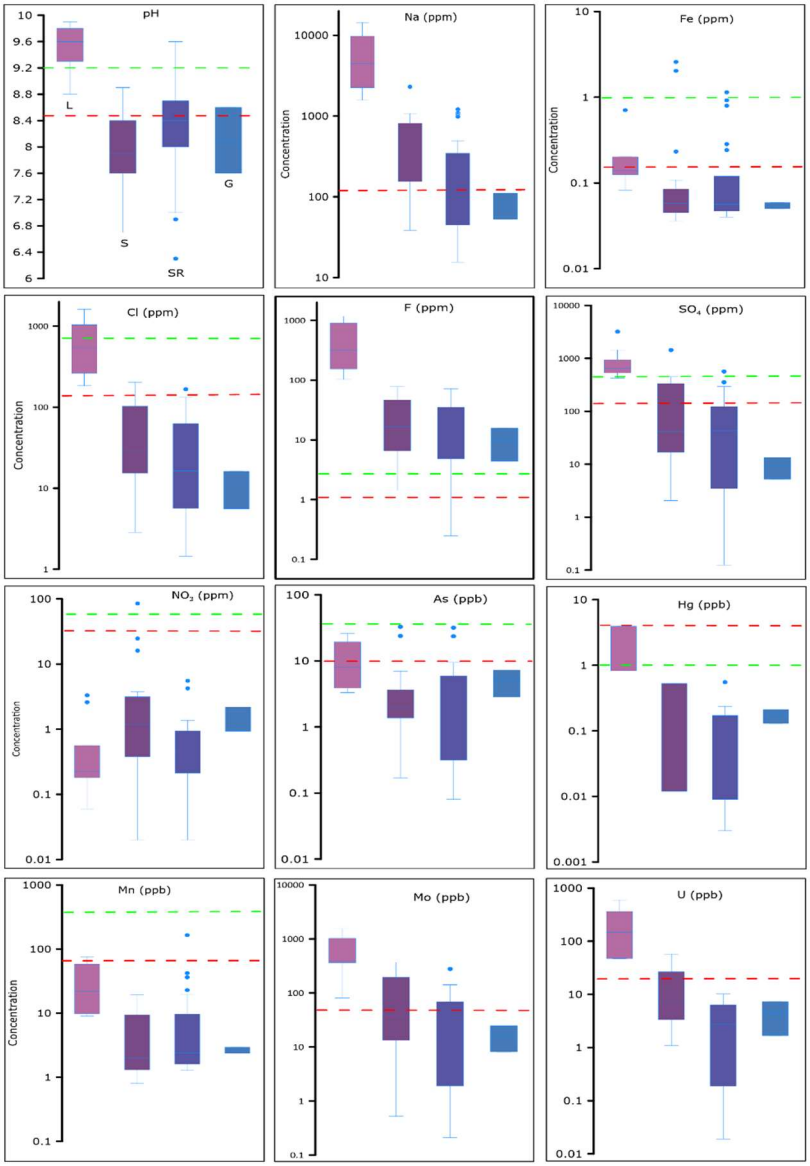

Figure 5- 13: Box and whisker plots showing parameters above the health limits in all the studied waters. The letters L is for lakes, S is for springs, SR is for streams and rivers, and G is for groundwater. The dotted green line is the Tanzanian health limit (TBS, 2008) and the red dotted line is the international health limit (WHO, 2022).

Table 4: Comparison of the studied waters chemical composition against the international guidelines (WHO, 2022) and Tanzanian guidelines (TBS, 2008). The numbers in red indicate concentration above the guidelines. The abbreviation bdl=below detection limit.

	pH	Na	Ca	Mg	Fe	F	Cl	SO_4	NO_3	Pb	As	B	Ba	Cd	Cr	Cu	Hg	Mn	Mo	Ni	Sb	U
		ppm	ppm	ppm	ppm	ppm	ppm	ppm	ppm	ppb	ppb	ppb	ppb	ppb	ppb	ppb	ppb	ppb	ppb	ppb	ppb	ppb
TBS 2008	9.2		300	100	1	4	800	600	75	100	50	-	1000	50	50	3000	1	500	-	-	-	-
WHO 2022	8.5	200	50	75	0.3	1.5	250	250	50	10	10	2400	1300	3	50	2000	6	80	70	70	20	30
TP-18	7.9	1075	5.53	2.95	0.036	64.9	176	375	0.23	0.203	32.8	629	6.49	0.227	11.1	0.881	0.526	3.69	68	18.1	0.33	31.7
TP-58	7.8	1064	5.67	2.92	0.069	50.0	181	379	0.02	0.3	23.9	376	6.3	0.24	8.6	1	bdl	1.3	288	4.4	0.24	29.2
TO-55	8.2	767	9.59	3.03	0.039	26.4	103	448	16	0.9	3.34	60	175	0.07	9.7	3.9	bdl	6	369	4.6	0.12	57
TP-79	8.3	816	2.12	1.94	0.070	46.9	104	336	0.04	na	0.17	117	0.9	0.07	0.4	0.6	na	0.8	195	na	na	na
TP-80	8.3	2294	16.5	4.97	2.584	77.9	203	1437	0.444	na	na	na	na	na	na	na	na	na	na	na	na	na
TP-88	8.9	876	4.95	1.55	0.233	58.5	71.7	288	1.48	0.4	3.56	151	1.8	0.05	9.4	1.8	bdl	19.5	209	4.7	0.09	26.7
TO-02	6.7	141	20.8	6.78	0.048	3.03	6.48	11.9	85.2	0.194	0.24	9.6	5.1	0.003	7.4	0.944	0.012	9.41	1.21	3.9	0.062	3.85
TO-04	7.9	38.5	5.61	1.88	0.053	1.55	2.86	2.07	1.96	0.186	0.28	3.73	1.75	0.007	7.5	0.554	bdl	1.27	0.52	3.82	0.036	1.09
TP-07	8.6	215	4.62	0.675	0.045	22.7	26.1	36.3	0.628	0.165	3.48	29.9	0.498	0.013	7.6	0.448	0.092	1.03	7.92	3.52	0.158	9.6
TO-50	7.5	204	15.2	4.15	0.040	7.81	19.4	46.2	24.6	0.21	2.02	46	2.84	0.012	8.73	2.03	bdl	1.2	36.3	4.1	0.107	15.9
TO-52	7.7	162	12.9	2.21	0.108	6.64	15.3	16.9	2.87	0.23	1.83	13	6.01	0.015	8.44	0.76	bdl	2.07	13.3	3.9	0.095	6.36
TO-53	8.7	213	3.38	0.462	0.077	10.7	31.8	29.4	0.89	0.22	3.64	28	4.19	0.014	8.58	0.68	bdl	1.97	37.4	4.1	0.213	12.1
TO-54	7.6	155	9.04	2.56	0.038	6.54	17.1	26.7	3.15	0.2	1.9	25	3.68	0.013	8.05	0.83	bdl	10.1	26.1	3.9	0.081	6.51
TO-56	7.8	206	16.7	3.16	0.058	7.92	17.6	28.8	2.28	0.23	1.37	32	10.7	0.012	9.08	1.62	bdl	13.4	20	4.5	0.056	7.55
TO-57	7.2	88.3	3.26	0.606	0.048	4.54	8.4	8.52	3.76	0.19	1.56	16	1.79	0.009	7.97	1.71	bdl	1.35	11	3.7	0.149	3.34
TP-59	8.6	268	1.01	0.351	0.058	28.5	31.8	74.7	0.23	0.21	7	98	0.56	0.018	8.39	0.71	bdl	1.5	85	4.1	0.1	1.65
TP-90	6.8	43.4	8.12	3.72	2.031	1.43	6.64	8.81	0.379	bdl	bdl	bdl	bdl	bdl	bdl	bdl	bdl	bdl	bdl	bdl	bdl	na
TO-78	8.4	402	2.05	1.42	0.085	22.5	58.5	106	0.681	0.5	0.401	111	0.9	0.1	16.2	3.2	bdl	4.3	102	8.1	0.06	3.23
TP-08	9.3	2790	2.08	7.12	bdl	223	403	745	0.19	bdl	bdl	bdl	bdl	bdl	bdl	bdl	bdl	bdl	bdl	bdl	bdl	bdl
TP-09	9.7	11710	9.32	8.13	bdl	1070	1570	1442	0.24	bdl	bdl	bdl	bdl	bdl	bdl	bdl	bdl	bdl	bdl	bdl	bdl	bdl
TP-10	9.8	14350	9.60	9.31	0.202	1180	1611	3186	0.31	0.208	25.9	2044	22	1.1	8.7	0.525	3.95	58.4	410	3.35	0.548	363
TP-11	9.8	9770	7.70	3.58	bdl	900	1039	505	0.18	bdl	bdl	bdl	bdl	bdl	bdl	bdl	bdl	bdl	bdl	bdl	bdl	bdl
TP-13	9.5	2610	1.09	3.95	0.082	245	262	678	0.06	0.206	3.9	480	5.53	0.161	9.6	0.759	0.822	8.97	81	4.21	0.124	47
TP-82	9.3	2247	1.61	4.79	0.139	154	242	624	0.208	0.4	3.32	409	6.1	0.14	9.7	1	bdl	9.8	378	4.4	0.08	47.3
TP-83	9.0	2165	3.26	5.62	0.125	129	317	623	2.6	0.3	5.69	440	6.4	0.12	9.8	2.6	bdl	21.7	362	4.3	0.2	67.8

TP-84	9.7	6805	7.66	4.6	0.150	436	924	935	0.176	bdl	19.4	1657	27	0.8	12.3	5.3	bdl	76	1558	bdl	bdl	598
TP-86	8.8	1569	10.9	2.91	0.708	103	184	530	3.32	bdl	bdl	bdl	bdl	bdl	bdl	bdl	bdl	bdl	bdl	bdl	bdl	bdl
TP-87	9.9	6097	5.12	2.18	0.130	391	685	424	0.562	bdl	10.5	1271	bdl	1	12.2	3.9	bdl	bdl	1028	bdl	0.8	228
TP-17	8.7	339	5.85	1.76	0.060	24.4	47.3	106	0.94	0.216	3.17	109	1.86	0.018	10.1	1.05	0.119	2.1	22	4.61	0.09	6.39
TP-12	8.5	1090	3.32	2.1	bdl	71.9	126	296	0.21	bdl	bdl	bdl	bdl	bdl	bdl	bdl	bdl	bdl	bdl	bdl	bdl	bdl
TO-03	7.5	87.6	5.25	0.898	0.048	7.90	4.77	8.73	4.24	0.184	1.83	9.93	0.977	0.006	8.2	0.576	bdl	1.35	3.03	4.04	0.149	2.08
TO-05	8.0	30.4	3.47	0.986	0.045	2.48	2.28	1.96	1.03	0.167	0.51	4.04	0.387	0.007	7.8	0.872	bdl	1.28	0.54	3.96	0.037	0.188
TP-19	6.3	18.9	6.32	1.32	0.046	0.248	2.63	3.48	5.52	0.265	0.08	28.6	5.66	0.014	14.4	1.84	0.008	9.01	0.75	32.6	0.022	0.019
TP-21	8.0	55.5	3.25	0.997	0.057	12.1	1.45	8.14	0.025	1.31	0.1	10.5	13.1	0.02	13.1	3.64	0.003	36.1	0.21	8.71	0.068	0.058
TP-67	7.7	38.0	5.69	1.08	0.242	1.01	5.82	1.7	0.22	0.27	0.18	15	1.44	0.011	8.23	1.58	bdl	42.1	1.91	4.1	0.03	0.071
TP-72	7.6	22.7	1.94	0.584	0.120	0.66	5.02	0.124	bdl	0.21	0.103	7	0.45	0.05	8.51	1.15	bdl	9.66	1.12	4.3	0.023	0.044
TP-81	8.4	1211	6.41	2.33	0.919	57.9	132	564	0.069	na	na	na	na	na	na	na	na	na	na	na	na	na
TP-14	8.8	495	6.76	2.16	0.045	35.3	84.3	179	0.43	0.195	9.48	264	4.73	0.052	10.1	1.88	0.236	2.4	40.9	5.01	0.191	10.2
TP-15	8.6	281	3.71	0.896	0.042	39.4	31.0	80.8	1.03	0.146	4.7	93.2	1.05	0.018	7.4	1.09	0.123	1.29	16.6	3.57	0.124	5.46
TO-06	8.4	37.1	1.87	0.451	0.066	4.85	2.44	1.97	0.713	0.202	1.79	4.05	0.91	0.009	7.4	0.76	bdl	1.57	0.64	3.68	0.154	0.282
TP-23	8.0	77.3	1.53	0.245	0.070	11.7	5.91	7.90	0.625	0.224	31.7	667	5.07	0.212	11.5	0.943	0.55	2.69	68.8	5.42	0.362	30.8
TP-24	8.4	186	1.67	0.43	0.044	32.2	16.0	42.8	0.533	0.298	5.92	51.2	0.427	0.013	14.6	1.66	0.037	4.18	4.23	10.2	0.26	1.37
TP-25	8.2	291	3.59	0.882	0.047	39.2	31.1	81.0	0.932	0.263	9.28	137	1.41	0.017	13.9	1.87	0.171	2.98	15.8	7.11	0.204	4.22
TO-63	7.0	44.8	12.8	2.99	1.142	1.75	6.37	1.30	0.38	0.38	0.316	17	5.9	0.027	9.49	5.74	bdl	19.7	3.92	5	0.05	0.923
TP-66	8.8	346	5.13	1.54	0.057	22.4	62.8	124	0.81	0.2	5.52	138	4.5	0.04	9.4	1.5	bdl	2.2	119	4.2	0.2	6.64
TP-68	6.9	15.5	18.7	5.2	0.284	0.732	5.64	0.403	0.02	0.26	0.161	28	10.3	0.033	9.67	4.6	bdl	165	2.01	4.9	0.037	0.051
TP-92	8.2	145	5.82	1.17	0.799	11.06	16.3	17.8	0.467	0.26	2.28	26	1.06	0.014	9.05	3.7	bdl	23	23.3	4.7	0.1	4.43
TP-73	8.3	160	1.42	0.358	0.049	19.0	14.6	36.9	0.34	0.2	5.79	60	0.65	0.006	8.32	1.74	bdl	1.48	50	4	0.246	2.73
TP-74	8.7	261	3.39	0.795	0.049	28.2	29.3	76.4	1.36	0.2	4.93	98	1.27	0.016	8.36	1.39	bdl	1.89	87.2	4.1	0.134	5.54
TP-22	9.6	1030	5.46	2.8	0.040	65.2	167	358	0.04	0.326	3.18	18.9	0.299	0.01	15.5	1.25	0.009	5.99	3.73	9.12	0.13	0.247
TP-76	8.9	404	5.64	1.69	0.048	26.8	72.7	155	0.186	0.3	8.34	177	4	0.07	8.4	1.3	bdl	1.6	141	4.4	0.13	8.17
TP-77	9.1	979	5.38	2.6	0.056	52.6	167	356	0.212	0.3	23.5	374	4.9	0.27	8.2	1	bdl	1.7	280	4.5	0.28	26.2
TP-65	8.9	332	5.21	1.54	0.068	21.2	58.3	122	0.85	0.3	5.64	128	3.8	0.04	8.7	1.9	bdl	2.3	113	4.3	0.07	6.16
TO-26	7.6	52.6	2.86	0.675	0.059	4.39	5.56	5.22	2.19	0.281	7.29	212	1.54	0.021	14.4	1.9	0.211	2.94	24.6	6.94	0.17	7.32
TO-27	8.6	111	3.02	0.431	0.050	15.7	16.2	13.4	0.931	0.888	2.84	84.1	1.31	0.02	13.5	4.44	0.129	2.36	8.11	6.98	0.073	1.67

This study has identified the concentration of As, U, Mo, Hg, Fe, Na, Cl, SO_4, NO_3, Mn in some of the studied water sources above the health limits while the concentration of F was above the health limits in nearly all the studied waters (Figure 5- 13). The concentration of these elements above the health limits was identified in the springs with reacted water, saline-alkaline lakes and the rivers incorporating water from these springs, but not in groundwater. This indicates that the springs with reacted water have considerable influence on the water quality in the area as indicated by mixing plots.

In this study more trace elements including Al, Be, Bi, Ce, Co, Cs, Dy, Er, Eu, Ga, Gd, Ge, Hf, Ho, In, La, Li, Lu, Nb, Nd, Pr, Rb, Sc, Sm, Sn, Sr, Ta, Tb, Te, Th, Ti, Tl, Tm, V, W, Y, Yb, and Zr were also analyzed. However, no standards found for comparison for these elements to see whether their concentration levels are likely to cause toxicity to humans and other communities relying on these water sources.

5.8 Hydrogeology of Mt. Meru

The hydrogeology and geochemistry of the natural waters at Mt. Meru reflects various elemental sources, progressive water-rock interaction and mixing of various water components. The waters are of meteoric origin, and infiltrate through permeable formations and fractures at high altitude and flow downslope at surface but mainly as subsurface groundwater. Along the flow-path the groundwaters continue to react with the surrounding rocks and minerals resulting in increased concentrations of dissolved constituents (Figure 5-14). Mixing of variable reacted waters may also contribute to the gradient in water composition.

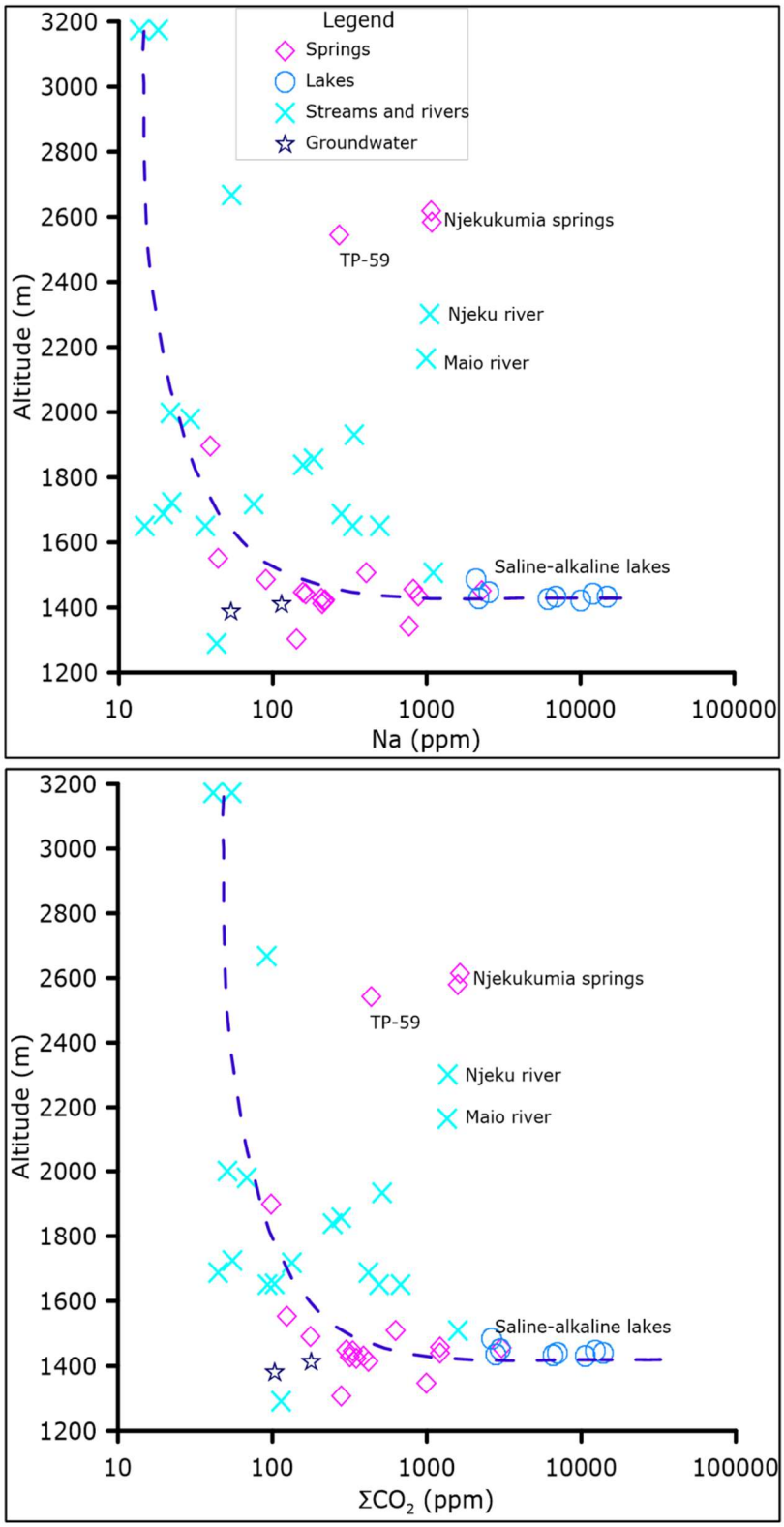

Figure 5- 14: Correlation plots for altitude and most abundant cation and anion in the studied waters. The hypothesized water chemistry evolution path is indicated by a blue dotted line. The Njekukumia springs with reacted water and Njeku and Maio rivers mixing with reacted waters evince high mineralization in the high altitude. The Lendoiya spring overlaps with saline-alkaline lakes.

At relatively high altitude, waters of the Njekukumia springs display high dissolved element concentration relative to the surrounding spring waters, suggesting a possible input of more reacted and/or thermal water. The Njekukumia springs may therefore represent a relatively shallow circulation of meteoric water gaining temperature by conduction from rocks and mixing with gases of deep provenance (Figure 5- 15). According to a mixing model, Maio, and Ngarenanyuki rivers incorporate significant amount of water from the presumably thermal Njekukumia springs.

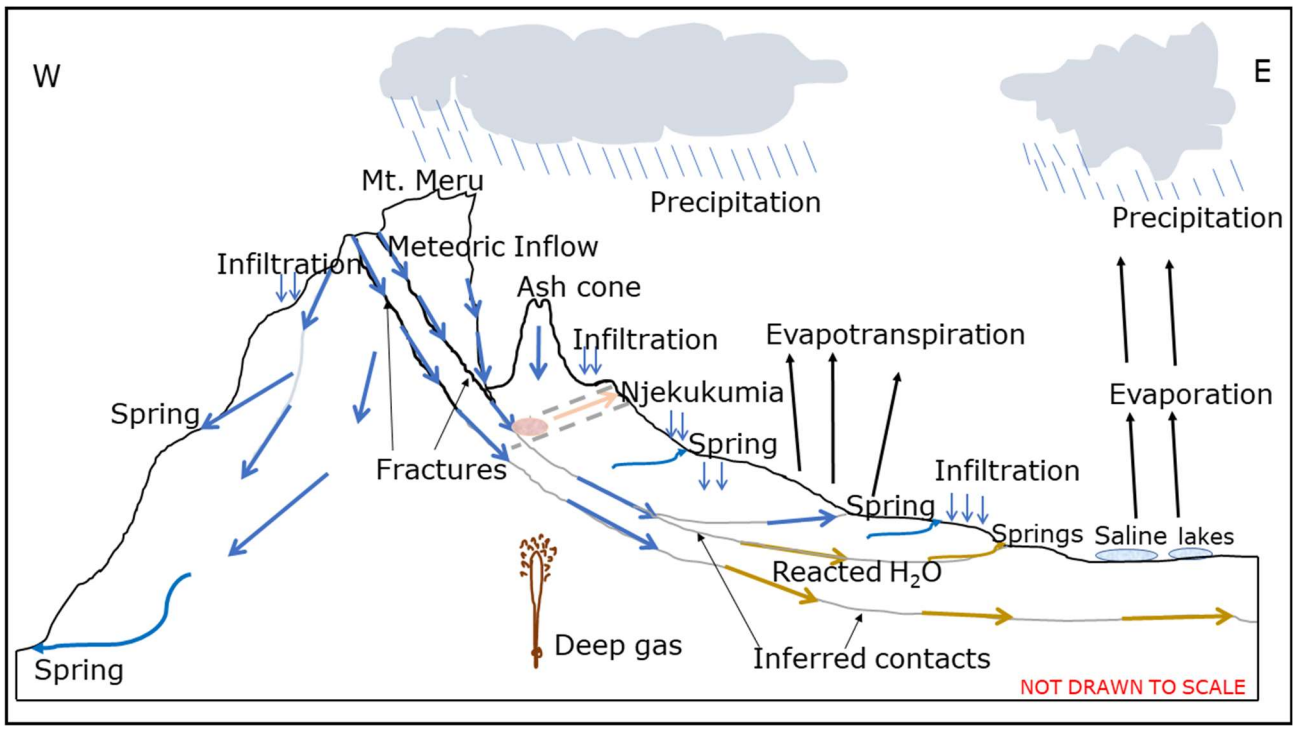

Figure 5- 15: Hypothesized waterflow model of the Mt. Meru volcano. Water infiltrates through the fractures/faults observed in the summit area and the crater at the top of ash cone. In the subsurface water could be flowing in the fractures or along lithological contacts.

The hydrological flow at Mt. Meru is hypothesized to be relatively fast due to the steep geomorphology of the area where the studied waters occur in the altitude between 1230 and 3554 m AMSL and the summit is 4565 m AMSL. No hydrological connection was identified on the surface between the saline-alkaline lakes and the Njekukumia springs and major rivers.

The waters in saline-alkaline lakes are of meteoric origin as well but have been modified by the open system evaporation as indicated by enrichment in heavy stable water isotopes (δ^2H and $\delta^{18}O$) and dissolved elements, both major and trace elements. No clear signs of thermal water input in these lakes were identified in this study. There was no major surface inflow to these lakes observed in the field nor mapped by remote sensing.

Figure 5- 16: Top photo was taken from ash cone showing fractures and veins (red lines) on the Mt. Meru summit collapse scar and the bottom photo was taken from the Mt. Meru summit showing the crater on the top of ash cone. The fractures and crater act as water percolation pathway. Photos by: Mathew Mwangomba (TGDC, 2021).

6 Conclusions

The investigated waters are of meteoric origin as indicated by $\delta^{2}H$-H_2O and $\delta^{18}O$-H_2O, with Na-HCO_3 composition. Their isotopic and chemical composition is affected by isotopic fractionation with altitude, evaporation, and condensation processes. The water precipitated at high altitude flows downslope partly at surface but mainly as subsurface groundwater.

The correlation between major constituents (Na, K, Mg, SO_4, and Cl) suggests progressive water rock interaction at low temperature as the dominant process controlling water composition. No significant input of geothermal water is observed. The saline alkaline lakes appear to be formed by evaporative concentration of waters sourced at higher altitude. Two possible end-member water compositions, non-reacted and more reacted, have been identified, with other spring-, river- and groundwaters falling between these two end members, suggesting mixing. The $\delta^{13}C$-CO_2 data suggest that main sources of dissolved inorganic carbon are dissolution of carbonates, mixing with biogenic CO_2 and input of deep volatiles.

Relative mobility of elements is generally low, only U and Cr have higher mobility than Na in the groundwater. Of the major elements, Na and K are the most mobile whereas other major cations show low mobility, suggesting that they are retained in alteration minerals upon water-rock interaction. Among trace elements U, Cr, Ni, Rb, V, Sr and Cu show the highest mobility, but Th and Ti are the least mobile, suggesting that the former are controlled by dissolution of primary rocks whereas the latter are incorporated into secondary minerals.

The multi-mineral equilibria geothermometer suggests an equilibrium temperature of 50-100 °C for the Njekukumia springs. No signs of intense geothermal activity or a high-temperature geothermal system are observed. The concentrations of As, U, Mn, Mo, Hg, Fe, Na, Cl, SO_4, and NO_3 are found to be above the local and international health limits in some waters while the concentration of F is above health limits in nearly all the studied waters. It is therefore recommended that potable water is treated so that all components are within the permissible limits before water is supplied to local communities.

References

Aiuppa, A., Allard, P., D'Alessandro, W., Michel, A., Parello, F., Treuil, M., & Valenza, M. (2000). Mobility and fluxes of major, minor and trace metals during basalt weathering and groundwater transport at Mt. Etna volcano (Sicily). *Geochimica et Cosmochimica Acta*, *64*(11), 1827–1841. https://doi.org/10.1016/S0016-7037(00)00345-8

Aiuppa, A., Avino, R., Brusca, L., Caliro, S., Chiodini, G., D'Alessandro, W., Favara, R., Federico, C., Ginevra, W., Inguaggiato, S., Longo, M., Pecoraino, G., & Valenza, M. (2006). Mineral control of arsenic content in thermal waters from volcano-hosted hydrothermal systems: Insights from island of Ischia and Phlegrean Fields (Campanian Volcanic Province, Italy). *Chemical Geology*, *229*(4), 313–330. https://doi.org/10.1016/j.chemgeo.2005.11.004

Aiuppa, A., Federico, C., Allard, P., Gurrieri, S., & Valenza, M. (2005). Trace metal modeling of groundwater–gas–rock interactions in a volcanic aquifer: Mount Vesuvius, Southern Italy. *Chemical Geology*, *216*(3), 289–311. https://doi.org/10.1016/j.chemgeo.2004.11.017

Allegre, C. J. (2008). *Isotope geology*. Cambridge University Press.

Arnórsson, S. (1985). The use of mixing models and chemical geothermometers for estimating underground temperatures in geothermal systems. *Journal of Volcanology and Geothermal Research*, *23*(3), 299–335. https://doi.org/10.1016/0377-0273(85)90039-3

Arnórsson, S., & Andrésdóttir, A. (1995). Processes controlling the distribution of boron and chlorine in natural waters in Iceland. *Geochimica et Cosmochimica Acta*, *59*(20), 4125–4146. https://doi.org/10.1016/0016-7037(95)00278-8

Benavente, O., Tassi, F., Reich, M., Aguilera, F., Capecchiacci, F., Gutiérrez, F., Vaselli, O., & Rizzo, A. (2016). Chemical and isotopic features of cold and thermal fluids discharged in the Southern Volcanic Zone between 32.5°S and 36°S: Insights into the physical and chemical processes controlling fluid geochemistry in geothermal systems of Central Chile. *Chemical Geology*, *420*, 97–113. https://doi.org/10.1016/j.chemgeo.2015.11.010

Bennett, G. (2022). *Hydrogeological investigation of a volcanic aquifer system on the flanks of mount Meru, Northern Tanzania* [PhD Thesis]. Ghent University.

Bennett, G., Reybrouck, J., Shemsanga, C., Kisaka, M., Tomašek, I., Fontijn, K., Kervyn, M., & Walraevens, K. (2022). Identification of low fluoride areas using conceptual groundwater flow model and hydrogeochemical system analysis in the aquifer system on the flanks of an active volcano: Mount Meru, Northern Tanzania. *Science of The Total Environment*, *814*, 152682. https://doi.org/10.1016/j.scitotenv.2021.152682

Bennett, G., Van Reybrouck, J., Shemsanga, C., Kisaka, M., Tomašek, I., Fontijn, K., Kervyn, M., & Walraevens, K. (2021). Hydrochemical Characterisation of High-Fluoride Groundwater and Development of a Conceptual Groundwater Flow Model Using a Combined Hydrogeological and Hydrochemical Approach on an Active Volcano: Mount Meru, Northern Tanzania. *Water*, *13*(16), Article 16. https://doi.org/10.3390/w13162159

BGR. (2018). *Petrography of Rocks collected during the geothermal Field Visit of Mt. Meru, in October 2016* (p. 109) [Unpublished TGDC Report].

Brady, P. V., & Walther, J. V. (1989). Controls on silicate dissolution rates in neutral and basic pH solutions at 25°C. *Geochimica et Cosmochimica Acta*, *53*(11), 2823–2830. https://doi.org/10.1016/0016-7037(89)90160-9

Braun, J.-J., Pagel, M., Herbilln, A., & Rosin, C. (1993). Mobilization and redistribution of REEs and thorium in a syenitic lateritic profile: A mass balance study. *Geochimica et Cosmochimica Acta*, *57*, 4419–4434. https://doi.org/10.1016/0016-7037(93)90492-F

Chacha, N., Njau, K. N., Lugomela, G. V., & Muzuka, A. N. N. (2018). Hydrogeochemical characteristics and spatial distribution of groundwater quality in Arusha well fields, Northern Tanzania. *Applied Water Science*, *8*(4), 118. https://doi.org/10.1007/s13201-018-0760-4

Chiodini, G., Caliro, S., Cardellini, C., Avino, R., Granieri, D., & Schmidt, A. (2008). Carbon isotopic composition of soil CO2 efflux, a powerful method to discriminate different sources feeding soil CO2 degassing in volcanic-hydrothermal areas. *Earth and Planetary Science Letters*, *274*(3), 372–379. https://doi.org/10.1016/j.epsl.2008.07.051

Chorowicz, J. (2005). The East African Rift System. *Journal of African Earth Sciences*, *43*, 379–410.

Craig, H. (1961). Isotopic Variations in Meteoric Waters. *Science*, *133*(3465), 1702–1703. https://doi.org/10.1126/science.133.3465.1702

Dawson, J. B. (1992). Neogene tectonics and volcanicity in the North Tanzania sector of the Gregory Rift Valley: Contrasts with the Kenya sector. *Tectonophysics*, *204*(1), 81–92. https://doi.org/10.1016/0040-1951(92)90271-7

Dawson, J. B. (2008). *The Gregory Rift Valley and Neogene—Recent Volcanoes of Northern Tanzania*. https://doi.org/10.1144/M33

Delalande, M., Bergonzini, L., Gherardi, F., Guidi, M., Andre, L., Abdallah, I., & Williamson, D. (2011). Fluid geochemistry of natural manifestations from the Southern Poroto–Rungwe hydrothermal system (Tanzania): Preliminary conceptual

model. *Journal of Volcanology and Geothermal Research*, *199*(1), 127–141. https://doi.org/10.1016/j.jvolgeores.2010.11.002

Delcamp, A., Kwelwa, S., Macheyeki, A., & Kervyn, M. (2013). *Multiple collapses at Mt Meru volcano, Tanzania: Remote sensing and field evidences from debris avalanche deposits.* 7775.

Delcamp, A., Roberti, G., & van Wyk de Vries, B. (2016). Water in volcanoes: Evolution, storage and rapid release during landslides. *Bulletin of Volcanology*, *78*. https://doi.org/10.1007/s00445-016-1082-8

Didas, M. M., Armadillo, E., Hersir, G. P., Cumming, W., & Rizzello, D. (2022). Regional thermal anomalies derived from magnetic spectral analysis and 3D gravity inversion: Implications for potential geothermal sites in Tanzania. *Geothermics*, *103*, 102431. https://doi.org/10.1016/j.geothermics.2022.102431

Foster, A. N., Ebinger, C., Mbede, E., & REX, D. (1997). Tectonic development of the northern Tanzania sector of the East African Rift System. *Journal of The Geological Society - J GEOL SOC*, *154*, 689–700. https://doi.org/10.1144/gsjgs.154.4.0689

Ghiglieri, G., Balia, R., Oggiano, G., & Pittalis, D. (2010). Prospecting for safe (low fluoride) groundwater in the Eastern African Rift: The Arumeru District (Northern Tanzania). *Hydrology and Earth System Sciences*, *14*(6), 1081–1091. https://doi.org/10.5194/hess-14-1081-2010

Ghiglieri, G., Pittalis, D., Cerri, G., & Oggiano, G. (2012). Hydrogeology and hydrogeochemistry of an alkaline volcanic area: The NE Mt. Meru slope (East African Rift – Northern Tanzania). *Hydrology and Earth System Sciences*, *16*(2), 529–541. https://doi.org/10.5194/hess-16-529-2012

Giggenbach, W. F. (1992). Isotopic shifts in waters from geothermal and volcanic systems along convergent plate boundaries and their origin. *Earth and Planetary Science Letters*, *113*(4), 495–510. https://doi.org/10.1016/0012-821X(92)90127-H

Gislason, S. (2008). Weathering in Iceland. *Jokull*, *58*, 387–408.

Gislason, S. R., Arnorsson, S., & Armannsson, H. (1996). Chemical weathering of basalt in Southwest Iceland; effects of runoff, age of rocks and vegetative/glacial cover. *American Journal of Science*, *296*(8), 837–907. https://doi.org/10.2475/ajs.296.8.837

Grassa, F., Capasso, G., Favara, R., & Inguaggiato, S. (2006). Chemical and Isotopic Composition of Waters and Dissolved Gases in Some Thermal Springs of Sicily and Adjacent Volcanic Islands, Italy. *Pure and Applied Geophysics*, *163*(4), 781–807. https://doi.org/10.1007/s00024-006-0043-0

Halldórsson, S., Hilton, D., Scarsi, P., Abebe, T., & Hopp, J. (2014). A common mantle plume source beneath the entire East African Rift System revealed by coupled helium-neon systematics. *Geophysical Research Letters*, *41*. https://doi.org/10.1002/2014GL059424

Jirsa, F., Gruber, M., Stojanovic, A., Omondi, S. O., Mader, D., Körner, W., & Schagerl, M. (2013). Major and trace element geochemistry of Lake Bogoria and Lake Nakuru, Kenya, during extreme draught. *Geochemistry*, *73*(3), 275–282. https://doi.org/10.1016/j.chemer.2012.09.001

Kaasalainen, H., & Stefánsson, A. (2012). The chemistry of trace elements in surface geothermal waters and steam, Iceland. *Chemical Geology*, *330–331*, 60–85. https://doi.org/10.1016/j.chemgeo.2012.08.019

Kebede, B. A. (2021). *The Relationship between the Tulu Moye Geothermal System, the Ziway–Asela Area and the Tectonic Structure of the Ethiopian Rift* [MS Thesis,

Faculty of Earth Science, University of Iceland]. https://skemman.is/handle/1946/40002

Le Gall, B., Nonnotte, P., Rolet, J., Benoit, M., Guillou, H., Mousseau-Nonnotte, M., Albaric, J., & Deverchère, J. (2008). Rift propagation at craton margin.: Distribution of faulting and volcanism in the North Tanzanian Divergence (East Africa) during Neogene times. *Tectonophysics*, *448*(1), 1–19. https://doi.org/10.1016/j.tecto.2007.11.005

Lyu, H., Watanabe, T., Kilasara, M., & Funakawa, S. (2018). Effects of climate on distribution of soil secondary minerals in volcanic regions of Tanzania. *CATENA*, *166*, 209–219. https://doi.org/10.1016/j.catena.2018.04.005

Mahecha, A. (2019). *Structural control of north Tanzania volcanic area and its implication to geothermal fluid pathways; a case study of lake Natron and Meru volcano* [MSc Thesis]. Kyushu University.

Mahecha, A., Saadi, N., Watanabe, K., & Josephat, S. (2021). The quest for fluid pathways at Meru volcanic area, Tanzania, using remote sensing and soil gas analysis. *Proceedings World Geothermal Congress 2020+1*, 8.

Makoba, E., & Muzuka, A. (2019). Water quality and hydrogeochemical characteristics of groundwater around Mt. Meru, Northern Tanzania. *Applied Water Science*, *9*, 120. https://doi.org/10.1007/s13201-019-0955-3

Malago, J., Makoba, E., & Muzuka, A. N. N. (2017). Fluoride Levels in Surface and Groundwater in Africa: A Review. *American Journal of Water Science and Engineering*, *3*(1), Article 1. https://doi.org/10.11648/j.ajwse.20170301.11

Malago, J., Makoba, E., & Muzuka, A. N. N. (2020). Spatial Distribution of Arsenic, Boron, Fluoride, and Lead in Surface and Groundwater in Arumeru District, Northern Tanzania. *Fluoride*, *53*(2), 356–386.

Middelburg, J. J., van der Weijden, C. H., & Woittiez, J. R. W. (1988). Chemical processes affecting the mobility of major, minor and trace elements during weathering of granitic rocks. *Chemical Geology*, *68*(3), 253–273. https://doi.org/10.1016/0009-2541(88)90025-3

Mutonga, M. (2015). *Stable Isotopic Composition of Geothermal Fields in Kenya; The Relationship Between Geothermal Fields and Kenya Rift Lakes Waters*.

Nanyaro, J. T., Aswathanarayana, U., Mungure, J. S., & Lahermo, P. W. (1984). A geochemical model for the abnormal fluoride concentrations in waters in parts of northern Tanzania. *Journal of African Earth Sciences (1983)*, *2*(2), 129–140. https://doi.org/10.1016/S0731-7247(84)80007-5

Parkhurst, D. L., & Appelo, C. A. J. (1999). User's guide to PHREEQC (Version 2): A computer program for speciation, batch-reaction, one-dimensional transport, and inverse geochemical calculations. In *User's guide to PHREEQC (Version 2): A computer program for speciation, batch-reaction, one-dimensional transport, and inverse geochemical calculations* (USGS Numbered Series No. 99–4259; Water-Resources Investigations Report, Vols. 99–4259). U.S. Geological Survey. https://doi.org/10.3133/wri994259

Ranta, E., Halldórsson, S. A., Barry, P. H., Ono, S., Robin, J. G., Kleine, B. I., Ricci, A., Fiebig, J., Sveinbjörnsdóttir, Á. E., & Stefánsson, A. (2023). Deep magma degassing and volatile fluxes through volcanic hydrothermal systems: Insights from the Askja and Kverkfjöll volcanoes, Iceland. *Journal of Volcanology and Geothermal Research*, *436*, 107776. https://doi.org/10.1016/j.jvolgeores.2023.107776

Reed, M., & Spycher, N. (1984). Calculation of pH and mineral equilibria in hydrothermal waters with application to geothermometry and studies of boiling and dilution.

Geochimica et Cosmochimica Acta, *48*, 1479–1492. https://doi.org/10.1016/0016-7037(84)90404-6

Roberts, M. A. (2002). *The Geochemical and Volcanological Evolution on the Mt. Meru Region, Northern Tanzania* [PhD Thesis]. Cambridge University.

Sharp, Z. (2017). Principles of Stable Isotope Geochemistry, 2nd Edition. *Open Textbooks*. https://doi.org/ https://doi.org/10.25844/h9q1-0p82

Stefansson, A., Arnórsson, S., Sveinbjörnsdottir, A., Heinemaier, J., & Kristmannsdóttir, H. (2019). Isotope (δD, δ18O, 3H, δ13C, 14C) and chemical (B, Cl) Constrains on water origin, mixing, water-rock interaction and age of low-temperature geothermal water. *Applied Geochemistry*, *108*, 104380. https://doi.org/10.1016/j.apgeochem.2019.104380

TBS. (2008). *Tanzania Standard: Drinking (potable) water – Specification (TZS 789: 2008)*. Tanzania Bureau of Standards.

Tomašek, I., Mouri, H., Dille, A., Bennett, G., Bhattacharya, P., Brion, N., Elskens, M., Fontijn, K., Gao, Y., Gevera, P. K., Ijumulana, J., Kisaka, M., Leermakers, M., Shemsanga, C., Walraevens, K., Wragg, J., & Kervyn, M. (2022). Naturally occurring potentially toxic elements in groundwater from the volcanic landscape around Mount Meru, Arusha, Tanzania and their potential health hazard. *Science of The Total Environment*, *807*, 150487. https://doi.org/10.1016/j.scitotenv.2021.150487

Wayne Nesbitt, H. (1979). Mobility and fractionation of rare earth elements during weathering of a granodiorite. *Nature*. https://doi.org/10.1038/279206a0

White, W. M. (2020). *Geochemistry* (2nd Edition). Wiley Professional, Reference & Trade (Wiley K&L). https://www.wiley.com/en-us/Geochemistry%2C+2nd+Edition-p-9781119438052

WHO. (2022). *Guidelines for drinking-water quality: Fourth edition incorporating the first and second addenda*. https://www.who.int/publications-detail-redirect/9789240045064

Wilkinson, P., Mitchell, J. G., Cattermole, P. J., & Downie, C. (1986). Volcanic chronology of the Meru–Kilimanjaro region, Northern Tanzania. *Journal of the Geological Society*, *143*(4), 601–605. https://doi.org/10.1144/gsjgs.143.4.0601